Population dynamics in patchy landscapes: steady states and pattern formation

Nazanin Zaker

A thesis submitted in partial fulfillment of the requirements for the degree of Doctorate in Philosophy Mathematics and Statistics[1]

Department of Mathematics and Statistics
Faculty of Science
University of Ottawa

[1]The Ph.D. program is a joint program with Carleton University, administered by the Ottawa-Carleton Institute of Mathematics and Statistics

Abstract

Many biological populations reside in increasingly fragmented landscapes, which arise from human activities and natural causes. Landscape characteristics may change abruptly in space and create sharp transitions (interfaces) in landscape quality. How patchy landscape affects ecosystem diversity and stability depends, among other things, on how individuals move through the landscape. Individuals adjust their movement behaviour to local habitat quality and show preferences for some habitat types over others. In this dissertation, we focus on how landscape composition and the movement behaviour at an interface between habitat patches of different quality affects the steady states of a single species and a predator–prey system.

First, we consider a model for population dynamics in a habitat consisting of two homogeneous one-dimensional patches in a coupled ecological reaction-diffusion equation. Several recent publications by other authors explored how individual movement behaviour affects population-level dynamics in a framework of reaction-diffusion systems that are coupled through discontinuous boundary conditions. The movement between patches is incorporated into the interface conditions. While most of those works are based on linear analysis, we study positive steady states of the nonlinear equations. We establish the existence, uniqueness and global asymptotic stability of the steady state, and we classify their qualitative shape depending on movement behaviour. We clarify the role of nonrandom movement in this context, and we apply our analysis to a previous result where it was shown that a randomly diffusing population in a continuously varying habitat can exceed the carrying capacity at steady state. In particular, we apply our results to study the question of why and under which conditions the total population abundance at steady state may exceed the total carrying capacity of the landscape.

Secondly, we model population dynamics with a predator–prey system in a coupled ecological reaction-diffusion equation in a heterogeneous landscape to study Turing patterns that emerge from diffusion-driven instability (DDI). We derive the DDI conditions, which consist of necessary and sufficient conditions for initiation of spatial patterns in a one-dimensional homogeneous landscape. We use a finite difference scheme method to numerically explore the general conditions using the May model,

and we present numerical simulations to illustrate our results. Then we extend our studies on Turing-pattern formation by considering a predator–prey system on an infinite patchy periodic landscape. The movement between patches is incorporated into the interface conditions that link the reaction-diffusion equations between patches. We use a homogenization technique to obtain an analytically tractable approximate model and determine Turing-pattern formation conditions. We use numerical simulations to present our results from this approximation method for this model. With this tool, we then explore how differential movement and habitat preference of both species in this model (prey and predator) affect DDI.

Dedications

This study is wholeheartedly dedicated to my beloved family, who have been my source of inspiration and gave me strength when I was discouraged. Thanks mom for always believing in me and for encouraging me to strive for my dreams.

I also dedicate this dissertation with love to my husband, Mohsen, who has offered unlimited support, warmth and encouragement during the past two years of my doctoral journey to follow my dreams.

Acknowledgement

First and foremost, I would like to express the deepest appreciation to my supervisor Professor Frithjof Lutscher for his excellent guidance and support throughout this thesis. Without his guidance and persistent help, this dissertation would not have been possible. I am also grateful for his financial support through research grants and conference funds.

I would like to thank my thesis examining committee, Prof. Huaiping Zhu, Prof. Abbas Momeni, Prof. Stacey Smith? and Prof. Hongbin Guo for accepting to review my thesis.

Last but not least, I take this opportunity to express my acknowledgement to the Faculty of Graduate and Postdoctoral Studies and the Department of Mathematics and Statistics at the University of Ottawa for their scholarships and financial support during my Ph.D. study.

Contents

List of Figures

List of Tables

Chapter 1

Introduction

The study of spatial population dynamics relates to some of the most fundamental questions in theoretical ecology: Why are organisms where they are? How does landscape structure affect population distribution in space? What effect does movement in response to habitat variation have on population density? How are interactions between individuals and populations affected by habitat fragmentation? These questions are of increasing importance as natural events and human activities create increasingly fragmented landscapes in which some biological populations may thrive while others struggle to survive. In this thesis, we answer some of these questions via mathematical modelling, analysis and numerical simulation.

1.1 Modelling Background

Whether a biological population can persist and spread in a given landscape depends on the interplay of population dynamics (growth, reproduction and death), individual movement through the landscape and landscape characteristics (favorable and unfavorable conditions). Hence, mathematical models need to take these processes into account.

In this section, we introduce some population dynamics models, including the logistic growth model [37] for a single population and the May model [48] for a predator–prey community. We then describe how individual movement in space can be modeled by diffusion and how biologically reasonable boundary conditions can be imposed. Joining the reaction models for population dynamics with diffusion models for movement, we arrive at reaction-diffusion equations, which are the mathematical modelling framework that we use to study some of the questions described above.

We approach population dynamics in spatially varying landscapes by considering

landscapes that consist of patches: regions in space that are homogeneous within—but different from—their neighbouring patches. Hence, we include heterogeneity into our models by dividing the landscape into patches. Each patch presents a particular landscape type and has its own population dynamics and movement characteristics that are constant throughout the patch. At the interface between patches, we impose appropriate matching conditions for population density and flux that are consistent with the random-walk model from which the diffusion equation can be derived.

1.1.1 Modelling population dynamics

To model how individuals reproduce and die, we write the ordinary differential equation

$$\frac{\mathrm{d}u(t)}{\mathrm{d}t} = F(u), \tag{1.1.1}$$

for the density $u(t)$ of a population at time t. The function F is the net growth rate of the species. A famous example is the logistic growth function

$$F(u) = ru(1 - u/K), \tag{1.1.2}$$

which is frequently used in mathematical biology [37]. Parameters r and K denote the intrinsic growth rate and the carrying capacity for the population, respectively. Both parameters are positive. Equation (1.1.1) with logistic growth function (1.1.2) has two steady states: $u = 0$ and $u = K$. The zero state is unstable, and $u = K$ is globally asymptotically stable. To describe the decline of species in some unfavourable environment, we use the simple linear mortality function

$$F(u) = -mu, \tag{1.1.3}$$

where the positive parameter m denotes the mortality rate.

To model the interaction of two species, we write a pair of coupled differential equations, one for each species. In general, such a system can be written as

$$\frac{\mathrm{d}u(t)}{\mathrm{d}t} = f(u, v), \quad \frac{\mathrm{d}v(t)}{\mathrm{d}t} = g(u, v), \tag{1.1.4}$$

where $u(t)$ and $v(t)$ denote the density of the two species at time t. More specifically, we are interested in a predator–prey interaction, where the predator consumes the prey. Hence, the prey's growth rate decreases when the predator density increases and the predator's growth rate increases when the prey density increases. If we denote by u the density of the prey and by v that of the predator, then the general model above should have the property $\frac{\partial f}{\partial v} < 0$ and $\frac{\partial g}{\partial u} > 0$.

There are many examples of predator–prey models, for example the Lotka–Volterra model [71] and the Rosenzweig–MacArthur model [62]. For reasons that

will become clear later, we will work with the May model [48]. In nondimensional form, this model can be written as

$$\frac{\mathrm{d}u}{\mathrm{d}t} = u(1-u) - \frac{uv}{b+u}, \quad \frac{\mathrm{d}v}{\mathrm{d}t} = sv\left(1 - \frac{v}{qu}\right). \tag{1.1.5}$$

The prey follows a logistic growth function and is consumed according to a Holling type II functional response [33, 34]. The functional response, $\frac{u}{b+u}$, is the rate at which each predator captures prey. The predator is modeled by a logistic equation with intrinsic growth rate s and prey-dependent carrying capacity qu.

The May model is not defined when the prey density is zero. However, we will only be interested in the positive coexistence steady state. Hence, our results will not be affected by singularity in the predator equation at zero.

1.1.2 Modelling movement in space

The diffusion equation is frequently used to model random movement of individuals in space. This equations can be derived in several ways, one of which begins with an unbiased random walk on an equidistant grid [13, 68]. After an appropriate scaling, one arrives at the diffusion equation

$$\frac{\partial u}{\partial t} = D\frac{\partial^2 u}{\partial x^2}, \tag{1.1.6}$$

for the density $u(x,t)$ of individuals at location x and time t. The diffusion coefficient D measures the mean squared displacement of organisms per unit time. Therefore, throughout the entire thesis, all diffusion coefficients are positive. We denote the spatial domain of interest by Ω. If Ω is a bounded domain, say some interval $[0, L]$, we need to introduce boundary conditions to describe individual movement behaviour at a boundary. The two standard boundary conditions are the Dirichlet (or hostile) conditions

$$u(0,t) = u(L,t) = 0, \tag{1.1.7}$$

which models the situation that individuals leave the domain and never return, and the Neumann (or no-flux) conditions

$$\frac{\partial u(0,t)}{\partial x} = \frac{\partial u(L,t)}{\partial x} = 0, \tag{1.1.8}$$

which model the situation that individuals never leave the domain.

1.1.3 Reaction-diffusion equations

If the movement and population dynamics occur on the same timescale, we can combine the dynamics from (1.1.1) with (1.1.6) and obtain the reaction-diffusion equation

$$\frac{\partial u}{\partial t} = D\frac{\partial^2 u}{\partial x^2} + F(u). \tag{1.1.9}$$

Reaction-diffusion equations are a common and highly versatile tool to study spatial population dynamics [13].

The above equation is derived for a single species. If we assume that two interacting species move independently of one another, we can formulate a corresponding system of two reaction-diffusion equations as

$$\frac{\partial u}{\partial t} = D^u\frac{\partial^2 u}{\partial x^2} + f(u,v), \quad \frac{\partial v}{\partial t} = D^v\frac{\partial^2 v}{\partial x^2} + g(u,v), \tag{1.1.10}$$

where D^u and D^v are the diffusion coefficients for two species.

1.1.4 Landscape heterogeneity

As formulated, the reaction-diffusion equations above imply that movement and population dynamics are identical at all spatial locations (homogeneous). A relatively straightforward way of introducing heterogeneity into reaction-diffusion equations is to allow the population growth function $F(u)$ in (1.1.9) to depend on space. To acknowledge this spatial dependence explicitly, we write $F(u,x)$. The general reaction-diffusion equation for the density $u(x,t)$ of a species at location x and time t becomes

$$\frac{\partial u}{\partial t} = D\frac{\partial^2 u}{\partial x^2} + F(u,x). \tag{1.1.11}$$

For example, the diffusive logistic equation is

$$\frac{\partial u}{\partial t} = D\frac{\partial^2 u}{\partial x^2} + r(x)u\left(1 - \frac{u}{K(x)}\right). \tag{1.1.12}$$

Spatially varying movement behaviour can be included in (1.1.12) in a number of different ways, such as a Fickian diffusion term $\partial_x(D(x)\partial_x u)$ or an "ecological" diffusion term $\partial_x^2(D(x)u)$ [68]. The two cases show qualitatively different behaviour in analysis and simulations.

Analyzing a spatially dependent reaction-diffusion equation is quite difficult. Many analytical results remain relatively abstract (e.g., existence of solutions, monotonicity). Another drawback of these equations is that large amounts of data are

required to estimate the spatially varying parameter functions $r(\cdot)$ and $K(\cdot)$. In addition, when landscape quality varies in space, the assumption of a spatially constant random diffusion process is unrealistic. Most organisms adapt their movement to habitat quality and show bias towards better habitats [18, 46].

Another method to include landscape heterogeneity into reaction-diffusion equations is to divide a landscape into two or more homogeneous patches, where growth and diffusion coefficients may be different between patches but are constant within patches [65, 26]. One then formulates a reaction-diffusion equation with constant coefficients on each patch and connects the equations for adjacent patches by matching conditions for the density and flux. This modelling approach was pioneered by Pacala and Roughgarden [56] for two patches and by Shigesada et al. [65] for infinite landscapes, which was continued by Freedman et al. [26], Cruywagen et al. [19], Lutscher et al. [43] and others.

A major advancement on these earlier models occurred when Maciel and Lutscher [46] introduced novel interface matching conditions. Those conditions are based on the work by Ovaskainen and Cornell [55], who had derived these interface conditions from the same kind of random walk that we mentioned earlier for the derivation of the diffusion equation.

We present the simplest scenario of a patchy one-dimensional landscape, consisting of two adjacent patches: Patch 1 and Patch 2. We denote Patch i by Ω_i and the population density on Patch i at location x and time t by $u_i(x,t)$.

On each patch, we have a reaction-diffusion equation of the form

$$\frac{\partial u_i(x,t)}{\partial t} = D_i \frac{\partial^2 u_i(x,t)}{\partial x^2} + F_i(u_i), \quad x \in \Omega_i, \quad i = 1,2, \tag{1.1.13}$$

where $D_i > 0$ is the diffusion coefficient in Patch i.

For our analysis and simulations in Chapter 3, we use the logistic growth function

$$F_i(u) = r_i u \left(1 - \frac{u}{K_i}\right), \tag{1.1.14}$$

where r_i and K_i are the intrinsic growth rate and the carrying capacity on Patch i.

When we extend the model to interacting species, we have coupled equations on each patch, which we write as

$$\frac{\partial u_i}{\partial t} = D_i^u \frac{\partial^2 u_i}{\partial x^2} + f_i(u_i, v_i), \quad \frac{\partial v_i}{\partial t} = D_i^v \frac{\partial^2 v_i}{\partial x^2} + g_i(u_i, v_i), \quad i = 1,2, \tag{1.1.15}$$

where D_i^u and D_i^v denote the diffusion coefficients for the two species on Patch i.

In our analysis and simulations in Chapter 5, we consider two different types of patches. On Type 1 patches, we use the May model from (1.1.5). On Type 2 patches,

we replace logistic growth for the prey by the simple death term in (1.1.3); i.e., we have

$$f_2 = -mu_2 - \frac{u_2 v_2}{b + u_2}, \quad g_2 = sv_2 \left(1 - \frac{v_2}{qu_2}\right). \tag{1.1.16}$$

The predation term $(\frac{u_i v_i}{b+u_i})$ is a common term on both type of patches.

Now that we have reaction-diffusion equations on each patch, we need to connect them via interface conditions. We choose the conditions derived by Ovaskainen and Cornell [55] and studied further by Maciel and Lutscher [46]. There are two conditions. One of them states that the population flux is continuous across the interface, which implies that no individuals are lost or gained from moving across the interface. Mathematically, continuity of the flux at the interface is expressed as

$$D_1 \frac{\partial u_1(0,t)}{\partial x} = D_2 \frac{\partial u_2(0,t)}{\partial x}, \quad t \geqslant 0. \tag{1.1.17}$$

The other condition relates the densities on the two sides of the interface. To understand this condition, we denote by p_1 and p_2 the probabilities that an individual at the interface moves to Patch 1 and Patch 2, respectively. We assume that individuals cannot stay at the interface, so that $p_1 + p_2 = 1$. We also refer to p_i as habitat preference. With this notation, the second interface condition [46, 55] reads

$$u_1(0,t) = ku_2(0,t), \quad k = \frac{p_1}{p_2}\frac{D_2}{D_1}, \quad t \geqslant 0. \tag{1.1.18}$$

We sometimes refer to the reaction-diffusion equations on each patch together with the interface conditions as "patchy reaction-diffusion equations".

The matching conditions not only allow us to include patch preference information, which is frequently collected in the field, into reaction-diffusion models, they also remove some biologically unrealistic behaviour that the early models showed; see Maciel and Lutscher [46] for a thorough discussion of this point. A number of recent studies use this new framework to study questions of persistence and spread [3, 47] and apply it to marine reserve design [2, 38]. However, most of their results are based on either linear analysis or numerical simulation (but see Maciel et al. [45]).

1.2 Outline of the thesis

We consider several questions in the theory of patchy reaction-diffusion equations, including analysis of existence of solutions, qualitative analysis of steady states and analytical and numerical aspects of Turing-pattern formation.

In Chapter 2, we prove the existence and uniqueness of solutions for the simplest meaningful patchy reaction-diffusion equation. We consider two adjacent patches with an interface at zero. We write the equations as follows

$$\begin{cases} \dfrac{\partial u_i(x,t)}{\partial t} = D_i \dfrac{\partial^2 u_i(x,t)}{\partial x^2} + F_i(u_i(x,t)), & (x,t) \in \Omega_i \times [0,\infty), \\ D_1 \dfrac{\partial u_1(0,t)}{\partial x} = D_2 \dfrac{\partial u_2(0,t)}{\partial x}, & t \geqslant 0, \\ u_1(0,t) = k u_2(0,t), & t \geqslant 0, \\ \dfrac{\partial u_1(-L_1,t)}{\partial x} = \dfrac{\partial u_2(L_2,t)}{\partial x} = 0, & t \geqslant 0, \end{cases} \tag{1.2.1}$$

where $\Omega_1 = [-L_1, 0]$ and $\Omega_2 = [0, L_2]$.

In Chapter 3, we study positive steady states of (1.2.1) on two patches. We first prove existence, uniqueness and global stability of a positive steady state. Then, assuming that we have logistic growth on each patch, we classify the qualitative shape of the steady state depending on movement behaviour. We apply our results to study the question of why and under which conditions the total population density at steady state may exceed the total carrying capacity of the landscape.

In Chapter 4, we give some background on the theory of diffusion-driven instability and Turing-pattern formation on a homogeneous landscape. We report the necessary and sufficient conditions for diffusion-driven instability and the initiation of spatial pattern in a one-dimensional homogeneous landscape. The general model in this context is

$$\begin{cases} \dfrac{\partial u}{\partial t} = D^u \dfrac{\partial^2 u}{\partial x^2} + f(u,v), & (x,t) \in \Omega \times [0,\infty), \\ \dfrac{\partial v}{\partial t} = D^v \dfrac{\partial^2 v}{\partial x^2} + g(u,v), & (x,t) \in \Omega \times [0,\infty), \\ \dfrac{\partial u(0,t)}{\partial x} = \dfrac{\partial u(L,t)}{\partial x} = 0, \quad \dfrac{\partial v(0,t)}{\partial x} = \dfrac{\partial v(L,t)}{\partial x} = 0, & t \geqslant 0, \\ u(x,0) = u_0 > 0, \quad v(x,0) = v_0 > 0. \end{cases} \tag{1.2.2}$$

We illustrate the general conditions using the May model (1.1.5) and present numerical simulations to illustrate the results.

In Chapter 5, we study Turing-pattern formation on patchy landscapes. More precisely, we consider an infinite landscape divided into periodically alternating patches of two different types. On Type 1 patches, we consider the May model; on Type 2 patches, we consider the case without prey growth (1.1.16). Thus, the model looks like

$$\begin{cases} \dfrac{\partial u_1(x,t)}{\partial t} = D_1^u \dfrac{\partial^2 u_1(x,t)}{\partial x^2} + u_1(1-u_1) - \dfrac{u_1 v_1}{b+u_1}, & t \geqslant 0, \\ \dfrac{\partial v_1(x,t)}{\partial t} = D_1^v \dfrac{\partial^2 v_1(x,t)}{\partial x^2} + s v_1 \left(1 - \dfrac{v_1}{q u_1}\right), & t \geqslant 0, \\ \dfrac{\partial u_2(x,t)}{\partial t} = D_2^u \dfrac{\partial^2 u_2(x,t)}{\partial x^2} - m u_2 - \dfrac{u_2 v_2}{b+u_2}, & t \geqslant 0, \\ \dfrac{\partial v_2(x,t)}{\partial t} = D_2^v \dfrac{\partial^2 v_2(x,t)}{\partial x^2} + s v_2 \left(1 - \dfrac{v_2}{q u_2}\right), & t \geqslant 0, \end{cases} \tag{1.2.3}$$

with appropriate interface conditions. To analyze the conditions for Turing-pattern formation in this model, we use the technique of homogenization to derive spatially homogeneous equations that we then analyze according to the theory from Chapter 4. We report the background and details of the homogenization procedure in Appendix A. We illustrate our results with numerical simulations.

Chapter 2

Existence and uniqueness theory for patchy reaction-diffusion models

In this chapter, we prove the existence and uniqueness of solutions for the simplest meaningful patchy reaction-diffusion equation with interface and boundary conditions; namely, system (1.2.1). We first present all the necessary background on semigroup theory and other analytical aspects. This chapter is based on [45] but contains more details and background.

2.1 Notation and background

In this section, we begin with the basic concepts and notation that we need to present the necessary background on semigroup theory, which is an appropriate tool to prove the existence and uniqueness of solutions for our patchy reaction-diffusion equation. The majority of definitions and theorems are from the famous books in semigroup theory by Friedman [28], Kato [35] and You and Sell [42]. Other references are indicated in the text.

2.1.1 Preliminary notions and notations

Let X and Y be Banach spaces; i.e., complete normed spaces over the real or complex numbers, with norms $\|.\|_X$ and $\|.\|_Y$, respectively. We denote by A a linear operator from X to Y and by $D(A)$ its domain. If $D(A)$ is dense in X, A is said to be densely defined. The linear subspace AX of Y is called the range of A and is denoted by

$R(A)$. The dimension of $R(A)$ is called the rank of A and is denoted by $\dim(R(A)) = \operatorname{rank}(A)$. The codimension of $R(A)$ with respect to Y is called the deficiency of A and is denoted by $\operatorname{def}(A)$. Then we have $\operatorname{rank}(A) + \operatorname{def}(A) = \dim(Y)$. The null space $N(A)$ of A is the set of all $u \in D(A)$, such that $Au = 0$. The dimension of $N(A)$ is called the nullity of A, which we shall denote by $\operatorname{nul}(A)$. Thus, we have $\operatorname{rank}(A) + \operatorname{nul}(A) = \dim(X)$. Also, we know that if $\operatorname{nul}(A) = \operatorname{def}(A) = 0$ then A maps X onto Y, one to one, and it is invertible. We denote the inverse by A^{-1} if it exists.

We say that A is a bounded linear operator if there exists some $M > 0$ such that for all $u \in D(A) \subseteq X$, we have $\|Au\|_Y \leqslant M\|u\|_X$. We denote the Banach algebra of all bounded linear operators on X by $\mathcal{L}(X)$.

An operator A from X to Y is continuous at $u_0 \in D(A)$ if $\|u_n - u_0\|_X \to 0$ implies $\|Au_n - Au_0\|_Y \to 0$ for all $\{u_n\} \subset D(A)$. If A is continuous at $u = 0$, then it is continuous everywhere in its domain. A linear operator is continuous if and only if it is bounded.

An operator $A\colon D(A) \subset X \to Y$ is said to be completely continuous if it is continuous and maps any bounded subset of $D(A)$ into a relatively compact subset of Y [60]. Hence, a completely continuous operator is bounded. A continuous operator $A\colon D(A) \subset X \to Y$ is completely continuous if and only if for every bounded sequence $\{u_k\} \subset D(A)$, the sequence $\{Au_k\}$ has a convergent subsequence [60].

Definition 2.1.1. *A linear operator $A\colon D(A) \to X$ is closed if for any sequence $\{f_n\} \subset D(A)$ such that, as $n \to \infty$, $f_n \to f$ and $Af_n \to g$, it follows that $f \in D(A)$ and $Af = g$.*

Proposition 2.1.2. *(Consequence of Closed Graph Theorem in [35]) If A is invertible, then A^{-1} is closed if and only if A is closed. A bounded linear operator on a Banach space is closed.*

Theorem 2.1.3. *(Theorem 5.3 in [35]) Let A be a linear operator. If A is invertible and A^{-1} is bounded, then it is automatically closed with nullity and deficiency* 0.

Definition 2.1.4. *(Definition 1.1 in [51]) Let $A\colon D(A) \subset X \to X$ be a closed linear operator on X. We call*

$$\rho(A) \coloneqq \{\lambda \in \mathbb{C} \mid \lambda - A\colon D(A) \to X \text{ is bijective}\},$$

the resolvent set and its complement $\sigma(A) \coloneqq \mathbb{C} \setminus \rho(A)$ the spectrum of A. For $\lambda \in \rho(A)$, the inverse

$$R(\lambda, A) \coloneqq (\lambda - A)^{-1},$$

is, by Proposition 2.1.2, a bounded operator on X and is called the resolvent (of A at the point λ).

In the following, we denote by H a non-trivial Hilbert space and by $(\cdot,\cdot)$ its inner product. As an example, the space $L^2(\Omega)$, where Ω is an open subset of $\mathbb{R}^n$, is a Hilbert space with inner product $(f,g)=\int_\Omega fg\,\mathrm{d}x$. The notion of the numerical range of a linear operator on H will play an important role. It is defined as follows.

Definition 2.1.5. *(Page 267 in [35]) Let A be a linear operator on H. The numerical range $\theta(A)$ of A is the set of all complex numbers (Au,u), where u ranges over all $u\in D(A)$ with $\|u\|_H=1$.*

Theorem 2.1.6. *(Theorem 3.2 in [35]) The numerical range, $\theta(A)$, is a convex set.*

Let us denote by Γ the closure of $\theta(A)$. Γ is a closed convex set. Let Δ be the complement of Γ in the complex plane. Since Γ is convex, Δ is a connected open set, except in the special case in which Γ is a strip bounded by two parallel straight lines (the limiting case is included in which the two lines coincide). In this exceptional case, Δ consists of two components Δ_1, Δ_2 which are half-planes.

Theorem 2.1.7. *(Theorem 3.2 in [35]) Let A be a closed operator and let Γ, Δ, Δ_1 and Δ_2 be as above. For any $\lambda\in\Delta$, $A-\lambda$ has closed range,* $\mathrm{nul}(A-\lambda)=0$ *and* $\mathrm{def}(A-\lambda)$ *is constant for $\lambda\in\Delta$, except in the special case mentioned above, in which* $\mathrm{def}(A-\lambda)$ *is constant in each of Δ_1 and Δ_2. If* $\mathrm{def}(A-\lambda)=0$ *for $\lambda\in\Delta$ ($\lambda\in\Delta_1$, $\lambda\in\Delta_2$), then Δ is a subset of $\rho(A)$ and* $\|R(\lambda,A)\|\leqslant\dfrac{1}{\mathrm{dist}(\lambda,\Gamma)}$.

We now define certain function spaces that we will use later. Let Ω be an open smooth domain in $\mathbb{R}^n$. We denote its closure by $\bar{\Omega}$. Let $C^k(\Omega)$ be the space of functions that are k-times differentiable for some integer $k\geq 0$ and $C^\infty(\Omega)$ the space of infinitely differentiable functions in Ω. Finally, let $C_c^\infty(\Omega)$ denote the space of infinitely differentiable functions with compact support in Ω [22].

Let u and v be two locally integrable functions defined in Ω and α a multi-index. We say that v is the α-th weak partial derivative of u, written $D^\alpha u=v$, provided

$$\int_\Omega uD^\alpha\phi\mathrm{d}x=(-1)^{|\alpha|}\int_\Omega v\phi\mathrm{d}x,$$

for all test functions $\phi\in C_c^\infty(\Omega)$ [22].

We introduce the Sobolev spaces $W^{k,p}(\Omega)$, which consist of all locally summable functions $u\colon\Omega\to\mathbb{R}$, such that for each multi-index α with $|\alpha|\leqslant k$, $D^\alpha u$ exists in the weak sense and belongs to $L^p(\Omega)$. $W^{k,p}(\Omega)$ is a Banach space. If $u\in W^{k,p}(\Omega)$, we define its norm to be

$$\|u\|_{W^{k,p}}:=\begin{cases}(\sum\limits_{|\alpha|\leqslant k}(\int_\Omega|D^\alpha u|^p\mathrm{d}x)^{\frac{1}{p}})^{\frac{1}{p}}, & 1\leqslant p<\infty,\\ \sum\limits_{|\alpha|\leqslant k}\mathrm{ess\,sup}_\Omega|D^\alpha u|, & p=\infty.\end{cases}$$

For $1 \leqslant p < \infty$, we have $\|u\|_{L^p(\Omega)} \leqslant \|u\|_{W^{k,p}(\Omega)}$. Hence, $W^{k,p}(\Omega)$ is embedded in $L^p(\Omega)$. If $p = 2$, we usually write $H^k(\Omega) = W^{k,p}(\Omega)$ for $k \in \mathbb{N}_0$. The letter H is used, since $H^k(\Omega)$ is a Hilbert space. Note that $H^0 = L^2(\Omega)$ [22].

Theorem 2.1.8. *(Theorem 3 in 5.3.3 in [22]) (Global approximation by functions smooth up to the boundary) Assume that Ω is bounded and $\partial\Omega$ is C^1. Suppose $u \in W^{k,p}(\Omega)$ for some $1 \leqslant p < \infty$. Then there exist functions $u_m \in C^\infty(\bar{\Omega})$ such that $u_m \to u$ in $W^{k,p}(\Omega)$.*

In the following, we provide two important theorems; the weak maximum principle and the strong maximum principle for second-order linear elliptic partial differential equations. We define the operator

$$Au \coloneqq -d_{ij}\partial_{ij}u + b_i\partial_i u + cu = -\sum_{i,j=1}^{N} d_{ij}\partial_{ij}u + \sum_{i=1}^{N} b_i\partial_i u + cu,$$

where $\partial_{ij}u$ shows the second partial derivative of u with respect to x_i and x_j, and the coefficients d_{ij}, b_i, c are continuous.

Theorem 2.1.9. *(Theorem 4.1 in [52]) (Weak maximum principle) Let $\Omega \subset \mathbb{R}^n$ be open and bounded and $u \in C^0(\bar{\Omega}) \cap C^2(\Omega)$. Suppose that $D = (d_{ij})$ is symmetric and that for any non-zero $\zeta \in \mathbb{R}^n$, we have $\zeta^t D\zeta > 0$ in $\bar{\Omega}$. Assume $Au \leqslant 0$ ($Au \geqslant 0$), $c = 0$ in Ω. Then the maximum (minimum) of u in $\bar{\Omega}$ is achieved on $\partial\Omega$; i.e.,*

$$\max_{\bar{\Omega}} u = \max_{\partial\Omega} u \qquad (\min_{\bar{\Omega}} u = \min_{\partial\Omega} u).$$

Remark 2.1.10. *(Page 345 in [22]) A function satisfying $Au \leqslant 0$ in Ω is called a subsolution. We are thus asserting that a subsolution attains its maximum on $\partial\Omega$. Similarly, if $Au \geqslant 0$ in Ω holds, u is a supersolution and attains its minimum on $\partial\Omega$.*

Theorem 2.1.11. *(Theorem 4.1 in [52]) (Strong maximum principle) Let the assumptions of Theorem 2.1.9 be satisfied except $c = 0$ in Ω. Then u is constant or, if not, we have:*

- *if $c = 0$, then u does not achieve its maximum (minimum) in Ω,*
- *if $c \geqslant 0$, then u does not achieve a non-negative maximum (non-positive minimum) in Ω,*
- *regardless the sign of c, u does not achieve a zero maximum (minimum) in Ω.*

Theorem 2.1.12. *(Remark 4.6 in [52]) (Hopf Lemma) Let the assumptions of Theorem 2.1.9 be satisfied except $c = 0$ in Ω. Assume furthermore that $\partial\Omega$ is a C^2 boundary near $x_0 \in \partial\Omega$, that $Au \geqslant 0$ in Ω, that $u(x) > u(x_0)$ for all $x \in \Omega$ near x_0 and that u is differentiable at x_0. Finally, we assume that one of the following holds:*

1. $c = 0$ *near* x_0.
2. $u(x_0) \leqslant 0$ *and* $c \geqslant 0$ *near* x_0.
3. $u(x_0) = 0$.

Then $\partial_\nu u(x_0) < 0$, *where* ν *is the outward unit normal vector to* $\partial\Omega$.

2.1.2 Background on semigroup theory

Our approach to prove the existence of solutions of system (1.2.1) is based on semigroup theory. Hence, we provide the background here, based on You and Sell [42].

We say that $T(t)$ is a semigroup of bounded linear operators on X if $T(t) \in \mathcal{L}(X)$, for all $t \in \mathbb{R}^+ = [0, \infty)$, and one has

$$\begin{cases} T(t+s) = T(t)T(s), & t, s \in [0, \infty), \\ T(0) = I. \end{cases} \tag{2.1.1}$$

A semigroup of bounded linear operators on X is a C_0-semigroup if one has

$$\lim_{t \to 0^+} T(t)x = x, \qquad \text{for every } x \in X. \tag{2.1.2}$$

The first equation of (2.1.1) is referred as the semigroup property; (2.1.2) is a statement of strong continuity of $T(t)$ at $t = 0$.

Let $T(t)$ be a C_0-semigroup on X. We define its (infinitesimal) generator A and its domain $D(A)$ by

$$Ax \coloneqq \lim_{h \to 0^+} \frac{T(h) - I}{h} x = \frac{d^+(T(t)x)}{dt} \mid_{t=0},$$

and $D(A) \coloneqq \{x \in X \mid Ax \text{ exists in } X\}$.

A typical example of a C_0-semigroup on a Banach space X comes from defining the operator-valued exponential function for any bounded operator A (see Nagel and Engel [51]) as

$$e^{tA} \coloneqq \sum_{k=0}^{\infty} \frac{t^k A^k}{k!}.$$

This is the reason that the semigroup $T(t)$ is often denoted by e^{At}, which we will use below.

In applications to partial differential equations, we typically encounter semigroups generated by unbounded operators. We present the necessary framework for these in the rest of this section.

Definition 2.1.13. *(Page 101 in [28]) Let φ be any number satisfying $0 < \varphi < \frac{\pi}{2}$, and let M be any positive constant. A linear operator A on X is said to be of type (φ, M) if:*

1) A is a closed, densely defined operator on X.

2) The resolvent set of A contains the sector

$$S_\varphi = \left\{ \lambda \mid \lambda \neq 0,\ \frac{\pi}{2} - \varphi < \arg \lambda < \frac{3\pi}{2} + \varphi \right\},$$

and

$$\| R(\lambda, A) \| = \| \left(\lambda - A\right)^{-1} \| \leqslant \frac{M}{|\lambda|}, \quad \text{if } \lambda \in S_\varphi.$$

Theorem 2.1.14. *(Theorem 2.1 in [28]) If A is of type (φ, M), then $-A$ generates a strongly continuous semigroup $T(t)$ with the following properties:*

1) $T(t)$ can be continued analytically into the sector $\Delta_\varphi = \{t :\ t \neq 0, |\arg t| < \varphi\}$.

2) $AT(t)$, $\frac{dT(t)}{dt}$ are bounded operators for each $t \in \Delta_\varphi$ and

$$\frac{dT(t)x}{dt} = -AT(t)x, \quad x \in X.$$

3) For any $0 < \varepsilon < \varphi$, there exists a constant $C = C(\varepsilon)$ such that

$$\| T(t) \| \leqslant C, \quad \| AT(t) \| \leqslant \frac{C}{|t|}, \quad \text{if } t \in \Delta_{\varphi - \varepsilon}.$$

4) For any $x \in X$ and $0 < \varepsilon < \varphi$, we have $T(t)x \to x$ if $t \to 0$ and $t \in \Delta_{\varphi - \varepsilon}$.

Definition 2.1.15. *(Page 102 in [28]) A strongly continuous semigroup with the additional properties (1)–(3) is called an analytic semigroup.*

Corollary 2.1.16. *(Page 102 in [28]) If A is of type (φ, M), then e^{-tA} is an analytic semigroup.*

Definition 2.1.17. *(Page 77 in [42]) For $\delta, \sigma \in (0, \pi)$, we define the following open sectors in the complex plane $\mathbb{C}$:*

$\Delta_\delta \coloneqq \{z \in \mathbb{C} \mid |\arg z| < \delta,\ z \neq 0\}$,

$\Delta_\delta(a) \coloneqq a + \Delta_\delta = \{z \in \mathbb{C} \mid |\arg(z-a)| < \delta,\ z \neq a\}$,

$\sum_\sigma \coloneqq \{z \in \mathbb{C} \mid |\arg z| > \sigma,\ z \neq 0\}$,

$\sum_\sigma(a) \coloneqq a + \sum_\sigma = \{z \in \mathbb{C} \mid |\arg(z-a)| > \sigma,\ z \neq a\}$.

A simple calculation shows that $\Delta_\delta(-a) = -\sum_\sigma(a)$, provided that $\delta = \pi - \sigma$. As a result, one has

$$\sum_\sigma(a) \subset \rho(A) \Longleftrightarrow \Delta_\delta(-a) \subset \rho(-A), \text{ where } \delta = \pi - \sigma, \tag{2.1.3}$$

for any linear operator $A : D(A) \to X$, where $D(A)$ is dense in X.

Definition 2.1.13 can be extended to what is nowadays called a sectorial operator. A sectorial operator generates an analytic semigroup as the following lemma shows.

Definition 2.1.18. *(Page 78 in [42]) A linear operator A is said to be a sectorial operator on X if $A\colon D(A) \to X$, where $D(A) \subset X$, satisfies the following two conditions:*

1) A is densely defined and closed.

2) There exist real numbers $a \in \mathbb{R}$, $\sigma \in \left(0, \frac{\pi}{2}\right)$ and $M \geqslant 1$ such that $\sum_\sigma(a) \subset \rho(A)$ and

$$\|R(\lambda, A)\| \leqslant \frac{M}{|\lambda - a|}, \quad \text{for all } \lambda \in \sum_\sigma(a). \tag{2.1.4}$$

A sectorial operator is said to be positive if it satisfies (2.1.4) for some $a > 0$.

Lemma 2.1.19. *(Lemma 36.1 in [42]) Let A be a sectorial operator on X. Then $-A$ is the infinitesimal generator of an analytic semigroup, e^{-At}, and there is a constant $M_0 \geqslant 1$ such that $\|e^{-At}\| \leqslant M_0 e^{-at}$, for all $t \geqslant 0$. Moreover, one has*

$$e^{-At} = \frac{1}{2\pi i} \int_\Gamma e^{-\lambda t} R(\lambda, -A) \mathrm{d}\lambda, \quad \text{for } t > 0, \tag{2.1.5}$$

and $e^{-At} = I$ at $t = 0$. Here, $\Gamma = \Gamma(\eta, \theta)$ is a contour in the resolvent set $\rho(-A)$, which is given by $\Gamma = \Gamma_1 \cup \Gamma_2 \cup \Gamma_3$, where

$$\Gamma_1 = \{\lambda = -a + re^{-i(\pi-\theta)} \mid r \geqslant \eta\}, \qquad \Gamma_2 = \{\lambda = -a + \eta e^{i\varphi} \mid |\varphi| \leqslant \pi - \theta\},$$
$$\Gamma_3 = \{\lambda = -a + re^{i(\pi-\theta)} \mid r \geqslant \eta\},$$

with θ satisfying $\sigma < \theta < \frac{\pi}{2}$ and η any positive constant. The path of integration along Γ in (2.1.5) is counterclockwise; see Figure 2.1. The integral in (2.1.5) exists in the uniform operator topology on $\mathcal{L}(X)$, for all $t > 0$.

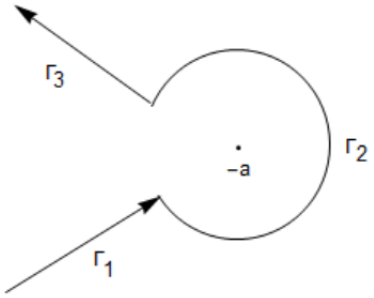

Figure 2.1: $\Gamma = \Gamma_1 \cup \Gamma_2 \cup \Gamma_3$

Now, we define the fractional power of an operator.

Definition 2.1.20. *(Page 95 in [42]) Let A be a positive sectorial operator on X. For any $\alpha > 0$ we define*

$$A^{-\alpha} := \frac{1}{\Gamma(\alpha)} \int_0^\infty t^{\alpha-1} e^{-At} \mathrm{d}t, \tag{2.1.6}$$

where e^{-At} is the analytic semigroup generated by $-A$, and $\Gamma(\alpha)$ is the Gamma function. If $\alpha = 1$, the operator defined in (2.1.6) is exactly the inverse of A.

Lemma 2.1.21. *(Theorem 37.3 in [42]) Let A be a positive, sectorial operator on X. For any $\alpha, \beta > 0$, $A^{-\alpha} \in \mathcal{L}(X)$ and $A^{-\alpha}A^{-\beta} = A^{-(\alpha+\beta)}$. Furthermore, each $A^{-\alpha}$ is one-to-one, and*

$$A^{-\alpha} = \frac{-\sin(\pi\alpha)}{\pi} \int_0^\infty \lambda^{-\alpha} R(\lambda, -A) \mathrm{d}\lambda, \qquad \text{for } 0 < \alpha < 1.$$

The fractional power A^α of the operator A is defined to be

$$A^\alpha = (A^{-\alpha})^{-1}, \qquad \text{for } 0 < \alpha < 1,$$

and its domain is given by $D(A^\alpha) := \mathcal{R}(A^{-\alpha})$. We also define $A^0 := I$, the identity operator on X.

2.1.3 Non-linear evolution equations

We consider the Cauchy problem

$$\frac{\mathrm{d}u}{\mathrm{d}t} + A(t,u)u = f(t,u), \tag{2.1.7}$$

$$u(0) = u_0, \tag{2.1.8}$$

where (2.1.7) is, in general, a nonlinear equation with respect to u and (2.1.8) is the initial condition.

We shall make the following assumptions based on Part 2 of Section 2 in [28]:

1. The operator $A_0 = A(0, u_0)$ is closed and densely defined, and
$$\|(\lambda I - A_0)^{-1}\| \leqslant \frac{C}{|\lambda| + 1}, \quad \text{for all } \lambda \text{ with } \mathrm{Re}\{\lambda\} \leqslant 0. \tag{2.1.9}$$
2. A_0^{-1} is a completely continuous operator.
3. For some constants $\alpha \in [0, 1)$ and $r > 0$, and for any $v \in X$ with $\|v\| < r$, the operator $A(t, A_0{}^{-\alpha} v)$ is well defined on D_0 for all $0 \leqslant t \leqslant t_0$. Furthermore, for any t, τ in $[0, t_0]$ and v,w in X with $\|v\|, \|w\| < r$,
$$\|[A(t, A_0^{-\alpha} v) - A(\tau, A_0^{-\alpha} w)]A^{-1}(\tau, A_0^{-\alpha} w)\| \leqslant C(r)(|\mathrm{t} - \tau|^{\sigma} + \|v - w\|^{\rho}), \tag{2.1.10}$$
where $0 < \sigma, \rho \leqslant 1$.
4. For every t, τ in $[0, t_0]$ and v,w in X with $\|v\|, \|w\| < r$,
$$\|f(t, A_0^{-\alpha} v) - f(\tau, A_0^{-\alpha} w)\| \leqslant C(r)(|\mathrm{t} - \tau|^{\sigma} + \|v - w\|^{\rho}). \tag{2.1.11}$$
5. We have $u_0 \in D(A_0^{\beta})$ for some $\beta > \alpha$ and
$$\|A_0^{\alpha} u_0\| < \mathrm{r}. \tag{2.1.12}$$

Theorem 2.1.22. *(Theorem 16.1 in [28]) Let assumptions* 1–5 *hold. Then there exists a number* t^*, $0 < t^* \leqslant t_0$, *such that there exists at least one continuously differentiable solution of (2.1.7) for* $0 < t \leqslant t^*$ *that satisfies (2.1.8).*

Theorem 2.1.23. *(Theorem 16.2 in [28]) Let assumptions* 1,3–5 *hold with* $\rho = 1$. *Then the assertion of Theorem 2.1.22 is valid and the solution is unique.*

2.2 Existence of solutions

In this section, we prove the existence and uniqueness of solutions for the patchy reaction-diffusion equation with its boundary and interface conditions (1.2.1), where $F_i(u_i) = u_i f_i(u_i)$. We show that solutions of this system exist globally in time. In the following section, we show that the solutions to non-negative initial conditions are positive.

The key idea is to write the above problem abstractly as

$$\frac{\mathrm{d}u}{\mathrm{d}t} + Au = F(u), \quad t \geqslant 0, \tag{2.2.1}$$

where A is the generator of an analytic semigroup. Then we use theory from the previous section to show that global solutions of this problem exist. When we compare (2.2.1) with (2.1.7), we notice that operator A is independent of t and u and that F only depends on u. This means that conditions 1–5 in the previous part will simplify accordingly. We rewrite the equations of system (1.2.1) as follows:

$$\begin{cases} \dfrac{\partial u_1}{\partial t} - D_1 \dfrac{\partial^2 u_1}{\partial x^2} + u_1 = f_1(u_1)u_1 + u_1, & (x,t) \in \Omega_1 \times [0,\infty), \\ \dfrac{\partial u_2}{\partial t} - D_2 \dfrac{\partial^2 u_2}{\partial x^2} + u_2 = f_2(u_2)u_2 + u_2, & (x,t) \in \Omega_2 \times [0,\infty), \\ D_1 \dfrac{\partial u_1(0,t)}{\partial x} = D_2 \dfrac{\partial u_2(0,t)}{\partial x}, & t \geqslant 0, \\ u_1(0,t) = k u_2(0,t), & t \geqslant 0, \\ \dfrac{\partial u_1(-L_1,t)}{\partial x} = \dfrac{\partial u_2(L_2,t)}{\partial x} = 0, & t \geqslant 0, \end{cases} \tag{2.2.2}$$

where $\Omega_1 = [-L_1, 0]$ and $\Omega_2 = [0, L_2]$. In this model, $x = 0$ is the interface where the two patches meet, and $x = -L_1$ and $x = L_2$ are the boundary of our landscape.

We let $u = \begin{pmatrix} u_1 \\ u_2 \end{pmatrix}$, $Au = \begin{pmatrix} -D_1 \dfrac{\partial^2 u_1}{\partial x^2} + u_1 \\ -D_2 \dfrac{\partial^2 u_2}{\partial x^2} + u_2 \end{pmatrix}$ and $F(u) = \begin{pmatrix} u_1 f_1(u_1) + u_1 \\ u_2 f_2(u_2) + u_2 \end{pmatrix}$. Then the first two equations in (2.2.2) are in the form (2.2.1).

2.2.1 Linear theory

We provide the appropriate space on which to consider the operator A and its properties.

Domain of the operator A, $D(A)$

We want to build the interface conditions into the definition of the domain of A. Since the model is set in one dimensional space, it is possible to set up the problem

in Hilbert spaces built from L^2 and $W^{2,2}$ spaces on Ω_1 and Ω_2. We define the basic space as
$H = L^2(\Omega_1) \times L^2(\Omega_2)$ and the domain of A, which is a subset of $X = W^{2,2}(\Omega_1) \times W^{2,2}(\Omega_2)$, as

$$D(A) = \left\{ u \in X \mid D_1 \frac{\partial u_1}{\partial x}(0) = D_2 \frac{\partial u_2}{\partial x}(0), u_1(0) = k u_2(0), \frac{\partial u_1}{\partial x}(-L_1) = \frac{\partial u_2}{\partial x}(L_2) = 0 \right\}. \tag{2.2.3}$$

We define a norm on H as

$$\|u\|_H^2 = \|u_1\|_{L^2(\Omega_1)}^2 + k\|u_2\|_{L^2(\Omega_2)}^2. \tag{2.2.4}$$

Properties of the operator A

Lemma 2.2.1. *$D(A)$ is dense in H.*

Proof: Based on the definition of C_c^∞, we see that any function in $C_c^\infty([-L_1, 0]) \times C_c^\infty([0, L_2])$ belongs to our domain, $D(A)$. On the other hand, based on standard regularity results [12], we know that C_c^∞ is dense in L^2. As a result, we can conclude that our domain is also dense in H. ∎

Lemma 2.2.2. *A is a closed linear operator.*

Proof: We can easily see that the operator A is linear on H. Thus, we just need to show that A is a closed operator. Based on Theorem 2.1.3, it is sufficient to show that A is invertible and A^{-1} is bounded. Inverting the operator A is equivalent to solving the following system

$$\begin{cases} -D_1 u_{1xx} + u_1 = v_1, & x \in \Omega_1, \\ -D_2 u_{2xx} + u_2 = v_2, & x \in \Omega_2, \\ D_1 u_{1x}(0) = D_2 u_{2x}(0), & \\ u_1(0) = k u_2(0), \quad u_{1x}(-L_1) = u_{2x}(L_2) = 0, & \end{cases} \tag{2.2.5}$$

where $(u_1, u_2) \in D(A)$ and $(v_1, v_2) \in H$.

To solve (2.2.5), we will first obtain the solution of the following problem

$$\begin{cases} -D_1 u_{1xx} + u_1 = v_1, & x \in \Omega_1, \\ -D_2 u_{2xx} + u_2 = v_2, & x \in \Omega_2, \\ u_{1x}(-L_1) = u_{1x}(0) = 0, \quad u_{2x}(L_2) = u_{2x}(0) = 0. & \end{cases} \tag{2.2.6}$$

To show that a solution of (2.2.6) exists, we use the method of Green's functions for solving inhomogenous boundary value problems; see e.g., Bender and Orszag [9]. We consider the system as the two separate systems

$$\begin{cases} -D_1 u_{1xx} + u_1 = v_1, & x \in \Omega_1, \\ u_{1x}(-L_1) = u_{1x}(0) = 0, \end{cases} \tag{2.2.7}$$

and

$$\begin{cases} -D_2 u_{2xx} + u_2 = v_2, & x \in \Omega_2, \\ u_{2x}(L_2) = u_{2x}(0) = 0. \end{cases} \tag{2.2.8}$$

The solutions have the following forms

$$\tilde{u}_1(x) = \int_{-L_1}^{0} v_1(s) G_1(x,s) \mathrm{d}s \quad \text{and} \quad \tilde{u}_2(x) = \int_{0}^{\mathrm{L}_2} v_2(s) G_2(x,s) \mathrm{d}s,$$

where $G_1(x,s)$ and $G_2(x,s)$ are the Green's functions of system (2.2.7) and (2.2.8), respectively.

Consider the following systems

$$\begin{cases} -y_{1xx} + y_1 = 0, & x \in \Omega_1, \\ y_1(-L_1) = 1, \quad y_{1x}(-L_1) = 0, \end{cases} \tag{2.2.9}$$

and

$$\begin{cases} -y_{2xx} + y_2 = 0, & x \in \Omega_2, \\ y_2(L_2) = 1, \quad y_{2x}(L_2) = 0. \end{cases} \tag{2.2.10}$$

Let y_1 be the solution of (2.2.9) and y_2 be the solution of (2.2.10). We show that $y_{1x}(x) > 0$ on $(-L_1, 0]$ and $y_1(x) \geqslant 1$ on $\Omega_1 = [-L_1, 0]$. By the same argument, we show that $y_{2x}(x) < 0$ on $[0, L_2)$ and $y_2(x) \geqslant 1$ on $\Omega_2 = [0, L_2]$.

At $x = -L_1$, we have $y_{1xx}(-L_1) = y_1(-L_1) = 1 > 0$. Thus, in some interval $(-L_1, -L_1 + \delta)$, for some $\delta > 0$, we have $y_{1x}(x) > 0$, so that $y_1(x) > 1$. Suppose $y_{1x}(x) = 0$ somewhere in $[-L_1 + \delta, 0]$, and let $x_0 = \inf\{x \in [-L_1 + \delta, 0] \mid y_{1x}(x) = 0\}$. For $x < x_0$, we have $y_1(x) > 1$ and $y_{1x}(x) > 0$. Therefore, we must have $y_{1xx}(x_0) \leqslant 0$. But $y_{1xx}(x_0) = y_1(x_0) > 1 > 0$. Thus, we have a contradiction. Hence, $y_{1x}(x) > 0$ for all $x \in (-L_1, 0]$ and $y_1(x) \geqslant 1$ for all $x \in \Omega_1 = [-L_1, 0]$.

By a similar argument, we can see that $y_{2x}(x) < 0$ and $y_2(x) \geqslant 1$ on $[0, L_2]$. Hence, we have $y_1(0) > 0$, $y_{1x}(0) > 0$, $y_2(0) > 0$, $y_{2x}(0) < 0$.

We combine solutions (2.2.6) and (2.2.9)–(2.2.10) to solve system (2.2.5). We define the solution operator as follows:

$$u_1 = \tilde{u}_1 + \alpha_1 y_1 \quad \text{and} \quad u_2 = \tilde{u}_2 + \alpha_2 y_2, \tag{2.2.11}$$

where α_1 and α_2 will be determined by the interface conditions. Solution (2.2.11) satisfies the interface conditions when α_1 and α_2 satisfy the following equations:

$$\begin{cases} y_1(0)\alpha_1 - ky_2(0)\alpha_2 = k\tilde{u}_2(0) - \tilde{u}_1(0), \\ D_1 y_{1x}(0)\alpha_1 - D_2 y_{2x}(0)\alpha_2 = 0. \end{cases} \tag{2.2.12}$$

Since $\begin{vmatrix} y_1(0) & y_2(0) \\ y_{1x}(0) & y_{2x}(0) \end{vmatrix} = y_1(0)y_{2x}(0) - y_2(0)y_{1x}(0) < 0$, problem (2.2.12) always has a solution for α_1 and α_2 as a linear combination of $\tilde{u}_1, \tilde{u}_2$, with coefficients depending on k, D_1 and D_2 but not on v_1 and v_2.

We need to prove that we have the following inequality in order to conclude that A^{-1} is bounded:

$$\|u_1\|_{L^2(\Omega_1)} + k\|u_2\|_{L^2(\Omega_2)} \leqslant C(\|v_1\|_{L^2(\Omega_1)} + k\|v_2\|_{L^2(\Omega_2)}). \tag{2.2.13}$$

By applying standard regularity theory for elliptic partial differential equations with Neumann boundary conditions [61], we can conclude that $\|\tilde{u}_1\|_{W^{2,2}(\Omega_1)} \leqslant C_1\|v_1\|_{L^2(\Omega_1)}$ and $\|\tilde{u}_2\|_{W^{2,2}(\Omega_2)} \leqslant C_2\|v_2\|_{L^2(\Omega_2)}$. Since $W^{2,2}$ is embedded in L^2, we have $\|\tilde{u}_1\|_{L^2(\Omega_1)} \leqslant C_1\|v_1\|_{L^2(\Omega_1)}$ and $\|\tilde{u}_2\|_{L^2(\Omega_2)} \leqslant C_2\|v_2\|_{L^2(\Omega_2)}$. Then from (2.2.11) we obtain

$$\|u_1\|_{L^2(\Omega_1)} = \|\tilde{u}_1 + \alpha_1 y_1\|_{L^2(\Omega_1)} \leqslant \|\tilde{u}_1\|_{L^2(\Omega_1)} + |\alpha_1|\|y_1\|_{L^2(\Omega_1)}$$

and

$$k\|u_2\|_{L^2(\Omega_2)} = k\|\tilde{u}_2 + \alpha_2 y_2\|_{L^2(\Omega_2)} \leqslant k\|\tilde{u}_2\|_{L^2(\Omega_2)} + k|\alpha_2|\|y_2\|_{L^2(\Omega_2)}.$$

Since α_1 and α_2 can be written as a linear combination of $\tilde{u}_1$ and $\tilde{u}_2$, we get

$$\begin{aligned} \|u_1\|_{L^2(\Omega_1)} + k\|u_2\|_{L^2(\Omega_2)} &\leqslant C_1\|v_1\|_{L^2(\Omega_1)} + kC_2\|v_2\|_{L^2(\Omega_2)} \\ &\quad + C_3(\|\tilde{u}_1\|_{L^2(\Omega_1)} + k\|\tilde{u}_2\|_{L^2(\Omega_2)}) \\ &\leqslant C(\|v_1\|_{L^2(\Omega_1)} + k\|v_2\|_{L^2(\Omega_2)}). \end{aligned}$$

∎

Lemma 2.2.3. *The resolvent set of A contains a sector S_φ, and we have $\|R(\lambda, A)\| \leqslant \frac{M}{|\lambda|}$, for all $\lambda \in S_\varphi$.*

Proof: To show that the resolvent set of A contains a sector S_φ, we use Theorem 2.1.7 and also Lemma 2 by Cosner [16]. We first find the numerical range of the operator $A, \theta(\mathrm{A}) \subseteq \mathbb{C}$. Then we show that $\Delta = \mathbb{C} \setminus \Gamma$ is connected, where Γ denotes the closure of $\theta(A)$. Since we proved that the operator A is closed, we have that A^{-1} is a

bounded operator in H, which shows that A has deficiency zero on Δ. If the deficiency is 0, then Δ is contained in the resolvent set of A and $\|(\lambda - A)^{-1}\| \leqslant 1/\mathrm{dist}(\lambda, \Gamma)$, where $\mathrm{dist}(\lambda, \Gamma)$ is the distance from λ to Γ in $\mathbb{C}$. Hence, we must calculate the numerical range of A.

Let $u \in D(A)$ with $\|u\|_H = 1$ and denote by $\bar{u}$ the complex conjugate of the function u. We have

$$\begin{aligned}
\langle Au, u\rangle_H &= \int_{-L_1}^{0} Au_1\bar{u}_1 \mathrm{d}x + k\int_{0}^{L_2} Au_2\bar{u}_2 \mathrm{d}x \\
&= -\int_{-L_1}^{0} -D_1u_{1xx}\bar{u}_1 \mathrm{d}x + \int_{-L_1}^{0} u_1\bar{u}_1 \mathrm{d}x - k\int_{0}^{L_2} D_2u_{2xx}\bar{u}_2 \mathrm{d}x + k\int_{0}^{L_2} u_2\bar{u}_2 \mathrm{d}x \\
&= -D_1u_{1x}(0)\bar{u}_1(0) + D_1u_{1x}(-L_1)\bar{u}_1(-L_1) + \int_{-L_1}^{0} (D_1u_{1x}\bar{u}_{1x} + u_1\bar{u}_1)\mathrm{d}x \\
&\quad - kD_2u_{2x}(L_2)\bar{u}_2(L_2) + kD_2u_{2x}(0)\bar{u}_2(0) + k\int_{0}^{L_2} (D_2u_{2x}\bar{u}_{2x} + u_2\bar{u}_2)\mathrm{d}x.
\end{aligned}$$

By the boundary and interface conditions in system (1.2.1), the interface terms cancel, the boundary terms vanish, and we have

$$\langle Au, u\rangle_H = \int_{-L_1}^{0} D_1u_{1x}\bar{u}_{1x}\mathrm{d}x + k\int_{0}^{L_2} D_2u_{2x}\bar{u}_{2x}\mathrm{d}x + \langle u, u\rangle_H \geqslant \langle u, u\rangle_H = \|u\|_H^2 = 1.$$

Hence, the lower bound of $\langle Au, u\rangle_H$ is 1. Thus, we have $\theta(A) \subseteq [1, \infty)$. Therefore, the closure of this numerical range also satisfies $\Gamma \subseteq [1, \infty) \subset \mathbb{C}$. Hence, we conclude that $\Delta = \mathbb{C} \setminus \Gamma$ is connected and, based on Theorem 2.1.7, we have $S_\varphi \subset \rho(A)$ and also

$$\|(\lambda - A)^{-1}\| \leqslant \frac{1}{\mathrm{dist}(\lambda, \Gamma)}.$$

Now, we need to show that $\|R(\lambda, A)\| = \|\,(\lambda - A)^{-1}\,\| \leqslant \dfrac{M}{|\lambda|}$ for $\lambda \in S_\varphi$. But if $\|R(\lambda, A)\| = \|\,(\lambda - A)^{-1}\,\| \leqslant \dfrac{M}{1 + |\lambda|}$, for $\lambda \in S_\varphi$, we will get our desired result because $\dfrac{M}{1 + |\lambda|} < \dfrac{M}{|\lambda|}$. Based on the above explanation, we just need to show that $\dfrac{1}{\mathrm{dist}(\lambda, \Gamma)} \leqslant \dfrac{M}{1 + |\lambda|}$, for $\lambda \in S_\varphi$ or, equivalently,

$$1 + |\lambda| \leqslant M\,\mathrm{dist}(\lambda, \Gamma), \quad \text{for } \lambda \in S_\varphi. \tag{2.2.14}$$

Based on $|\lambda|$, we have three cases; see Figure 2.2. We abbreviate $d = \mathrm{dist}(\lambda, \Gamma)$.

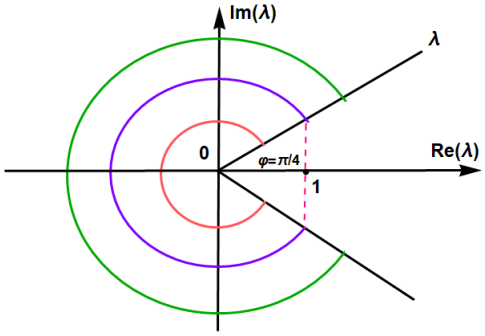

Figure 2.2: Three sectors based on the value of $|\lambda|$

We know that λ can be written in polar form as $\lambda = ze^{i\varphi} = z(\cos(\varphi) + i\sin(\varphi))$, where $z := |\lambda|$. By symmetry, we can prove inequality (2.2.14) just for the upper half plane. Moreover, to prove this inequality for a given $\lambda \in S_\varphi$, it is enough to show it for the line $\lambda = ze^{i\varphi}$ rather than showing for the whole sector corresponding to this λ. We choose $\varphi = \frac{\pi}{4}$.

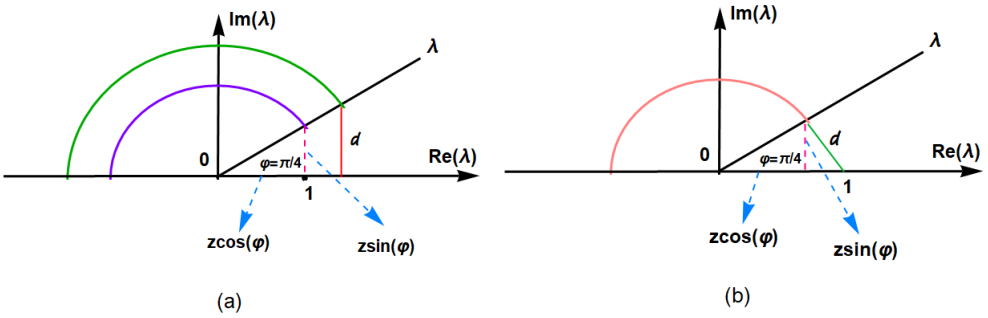

Figure 2.3: (a): $\mathrm{Re}(\lambda) \geqslant 1$. (b): $\mathrm{Re}(\lambda) < 1$. In figure (a), the $\mathrm{dist}(\lambda, \Gamma)$ for $\mathrm{Re}(\lambda) = 1$ and $\mathrm{Re}(\lambda) > 1$, corresponds to the dashed and solid line, respectively.

Figure 2.3 shows that we have two cases:

1. $\mathrm{Re}(\lambda) \geqslant 1$

   If $\mathrm{Re}(\lambda) \geqslant 1$, then $\mathrm{dist}(\lambda, \Gamma) = \mathrm{Im}(\lambda)$. We need to find some positive constant M such that $z + 1 \leqslant Mz\sin(\varphi)$ for $z \geqslant \frac{1}{\cos(\varphi)}$. Since we chose $\varphi = \frac{\pi}{4}$, this inequality can be written as $z + 1 \leqslant \dfrac{Mz}{\sqrt{2}}$ for $z \geqslant \sqrt{2}$.

   Clearly, we require $M > \sqrt{2}$. The inequality is an equality for $z = z^* = \frac{\sqrt{2}}{M - \sqrt{2}}$. Hence, we get the desired result if $z^* < \sqrt{2}$, or $M > \sqrt{2} + 1$.

2. $\mathrm{Re}(\lambda) < 1$

   Based on Figure 2.3, we see that

$$\mathrm{dist}(\lambda, \Gamma) = \sqrt{(z\sin((\varphi))^2 + (1 - z\cos(\varphi))^2} = \sqrt{\left(\frac{z}{\sqrt{2}}\right)^2 + \left(1 - \frac{z}{\sqrt{2}}\right)^2}.$$

   Then, by applying (2.2.14), we show that, for some positive constant M, we have $\dfrac{1}{M^2} \leqslant \dfrac{z^2 - \sqrt{2}z + 1}{(z+1)^2}$. Let $f(z) = \dfrac{z^2 - \sqrt{2}z + 1}{(z+1)^2}$. We see that $f(0) = 1$ and $\lim\limits_{z\to\infty} f(z) = 1$. Also, we get $f'(z) = \dfrac{(z-1)(2+\sqrt{2})}{(1+z)^3}$, which shows that $z = 1$ is the minimum point of $f(z)$. Thus, $f(1) = \dfrac{2-\sqrt{2}}{4}$ is the minimum value of this function. Now we can choose $\dfrac{1}{M^2} = \dfrac{2-\sqrt{2}}{4}$, or $M = \dfrac{2}{\sqrt{2-\sqrt{2}}}$.

   Therefore, for $M \geqslant \dfrac{2}{\sqrt{2-\sqrt{2}}}$, equation (2.2.14) is satisfied for all $\lambda \in S_{\frac{\pi}{4}}$.

∎

Based on Definition 2.1.13 and Lemmas 2.2.1–2.2.3, we conclude that our operator A is of type (φ, M), which implies that it is the generator of an analytic semigroup.

2.2.2 Existence

We prove the existence of local and global solutions of system (1.2.1) or equivalently, (2.2.2).

Existence of local solutions

We want to show that equation (2.2.1) has local solutions on $(0, T]$, for some finite time T. By applying Theorem 2.1.23, we see that it is enough to show that the function F is a Lipschitz function.

Let $u = (u_1, u_2)^T$ and $v = (v_1, v_2)^T$ be such that $\|u\|_H, \|v\|_H < r$. Since our function does not depend on t, based on equation (2.1.11) and Theorem 2.1.23, it is sufficient to show that $\|F(A^{-\alpha}u) - F(A^{-\alpha}v)\|_H \leqslant C(r)\|u - v\|_H$.

Since $\|u\|_H, \|v\|_H < r$ and based on the definition of the norm on H, we have $\|u_1\|^2_{L^2(\Omega_1)}, \|v_1\|^2_{L^2(\Omega_1)} < r$ and $k\|u_2\|^2_{L^2(\Omega_2)}, k\|v_2\|^2_{L^2(\Omega_2)} < r$. We define $(w_1^1, w_2^1) =$

$w^1 = A^{-\alpha}u$ and $(w_1^2, w_2^2) = w^2 = A^{-\alpha}v$, where $w^1, w^2 \in X$ and $w_1^i \in W^{2,2}(\Omega_1) \subset C^1(\Omega_1), w_2^i \in W^{2,2}(\Omega_2) \subset C^1(\Omega_2)$, for $i = 1, 2$. Thus, w_1^i, w_2^i for $i = 1, 2$, are bounded continuous functions. Then we have $\|w_1^i\|_\infty, \|w_2^i\|_\infty < C_r$ for $i = 1, 2$.

We calculate

$$\begin{aligned}
\|F(A^{-\alpha}u) - F(A^{-\alpha}v)\|_H &= \|F(w^1) - F(w^2)\|_H \\
&= \left\| \begin{pmatrix} w_1^1 f_1(w_1^1) - w_1^2 f_1(w_1^2) \\ w_2^1 f_2(w_2^1) - w_2^2 f_2(w_2^2) \end{pmatrix} + \begin{pmatrix} w_1^1 - w_1^2 \\ w_2^1 - w_2^2 \end{pmatrix} \right\|_H \\
&\leqslant \left\| \begin{pmatrix} w_1^1 f_1(w_1^1) - w_1^2 f_1(w_1^2) \\ w_2^1 f_2(w_2^1) - w_2^2 f_2(w_2^2) \end{pmatrix} \right\|_H + \left\| \begin{pmatrix} w_1^1 - w_1^2 \\ w_2^1 - w_2^2 \end{pmatrix} \right\|_H \\
&= \|w_1^1 f_1(w_1^1) - w_1^2 f_1(w_1^2)\|^2_{L^2(\Omega_1)} \\
&\quad + k\|w_2^1 f_2(w_2^1) - w_2^2 f_2(w_2^2)\|^2_{L^2(\Omega_2)} + \|w^1 - w^2\|_H.
\end{aligned}$$

We need to show that $\|w_1^1 f_1(w_1^1) - w_1^2 f_1(w_1^2)\|^2_{L^2(\Omega_1)} \leqslant \tilde{C}_1(r)\|w_1^1 - w_1^2\|^2_{L^2(\Omega_1)}$ and $k\|w_2^1 f_2(w_2^1) - w_2^2 f_2(w_2^2)\|^2_{L^2(\Omega_2)} \leqslant \tilde{C}_2(r)k\|w_2^1 - w_2^2\|^2_{L^2(\Omega_2)}$. First we prove $\|w_1^1 f_1(w_1^1) - w_1^2 f_1(w_1^2)\|^2_{L^2(\Omega_1)} \leqslant \tilde{C}_1(r)\|w_1^1 - w_1^2\|_{L^2(\Omega_1)}$. For this purpose, we denote a quadratic function $\tilde{F}(w_1^i) = w_1^i f_1(w_1^i)$ for $i = 1, 2$, and we also define the function $h(s)$ as follows

$$\begin{aligned}
h(s): \ [0,1] &\longrightarrow X \\
s &\longrightarrow sw_1^1 + (1-s)w_1^2.
\end{aligned}$$

Then we have

$$w_1^1 f_1(w_1^1) - w_1^2 f_1(w_1^2) = \tilde{F}(w_1^1) - \tilde{F}(w_1^2) = \tilde{F}(h(1)) - \tilde{F}(h(0)).$$

By applying the Fundamental Theorem of Calculus, we obtain

$$\tilde{F}(h(1)) - \tilde{F}(h(0)) = \int_0^1 D\tilde{F}(sw_1^1 + (1-s)w_1^2)(w_1^1 - w_1^2)\mathrm{d}s.$$

Now we can use the supremum norm over s in $[0, 1]$ for the linear function $D\tilde{F}(sw_1^1 - (1-s)w_1^2)$, because we have $\|w_1^i\|_\infty < C_r$. Hence, we get

$$\begin{aligned}
\left\| \int_0^1 D\tilde{F}(sw_1^1 + (1-s)w_1^2)(w_1^1 - w_1^2)\mathrm{d}s \right\|^2_{L^2(\Omega_1)} &\leqslant \sup_{s\in[0,1]} \|D\tilde{F}(sw_1^1 + (1-s)w_1^2)\| \\
&\quad \times \left\| \int_0^1 (w_1^1 - w_1^2)\mathrm{d}s \right\|^2_{L^2(\Omega_1)} \\
&\leqslant \tilde{C}_1(r)\|w_1^1 - w_1^2\|^2_{L^2(\Omega_1)}.
\end{aligned}$$

Similarly, we obtain $k\|w_2^1 f_2(w_1^2) - w_2^2 f_2(w_2^2)\|^2_{L^2(\Omega_2)} \leqslant \tilde{C}_2(r)k\|w_2^1 - w_2^2\|^2_{L^2(\Omega_2)}$. If we combine these two inequalities, we get

$$\begin{aligned}
\|F(A^{-\alpha}u) - F(A^{-\alpha}v)\|_H &\leqslant \tilde{C}_1(r)\|w_1^1 - w_1^2\|^2_{L^2(\Omega_1)} + \tilde{C}_2(r)k\|w_2^1 - w_2^2\|^2_{L^2(\Omega_2)} + \|w^1 - w^2\|_H \\
&\leqslant C'(r)(\|w_1^1 - w_1^2\|^2_{L^2(\Omega_1)} + k\|w_2^1 - w_2^2\|^2_{L^2(\Omega_2)}) + \|w^1 - w^2\|_H \\
&= (C'(r) + 1)\|w^1 - w^2\|_H \\
&= C''(r)\|w^1 - w^2\|_H \\
&= C''(r)\|A^{-\alpha}u - A^{-\alpha}v\|_H \\
&= C''(r)\|A^{-\alpha}(u - v)\|_H \\
&\leqslant C''(r)\|A^{-\alpha}\|\|u - v\|_H \\
&\leqslant C(r)\|u - v\|_H,
\end{aligned}$$

thus proving the desired result. Based on Theorem 2.1.23, equation (2.2.1) has local solutions.

Existence of global solutions

Finally, we show the global existence of non-negative solutions. Suppose that our solutions exist for a finite time. We need to show that $\|Au\|_H$ is bounded for any finite $T > 0$. Then we can continue to use the local existence theorem to extend the solutions in order to have the existence of global solutions. Since we have $u_t + Au = F(u)$, we obtain $\|Au\|_H \leqslant \|u_t\|_H + \|F(u)\|_H$. We see that

$$F(u) = \begin{pmatrix} u_1 f_1(u_1) + u_1 \\ u_2 f_2(u_2) + u_2 \end{pmatrix},$$

which can be also written as

$$F(u) = \begin{pmatrix} f_1(u_1) + 1 & 0 \\ 0 & f_2(u_2) + 1 \end{pmatrix} \begin{pmatrix} u_1 \\ u_2 \end{pmatrix}.$$

Based on the definition of $F(u)$, we conclude that $\|F(u)\|_H \leqslant C\|u\|_H$ for some positive constant C, because the function $u_i f_i(u_i) = r_i u_i(1 - \frac{u_i}{K_i})$ for $i = 1, 2$ is a logistic growth function, which shows that $u_i f_i(u_i) < r_i u_i$. Thus, it is enough to show that $\|u\|_H$ and $\|u_t\|_H$ are bounded. Here, we obtain the necessary bounds via a Lyapunov function. Let $E(t) = \frac{1}{2}(\|u\|^2_H + \|u_t\|^2_H)$. Then we have $E'(t) = \frac{1}{2}[(\|u\|^2_H)' + (\|u_t\|^2_H)']$. Thus, we need to estimate $(\|u\|^2_H)'$ and $(\|u_t\|^2_H)'$. We first find an expression for $(\|u\|^2_H)'$ as follows:

$$(\|u\|^2_H)' = (\langle u, u\rangle_H)' = 2\langle u, u_t\rangle_H = 2\langle u, -Au + F(u)\rangle_H = 2\langle u, -Au\rangle_H + 2\langle u, F(u)\rangle_H.$$

We compute each of the above terms separately. We have

$$\langle u, -Au\rangle_H = -\langle u, Au\rangle_H = -\int_{-L_1}^{0} D_1 u_{1x}^2 \mathrm{d}x - k\int_0^{L_2} D_2 u_{2x}^2 \mathrm{d}x - \langle u, u\rangle_H \leqslant -\langle u, u\rangle_H.$$

Since $u_i f_i(u_i) < r_i u_i$, we obtain $\langle u, F(u)\rangle_H \leqslant C\langle u, u\rangle_H = C\|u\|_H^2$ for some constant C. Therefore, we get $(\|u\|_H^2)' \leqslant 2C\|u\|_H^2$. Moreover, we calculate the second term $(\|u_t\|_H^2)'$ as follows:

$$\begin{aligned}(\|u_t\|_H^2)' &= (\langle u_t, u_t\rangle_H)' = 2\langle u_t, u_{tt}\rangle_H = 2\langle u_t, (-Au + F(u))_t\rangle_H \\ &= 2\langle u_t, (-Au_t + D_u F(u)u_t)\rangle_H = 2\langle u_t, -Au_t\rangle_H + 2\langle u_t, D_u F(u)u_t\rangle_H.\end{aligned}$$

By a similar calculation for $(\|u_t\|_H^2)'$, we get $(\|u_t\|_H^2)' \leqslant 2C\langle u_t, u_t\rangle_H = 2C\|u_t\|_H^2$. Substituting these estimates into the expression of $E'(t)$, we get:

$$E'(t) = \frac{1}{2}[(\|u\|_H^2)' + (\|u_t\|_H^2)'] \leqslant \frac{1}{2}C[\|u\|_H^2 + \|u_t\|_H^2] = CE(t).$$

Thus, $E'(t) \leqslant CE(t)$, for some positive constant C, which shows that $E(t) \leqslant e^{Ct}E_0$, where E_0 is a positive initial value for $E(t)$ and $t \in (0, T]$. Thus, $E(t)$ is bounded for any finite time, which is equivalent to the boundedness of $\|u\|_H$ and $\|u_t\|_H$. It follows that $\|Au\|_H$ is also bounded. Therefore, local solutions of (1.2.1) can be extended to global solutions.

Remark 2.2.4. *Theorem 2.1.23 shows that the solutions of (2.2.2) are continuously differentioble with respect to time. Furthermore, considering domain of operator A—$D(A)$ in (2.2.3)—along with the standard Sobolev embedding theorem—$W^{2,2}(\Omega_i)$ is embedded in $C^1(\Omega_i)$ for $i = 1, 2$—we can see that the solutions are also continuous in space. Then we can apply parabolic regularity [12] to conclude that the solutions of (2.2.2) are classical solutions on each interval.*

2.3 Positivity of solutions

In the last section of this chapter, we show that solutions to non-negative initial conditions are positive.

Lemma 2.3.1. *Any classical solution of (1.2.1)—or, equivalently, (2.2.2)—with non-negative initial conditions is positive on $(0, T]$.*

Proof: We suppose that u_1 and u_2 satisfy (1.2.1) for $t \in [0, T]$. We may assume that $f_i(u_i(x, t))$ for $i = 1, 2$ are positive. If not, we can choose $\gamma > 0$ large enough and

replace u_1 and u_2 with $\tilde{u}_1 = e^{\gamma t}u_1$, and $\tilde{u}_2 = e^{\gamma t}u_2$ such that $f_i(e^{-\gamma t}\tilde{u}_i(x,t)) + \gamma > 0$ for $i = 1, 2$. Then the new system is

$$\begin{cases} \tilde{u}_{1t} = D_1\tilde{u}_{1xx} + (f_1(e^{-\gamma t}\tilde{u}_1) + \gamma)\tilde{u}_1, & (x,t) \in \Omega_1 \times [0,T), \\ \tilde{u}_{2t} = D_2\tilde{u}_{2xx} + (f_2(e^{-\gamma t}\tilde{u}_2) + \gamma)\tilde{u}_2, & (x,t) \in \Omega_2 \times [0,T). \end{cases}$$

Thus, we can assume that $f_i(u_i)$, $i = 1, 2$, are positive.

Let $v_1(x,t) = u_1(x,t) + k\epsilon e^t$ and $v_2(x,t) = u_2(x,t) + \epsilon e^t$. Then the interface and boundary conditions in terms of $v(x,t)$ are: $D_1\dfrac{\partial v_1(0,t)}{\partial x} = D_2\dfrac{\partial v_2(0,t)}{\partial x}$, $v_1(0,t) = kv_2(0,t)$, $\dfrac{\partial v_1(-L_1,t)}{\partial x} = \dfrac{\partial v_2(L_2,t)}{\partial x} = 0$ and $v_i(x,0) > 0$, $i = 1, 2$. Moreover, v_1 and v_2 satisfy the first equation of (1.2.1) with strict inequalities. Thus, the functions v_i satisfy the following system of inequalities and interface and boundary conditions

$$\begin{cases} v_{1t} > D_1v_{1xx} + f(v_1)v_1, & (x,t) \in \Omega_1 \times [0,T), \\ v_{2t} > D_2v_{2xx} + f(v_2)v_2, & (x,t) \in \Omega_2 \times [0,T), \\ D_1v_{1x}(0,t) = D_2v_{2x}(0,t), & \\ v_1(0,t) = kv_2(0,t), v_{1x}(-L_1,t) = v_{2x}(L_2,t) = 0. & \end{cases}$$

We show that v_1 and v_2 are positive for $x \in [-L_1, L_2]$ and $t \in (0,T]$. Suppose that v_1 or v_2 is not positive for some $x \in [-L_1, L_2]$ and $t \leqslant T$. Let t_0 be the supremum of $\{t \mid v_1(x,t) > 0 \text{ for } -L_1 \leqslant x \leqslant 0, \text{ and } v_2(x,t) > 0 \text{ for } 0 \leqslant x \leqslant L_2\}$. Since v_1 and v_2 are positive for $t = 0$, we have $t_0 > 0$. For this t_0, there will be an $x_0 \in [-L_1, L_2]$ such that $v_1(x_0,t_0) = 0$ or $v_2(x_0,t_0) = 0$, whereas for $t \in (0,t_0]$ and $x \in [-L_1, L_2]$, we have $v_1, v_2 \geqslant 0$. We have the following cases:
1. If $x_0 \in (-L_1, 0)$, we have

$$v_{1t}(x_0,t_0) = \lim_{h\to 0}\frac{v_1(x_0,t_0+h) - v_1(x_0,t_0)}{h}.$$

Since $v_1(x_0,t_0) = 0$ and $v_1(x_0,t_0+h) \leqslant 0$ for some $h > 0$, we get $v_{1t}(x_0,t_0) \leqslant 0$. Also, since $v_1(x,t_0) > 0$ on $x \in [-L_1, 0] \setminus \{x_0\}$ and $v_1(x_0,t_0) = 0$, we get

$$v_{1x}(x_0^+,t_0) = \lim_{x\to x_0^+}\frac{v_1(x,t_0) - v_1(x_0,t_0)}{x - x_0} \geqslant 0,$$

and

$$v_{1x}(x_0^-,t_0) = \lim_{x\to x_0^-}\frac{v_1(x,t_0) - v_1(x_0,t_0)}{x - x_0} \leqslant 0.$$

Hence, we conclude that $v_{1xx}(x_0,t_0) \geqslant 0$, so that we have $v_{1t}(x_0,t_0) - D_1v_{1xx}(x_0,t_0) \leqslant 0$. On the other hand, by the definition of v_1, we get $v_{1t} - D_1v_{1xx} > f_1(v_1)v_1 \geqslant 0$.

Thus, we have a contradiction.
2. If $x_0 \in (0, L_2)$, then the same argument can be used to get a contradiction.
3. If $x_0 = 0$, then $v_1(0, t_0) = kv_2(0, t_0) = 0$. By assumption, v_1 and v_2 are non-negative for $t \in (0, t_0]$ and $x \in [-L_1, L_2] \setminus \{0\}$. Hence, $D_1 v_{1x}(0, t_0) \leqslant 0$ and $D_2 v_{2x}(0, t_0) \geqslant 0$ by the definition of the derivative. But because $D_1 v_{1x}(0, t_0) = D_2 v_{2x}(0, t_0)$, we must have $v_{1x}(0, t_0) = v_{2x}(0, t_0) = 0$. The strong maximum principle and Theorem 2.1.12 imply that if there is an interval $(-\delta, 0)$ with $v_1(x, t_0) > 0$, then $D_1 v_{1x}(0, t_0) < 0$. Also, if there exists an interval $(0, \delta)$ with $v_2(x, t_0) > 0$, then $-D_2 v_{2x}(0, t_0) < 0$. Thus, we get a contradiction. Hence, we must have $v_1(x, t_0) = 0$ somewhere in $(-L_1, 0)$ and $v_2(x, t_0) = 0$ somewhere in $(0, L_2)$. Thus, $v_1, v_2 \equiv 0$ for $t \in (0, t_0]$ and $x \in [-L_1, L_2]$, which is a contradiction to our assumption $v_i(x, t)>0$.
4. If $x_0 = -L_1$, then $v_1(-L_1, t_0) = 0$. We have

$$v_{1x}(-L_1, t_0) = \lim_{x \to -L_1} \frac{v_1(x, t_0) - v_1(-L_1, t_0)}{x + L_1},$$

which shows that $v_{1x}(-L_1, t_0) \geqslant 0$. By the boundary condition, we have $v_{1x}(-L_1, t) = 0$ for $0 < t < T$. Thus, $v_{1x}(-L_1, t_0)$ must be zero. Then, by the same argument as in Case 3, using the strong maximum principle and Theorem 2.1.12, we have $v_1(x, t) = 0$ somewhere in $(-L_1, 0)$ for $t \in (0, t_0]$, which is a contradiction.
5. If $x_0 = L_2$, we obtain a contradiction by an analogous argument.

As a result, we must have $v_1, v_2 > 0$ on $[-L_1, L_2] \times (0, T]$. Since $\epsilon > 0$ is arbitrary, we get $u_1 \geqslant 0, u_2 \geqslant 0$. Moreover, if u_i for $i = 1, 2$, are not identically zero and $u_1(x, t_0) = 0$ somewhere in $[-L_1, 0]$, and $u_2(x, t_0) = 0$ somewhere in $[0, L_2]$ for some $t_0 > 0$, then the same arguments based on the strong maximum principle and Theorem 2.1.12 imply that $u_1 = u_2 = 0$ for $0 < t \leqslant t_0$, which is a contradiction. Thus, $u_i > 0$, $i = 1, 2$ for $t > 0$. ∎

Chapter 3

The effect of movement behaviour on population density in patchy landscapes

Many biological populations reside in increasingly fragmented landscapes, where habitat quality may change abruptly in space. Individuals adjust their movement behaviour to local habitat quality and show preferences for some habitat types over others. Several recent publications explore how such individual movement behaviour affects population-level dynamics in a framework of reaction-diffusion systems that are coupled through discontinuous boundary conditions. While most of those works are based on linear analysis [2, 38, 44, 46, 47], we study positive steady states of the nonlinear equations. We prove the existence, uniqueness and global stability of steady states, and we classify their qualitative shapes depending on movement behaviour. We apply our results to study the question of why and under which conditions the total population abundance at steady state may exceed the total carrying capacity of the landscape.

We begin this chapter with a detailed description of the biological and mathematical background and a precise statement of the questions that we will answer. The proof of existence and uniqueness of a positive steady state, as well as its global stability, is given in Section 3.2. Illustrations of our results, the classification of steady-state profiles and the relation between the total steady-state density and the total carrying capacity are given in Section 3.3. Most content in this chapter is in Zaker et al. [76], but we give more details here.

3.1 Introduction and model presentation

The study of spatial population dynamics relates to some of the most fundamental questions in theoretical ecology: Why are individuals where they are? How does landscape structure affect population distribution in space? What effect does movement in response to habitat variation have on population density? These questions are of increasing importance as natural events and human activities create increasingly fragmented landscapes in which some biological populations may thrive, while others struggle to survive.

Reaction-diffusion equations are a common and highly versatile tool to study such questions [13]. One fairly basic model for the density $u(x,t)$ of a species at location x and time t is the diffusive logistic equation

$$\frac{\partial u}{\partial t} = D\frac{\partial^2 u}{\partial x^2} + r(x)u\left(1 - \frac{u}{K(x)}\right). \tag{3.1.1}$$

Here, the diffusion coefficient D measures the mean-squared displacement of organisms under random motion, r is the low-density growth rate, and K denotes the local carrying capacity. In the non-spatial version of (3.1.1), which we discussed in Chapter 1, the steady state, u^*, is equal to the carrying capacity. With spatially constant parameters, this equation is widely used in applications [4]. For heterogeneous landscapes, large amounts of data are required to estimate the spatially varying parameter functions $r(\cdot)$ and $K(\cdot)$. In addition, when landscape quality varies in space, the assumption of a spatially constant random diffusion process is unrealistic. Most organisms adapt their movement to habitat quality and show bias towards better habitats [18, 46]. Spatially varying movement behaviour can be included in (3.1.1) in a number of different ways, such as a Fickian diffusion term $\partial_x(D(x)\partial_x u)$ or an "ecological" diffusion term $\partial_x^2(D(x)u)$ [68]. The two cases show different behaviour in simulations, but analytical results remain relatively abstract (e.g., existence of solutions, monotonicity).

A closely related but somewhat different approach to population dynamics in spatially varying landscapes is to consider landscapes that consist of "patches": regions in space that are homogeneous within but different from their neighbouring patches. One then formulates a reaction-diffusion equation with constant coefficients on each patch and connects the equations for adjacent patches by matching conditions for the density and flux. This modelling approach was pioneered by Pacala and Roughgarden [56] for two patches and by Shigesada et al. [65] for infinite landscapes, and continued by Freedman et al. [26], Cruywagen et al. [19], Lutscher et al. [43] and others. A major improvement on these earlier models occurred when Maciel and Lutscher in [46] introduced novel interface-matching conditions, based on the work by Ovaskainen and Cornell [55]. These matching conditions not only allow us to include patch-preference

data, which are frequently collected in the field, into reaction-diffusion models, they also remove some biologically unrealistic behaviour that the early models showed [46]. A number of recent studies use this new framework to study questions of persistence and spread [3, 47] and apply it to marine-reserve design [2, 38]. However, most of their results are based on either linear analysis or numerical simulation (but see Maciel et al. [45]).

In this chapter, we study the various aspects of a positive steady state of the nonlinear equations. More specifically, we prove the existence, uniqueness and global stability of such a state, and we classify the possible qualitative behaviours of this state, depending on model parameters. We also apply our results to the question of whether and how the total population abundance at steady state could exceed the total carrying capacity of a landscape, depending on movement behaviour. This latter question has puzzled theoretical ecologists since the discovery of the phenomenon by Freedman and Waltman [27]; see Zhang et al. [77] and Guo et al. [32] recent reviews on the subject. While the original discovery emerged in a spatially implicit patch model, formulated as ordinary differential equations, the phenomenon can also be observed in the spatially explicit reaction-diffusion model (3.1.1). Here, we want to compare the total density, $\int u^*(x)\mathrm{d}x$, to the total carrying capacity over the domain. Lou in his paper [41] proved that

$$\int_\Omega [u^*(x) - K(x)]\mathrm{d}x > 0, \tag{3.1.2}$$

for all $D > 0$, in the special case of nonconstant functions $r(x) = K(x)$. DeAngelis et al. [20] extended this result by showing that the same inequality holds when $r(\cdot)$ and $K(\cdot)$ are positively correlated and D is small. Such a result is surprising at first, because it says that the "carrying capacity" is not necessarily the upper limit of the population density on a landscape. The details of these results are given in Section 3.4. It is also relevant when studying competition of two species and the question of (mutual) invasion of one by the other. We will obtain some sufficient conditions for when the corresponding inequality holds in our patch model, and we will show that in certain limiting cases, these conditions are also necessary. However, we will also show that certain types of movement behaviour will ensure that the corresponding inequality cannot hold.

We consider the simplest scenario of a patchy one-dimensional landscape, consisting of two adjacent patches that are homogeneous within but differ from one another. We denote these patches by $\Omega_1 = [-L_1, 0]$ and $\Omega_2 = [0, L_2]$, respectively, and the population density on Patch i by $u_i(x, t)$. We refer to the point $x = 0$ where the two patches meet as the interface and to $x = -L_1$ and $x = L_2$ as the boundary of our landscape. On each patch, individual movement and population dynamics are described by a reaction-diffusion equation. These equations for the densities on Patch i are given in (1.1.13); see also (3.1.8) below. In this chapter, we write $F_i(u_i) = u_i f_i(u_i)$,

where we generally assume that the per capita growth functions $f_i \in C^2[0,\infty)$ satisfy the conditions (see, e.g., Freedman [25])

$$f_i(0) > 0,\ f_i'(u_i) < 0,\ \text{there exist } K_i > 0 \text{ such that } f_i(K_i) = 0. \tag{3.1.3}$$

In biological terms, the per capita growth rate decreases with population density because of intraspecific competition. The maximum per capita growth rate $r_i = f_i(0)$ occurs at low density. This assumption excludes Allee effect, where the maximum per capita growth rate occurs at intermediate density [17]. Parameter K_i denotes the carrying capacity of Patch i. In this chapter, for all explicit calculations and simulations, we use the logistic growth function (1.1.14), where $f_i(u_i)$ has the form

$$f_i(u_i) = r_i\left(1 - \frac{u_i}{K_i}\right). \tag{3.1.4}$$

In our model, we assume that no individuals cross the boundaries of the two-patch landscape. Hence, we impose Neumann (no-flux) boundary conditions at $x = -L_1$ and $x = L_2$; i.e.,

$$\frac{\partial u_1(-L_1,t)}{\partial x} = \frac{\partial u_2(L_2,t)}{\partial x} = 0, \quad t \geqslant 0. \tag{3.1.5}$$

With these conditions, our system can also be viewed as half a period of an infinite periodic landscape with alternating patches of lengths $2L_1$ and $2L_2$, respectively [45].

At the interface between patches—i.e., at $x = 0$—we impose the matching conditions for the population density

$$u_1(0,t) = ku_2(0,t), \qquad k = \frac{p_1}{p_2}\frac{D_2}{D_1}, \qquad t \geqslant 0, \tag{3.1.6}$$

and the flux

$$D_1\frac{\partial u_1(0,t)}{\partial x} = D_2\frac{\partial u_2(0,t)}{\partial x}, \qquad t \geqslant 0. \tag{3.1.7}$$

See Chapter 1 for more details.
Putting all the ingredients together, we have the following system of equations:

$$\begin{cases} \dfrac{\partial u_i(x,t)}{\partial t} = D_i\dfrac{\partial^2 u_i(x,t)}{\partial x^2} + u_i(x,t)f_i\left(u_i(x,t)\right), & (x,t) \in \Omega_i \times [0,\infty), \\ D_1\dfrac{\partial u_1(0,t)}{\partial x} = D_2\dfrac{\partial u_2(0,t)}{\partial x}, & t \geqslant 0, \\ u_1(0,t) = ku_2(0,t), & t \geqslant 0, \\ \dfrac{\partial u_1(-L_1,t)}{\partial x} = \dfrac{\partial u_2(L_2,t)}{\partial x} = 0, & t \geqslant 0. \end{cases} \tag{3.1.8}$$

Uniqueness and global existence of solutions of this time-dependent problem were proved in Chapter 2. In this chapter, we focus on the steady-state problem of equations (3.1.8). Denoting the steady state densities by $u_i = u_i(x)$, the defining equations are

$$\begin{cases} D_i \dfrac{\mathrm{d}^2 u_i(x)}{\mathrm{d}x^2} + u_i(x) f_i\left(u_i(x)\right) = 0, \quad i = 1, 2, \quad x \in \Omega_i, \\ D_1 \dfrac{\mathrm{d}u_1(0)}{\mathrm{d}x} = D_2 \dfrac{\mathrm{d}u_2(0)}{\mathrm{d}x}, \\ u_1(0) = k u_2(0), \\ \dfrac{\mathrm{d}u_1(-L_1)}{\mathrm{d}x} = \dfrac{\mathrm{d}u_2(L_2)}{\mathrm{d}x} = 0. \end{cases} \tag{3.1.9}$$

In the next section, we prove the uniqueness, existence, and global stability of the steady state.

3.2 Existence and global stability of a positive steady state

In this section, we first rescale our model and use some ideas from Freedman et al. [26] to prove existence and uniqueness of a positive solution of the steady-state problem (3.1.9). Then we prove that this positive solution is globally asymptotically stable, using monotonicity properties of the system. Finally, we classify the possible qualitative shapes of the positive steady-state solutions.

3.2.1 Scaling and continuous solutions

Freedman et al. [26] considered a steady-state problem of population dynamics on two adjacent patches, similar to our problem. Their model differed from ours in that they assumed continuity at the interface and a different set of boundary conditions. In order to apply their ideas, we first scale our model to obtain continuous interface conditions.

By following the idea of scaling in Maciel and Lutscher [47], we define new

variables for the time-dependent problem as

$$\begin{cases} v_1(\xi,t) = u_1(x,t), \quad \xi = x \in \widetilde{\Omega}_1 := [-L_1, 0]\,, \\ \\ v_2(\xi,t) = k u_2(x,t), \quad \xi = \frac{x}{k} \in \widetilde{\Omega}_2 := [0, \frac{L_2}{k}]. \end{cases} \tag{3.2.1}$$

In this new scaling, system (3.1.8) takes the form

$$\begin{cases} \dfrac{\partial v_1(\xi,t)}{\partial t} = \widetilde{D}_1 \dfrac{\partial^2 v_1(\xi,t)}{\partial \xi^2} + v_1(\xi,t)\widetilde{f}_1(v_1(\xi,t)), & \text{on } \widetilde{\Omega}_1 \times [0,\infty), \\ \\ \dfrac{\partial v_2(\xi,t)}{\partial t} = \widetilde{D}_2 \dfrac{\partial^2 v_2(\xi,t)}{\partial \xi^2} + v_2(\xi,t)\widetilde{f}_2(v_2(\xi,t)), & \text{on } \widetilde{\Omega}_2 \times [0,\infty), \\ \\ \widetilde{D}_1 \dfrac{\partial v_1(0,t)}{\partial \xi} = \widetilde{D}_2 \dfrac{\partial v_2(0,t)}{\partial \xi}\ , & t \geqslant 0, \\ \\ \dfrac{\partial v_1\left(-L_1,t\right)}{\partial \xi} = \dfrac{\partial v_2\left(L_2/k,t\right)}{\partial \xi} = 0\ , & t \geqslant 0, \\ \\ v_1(0,t) = v_2(0,t), & t \geqslant 0, \end{cases} \tag{3.2.2}$$

where $\widetilde{D}_1 = D_1$, $\widetilde{D}_2 = \dfrac{D_2}{k^2}$, $\widetilde{f}_1(v_1) = f_1(v_1)$, and $\widetilde{f}_2(v_2) = f_2(v_2/k)$. In this scaling, we have continuity of density and flux at the interface.

We denote $\tilde{L}_2 = \dfrac{L_2}{k}$, $\widetilde{K}_1 = K_1$ and $\widetilde{K}_2 = kK_2$. For simplicity of notation, we drop the ˜ from here on and revert to the original variable name $\xi = x$. As a result, we rewrite the above system as

$$\begin{cases} \dfrac{\partial v_1(x,t)}{\partial t} = D_1 \dfrac{\partial^2 v_1(x,t)}{\partial x^2} + v_1(x,t) f_1(v_1(x,t)), & \text{on } \Omega_1 \times [0,\infty), \\ \\ \dfrac{\partial v_2(x,t)}{\partial t} = D_2 \dfrac{\partial^2 v_2(x,t)}{\partial x^2} + v_2(x,t) f_2(v_2(x,t)), & \text{on } \Omega_2 \times [0,\infty), \\ \\ D_1 \dfrac{\partial v_1(0,t)}{\partial x} = D_2 \dfrac{\partial v_2(0,t)}{\partial x}\ , & t \geqslant 0, \\ \\ \dfrac{\partial v_1\left(-L_1,t\right)}{\partial x} = \dfrac{\partial v_2\left(L_2,t\right)}{\partial x} = 0\ , & t \geqslant 0, \\ \\ v_1(0,t) = v_2(0,t), & t \geqslant 0. \end{cases} \tag{3.2.3}$$

3.2.2 Existence and uniqueness of the positive steady state

In the rescaled variables, system (3.1.9) assumes the time-independent form:

$$\begin{cases} D_1 \dfrac{\mathrm{d}^2 v_1(x)}{\mathrm{d}x^2} + v_1(x) f_1(v_1(x)) = 0, & \text{on } \Omega_1 = [-L_1, 0], \\ D_2 \dfrac{\mathrm{d}^2 v_2(x)}{\mathrm{d}x^2} + v_2(x) f_2(v_2(x)) = 0, & \text{on } \Omega_2 = [0, L_2], \\ D_1 \dfrac{\mathrm{d}v_1(0)}{\mathrm{d}x} = D_2 \dfrac{\mathrm{d}v_2(0)}{\mathrm{d}x}, \quad v_1(0) = v_2(0), \\ \dfrac{\mathrm{d}v_1(-L_1)}{\mathrm{d}x} = 0, \quad \dfrac{\mathrm{d}v_2(L_2)}{\mathrm{d}x} = 0, \end{cases} \tag{3.2.4}$$

which is, of course, the steady-state problem of the rescaled dynamic system (3.2.3).

We note that if $K_2 = K_1$, the function $v_1(x) = v_2(x) = K_1$ is a solution of (3.2.4). The challenge is to find a solution when $K_1 \neq K_2$. Without loss of generality, we assume that $K_2 > K_1$. Our main result in this section is the following.

Theorem 3.2.1. *There exists a unique positive solution of system (3.2.4). This solution is monotone on each Ω_i.*

We begin the proof of this theorem with some general considerations. If we suppose that $0 < v_1(-L_1) \leq K_1 < K_2$, then, by the maximum principle, we necessarily have $v_1'(0) \leq 0$. By continuity, we then find $v_2(0) < K_2$ and $v_2'(0) \leq 0$. By the maximum principle again, this implies that $v_2'(L_2) < 0$ so that the boundary conditions cannot be met. Hence, we must have $v_1(-L_1) > K_1$. The same reasoning applies to show that $v_2(L_2) < K_2$. We now construct our desired solution such that $K_1 < v_1(-L_1) < v_2(L_2) < K_2$. We split the construction into several smaller steps that follow the ideas in Freedman et al. [26].

We define $q_1(x, \alpha_1)$, $x \in \Omega_1$ and $\alpha_1 > 0$ to be the unique solution of the first equation of (3.2.4) such that

$$\frac{\partial q_1(-L_1, \alpha_1)}{\partial x} = 0, \quad q_1(-L_1, \alpha_1) = \alpha_1 \tag{3.2.5}$$

and define $q_2(x, \alpha_2)$, $x \in \Omega_2$ and $\alpha_2 > 0$ the unique solution of the second equation of (3.2.4) such that

$$\frac{\partial q_2(L_2, \alpha_2)}{\partial x} = 0, \quad q_2(L_2, \alpha_2) = \alpha_2. \tag{3.2.6}$$

Existence and uniqueness of q_i is guaranteed by the general existence and uniqueness theorem for ordinary differential equations; see e.g., Perko [59].

If we can show that there exist unique α_1, α_2 such that

$$\begin{cases} q_1(0,\alpha_1) = q_2(0,\alpha_2), \\ D_1 \dfrac{\partial q_1(0,\alpha_1)}{\partial x} = D_2 \dfrac{\partial q_2(0,\alpha_2)}{\partial x}, \end{cases}$$

then we have shown the existence and uniqueness of a positive solution of model (3.2.4). The following three lemmas are key to achieve this goal.

Lemma 3.2.2. *If $\alpha_1 > K_1$ then*

$$\frac{\partial q_1(x,\alpha_1)}{\partial x} > 0, \qquad \text{on} \qquad -L_1 < x \leqslant 0.$$

Proof: Based on (3.2.5) and the assumption of this lemma, we have $q_1(-L_1,\alpha_1) = \alpha_1 > K_1$. By continuity, we can assume that there exists a small enough value $\varepsilon > 0$ such that $q_1(x,\alpha_1) > K_1$ on the interval $[-L_1, -L_1+\varepsilon)$. From the first equation of system (3.2.4), we see that $\dfrac{\partial^2 q_1(x,\alpha_1)}{\partial x^2} > 0$, so we conclude $\dfrac{\partial q_1(x,\alpha_1)}{\partial x} > \dfrac{\partial q_1(-L_1,\alpha_1)}{\partial x}$ on this interval. On the other hand, by (3.2.5) we have $\dfrac{\partial q_1(-L_1,\alpha_1)}{\partial x} = 0$. Thus, $\dfrac{\partial q_1(x,\alpha_1)}{\partial x} > 0$, which shows that $q_1(x,\alpha_1)$ is an increasing function on the interval $[-L_1, -L_1+\varepsilon)$.

If $q_1(x,\alpha_1)$ is not increasing everywhere in $[-L_1, 0]$, we can find a point $\bar{x}$, such that $\dfrac{\partial q_1(\bar{x},\alpha_1)}{\partial x} = 0$. By construction, q_1 satisfies the first equation in (3.2.4). We multiply this equation by $\mathrm{d}q_1/\mathrm{d}x$ and integrate from $-L_1$ to x. We obtain

$$\left(\frac{\partial q_1(x,\alpha_1)}{\partial x}\right)^2 = -\frac{2}{D_1}\int_{\alpha_1}^{q_1(x,\alpha_1)} \zeta f_1(\zeta)\mathrm{d}\zeta. \tag{3.2.7}$$

If we evaluate this expression at $\bar{x}$, then the left-hand side is zero, while the right-hand side is positive since $\zeta > \alpha_1$. Thus, we get a contradiction. ∎

Lemma 3.2.3. *If $\alpha_2 < K_2$ then*

$$\frac{\partial q_2(x,\alpha_2)}{\partial x} > 0, \qquad \text{on} \qquad 0 \leqslant x < L_2.$$

Proof: The idea of this proof is the same as that of the proof of Lemma 3.2.2. ∎

Lemma 3.2.4. *Define $H_i(\alpha) := q_i(0,\alpha)$, $i = 1, 2$. Then there exist $\hat{\alpha}_i$ such that*

$$H_1 : [K_1, \hat{\alpha}_1] \to [K_1, K_2] \qquad \text{and} \qquad H_2 : [\hat{\alpha}_2, K_2] \to [K_1, K_2]\,.$$

Furthermore, H_i are monotone functions. In particular, for every $\alpha_1 \in [K_1, \hat{\alpha}_1]$, there exists a unique $\alpha_2 \in [\hat{\alpha}_2, K_2]$ such that $q_1(0,\alpha_1) = q_2(0,\alpha_2)$.

Proof: We know that H_i are continuous. We start by showing that they are also monotone. It is enough to show that H_1 is monotone; the case for H_2 is similar. Suppose that $\tilde{\alpha} > \alpha > K_1$. We want to show that $H_1(\tilde{\alpha}) > H_1(\alpha) > K_1$. We know that $q_1(x,\alpha)$ is monotone increasing in x for $\alpha > K_1$; hence, $H_1(\alpha) > \alpha$ for all $\alpha > K_1$. By the definition of $q_1(x,\alpha)$, we have $q_1(-L_1,\tilde{\alpha}) = \tilde{\alpha} > \alpha = q_1(-L_1,\alpha) > K_1$. Hence, there is some interval $[-L_1, -L_1+\epsilon]$ such that $q_1(x,\tilde{\alpha}) > q_1(x,\alpha) > K_1$ on this interval. From the definition of q_1, we then have $q_1''(x,\tilde{\alpha}) > q_1''(x,\alpha) > 0$ on this interval. Since $q_1'(-L_1,\tilde{\alpha}) = q_1'(-L_1,\alpha) = 0$, we also have that $q_1'(x,\tilde{\alpha}) > q_1'(x,\alpha)$ on $[-L_1, -L_1+\epsilon]$. This then implies that $q_1(-L_1+\epsilon,\tilde{\alpha}) > q_1(-L_1+\epsilon,\alpha)$. We can continue this process. As long as $q_1(x,\tilde{\alpha}) > q_1(x,\alpha)$, we have $q_1'(x,\tilde{\alpha}) > q_1'(x,\alpha)$. Now suppose that there is a point $\tilde{x} \in (-L_1, 0]$ such that $q_1(\tilde{x},\tilde{\alpha}) = q_1(\tilde{x},\alpha)$. Then for the smallest such point, we must have $q_1'(\tilde{x},\tilde{\alpha}) \le q_1'(\tilde{x},\alpha)$. But this is impossible, by the preceding argument. Hence $q_1(x,\tilde{\alpha}) > q_1(x,\alpha)$ in $[-L_1, 0]$; in particular, $H_1(\tilde{\alpha}) > H_1(\alpha) > K_1$ as claimed.

Since $q_1(x,K_1) \equiv K_1$ is the constant solution, we have $H_1(K_1) = K_1$. Since $H_1(\alpha) > \alpha$ for $\alpha > K_1$, we have $H_1(K_2) > K_2$. By continuity and monotonicity, there exists a unique $\hat{\alpha}_1 \in [K_1, K_2]$ such that $H_1(\hat{\alpha}_1) = K_2$. Similarly, $H_2(K_2) = K_2$, and there exists a unique $\hat{\alpha}_2 \in [K_1, K_2]$ such that $H_2(\hat{\alpha}_2) = K_1$. By continuity and monotonicity, for each $\alpha_1 \in [K_1, \hat{\alpha}_1]$, there exists some $\alpha_2 \in [\hat{\alpha}_2, K_2]$ such that $H_1(\alpha_1) = H_2(\alpha_2)$. ∎

Now we prove Theorem 3.2.1, which is our first main result of this section.

Proof: By Lemma 3.2.4, for each $\alpha_2 \in [\hat{\alpha}_2, K_2]$, we can find $\alpha_1 \in [K_1, \hat{\alpha}_1]$ such that $q_1(0,\alpha_1) = q_2(0,\alpha_2)$. Hence, for each α_2, we have a continuous solution of (3.2.4). We write $\alpha_1 = h(\alpha_2)$. Based on the definition of $\hat{\alpha}_1$, $\hat{\alpha}_2$, we see that $h(K_2) = \hat{\alpha}_1$ and $h(\hat{\alpha}_2) = K_1$.

We now define

$$J(\alpha_2) \coloneqq D_1 \frac{\partial q_1(0, h(\alpha_2))}{\partial x} - D_2 \frac{\partial q_2(0,\alpha_2)}{\partial x}. \tag{3.2.8}$$

Then, for $\alpha_2 = \hat{\alpha}_2$ and $\alpha_2 = K_2$, we have the following expressions

$$J(\hat{\alpha}_2) = D_1 \frac{\partial q_1(0, h(\hat{\alpha}_2))}{\partial x} - D_2 \frac{\partial q_2(0, \hat{\alpha}_2)}{\partial x} \tag{3.2.9}$$

and

$$J(K_2) = D_1 \frac{\partial q_1(0, h(K_2))}{\partial x} - D_2 \frac{\partial q_2(0, K_2)}{\partial x}. \tag{3.2.10}$$

Since we have $q_1(x, h(\hat{\alpha}_2)) = q_1(x, K_1) = K_1$ and $q_2(x, K_2) = K_2$, which are constant, we can conclude that $\dfrac{\partial q_1(0, h(\hat{\alpha}_2))}{\partial x} = \dfrac{\partial q_2(0, K_2)}{\partial x} = 0$. Therefore, we have

$$J(\hat{\alpha}_2) = -D_2 \frac{\partial q_2(0, \hat{\alpha}_2)}{\partial x} < 0 \quad \text{and} \quad J(K_2) = D_1 \frac{\partial q_1(0, \hat{\alpha}_1)}{\partial x} > 0. \tag{3.2.11}$$

Hence, by applying the intermediate value theorem, there exists $\alpha_2 \in (\hat{\alpha}_2, K_2)$, such that $J(\alpha_2) = 0$. Moreover, by Lemmas 3.2.2–3.2.4 and continuity at the interface, we can conclude that any unique positive solution that we construct must be monotonic. ∎

Freedman et al. proved that the steady state of (3.2.4) is locally asymptotically stable under the sufficient condition that $\frac{d}{dv_2}(v_2 f(v_2)) < 0$ for $K_1 \leq v_2 \leq K_2$ [26]. This condition is too strong for many of the cases that we are interested in. We prove that the steady state of (3.2.4) is globally asymptotically stable under weaker conditions. Therefore, we prove the much stronger result that the positive steady state is unconditionally stable. This is the second main result of this section.

Theorem 3.2.5. *The positive steady-state solution of (3.2.3) is globally asymptotically stable.*

Proof: The proof is an adaptation of the proof of Proposition 3.2 in [13]. In Chapter 2, we showed the existence and uniqueness of solutions of (3.2.3). Maciel et al. showed that the equation possesses a comparison principle [45], which means that if we have two solutions with ordered initial conditions, then the solutions remain ordered. We proceed by finding a supersolution and a subsolution. We pick any constant $\tilde{K} > K_2$. Then the constant function $(\bar{K}, \bar{K})$ satisfies the interface and boundary conditions of system (3.2.3) and is a supersolution of the steady-state problem (3.2.4). If $\bar{v}(x,t)$ is the solution of (3.2.3), with $\bar{v}(x,0) = (\bar{K}, \bar{K})$, then $\bar{v}_t \mid_{t=0} < 0$ on $\Omega = \Omega_1 \cup \Omega_2$. Standard arguments of subsolution and supersolutions, together with monotonicity and regularity estimates, then imply that $\bar{v}(x,t)$ is decreasing in t and, since it is also bounded below, converging to a steady state.

To find a subsolution, we consider the linearization of (3.2.3) at $v = 0$. The eigenvalue problem for the linearized system (3.2.3) is given by

$$\begin{cases} \left(D_i \dfrac{\mathrm{d}^2}{\mathrm{d}x^2} + f_i(0)\right)\psi_i = \sigma\psi_i, & x \in \Omega_i, \\ \psi_1(0) = \psi_2(0), \quad D_1 \dfrac{\mathrm{d}\psi_1(0)}{\mathrm{d}x} = D_2 \dfrac{\mathrm{d}\psi_2(0)}{\mathrm{d}x}, \\ \dfrac{\mathrm{d}\psi_1(-L_1)}{\mathrm{d}x} = 0 = \dfrac{\mathrm{d}\psi_2(L_2)}{\mathrm{d}x}. \end{cases} \tag{3.2.12}$$

Maciel et al. [45] showed that this equation possesses a positive dominant eigenvalue, σ_0, with positive eigenfunction $\psi_0 = (\psi_{01}, \psi_{02})$. We construct a subsolution as an appropriate multiple of the eigenfunction. By the smoothness assumptions, we can write $v_i f_i(v_i) = v_i[f_i(0) + g_i(v_i)v_i]$, so that g_i is a C^1 function in v_i.

For $\epsilon > 0$ sufficiently small, we have

$$\begin{aligned} \left(D_1 \frac{\mathrm{d}^2}{\mathrm{d}x^2} + f_1(0) + g_1(\epsilon\psi_{01})\epsilon\psi_{01}\right)\epsilon\psi_{01} &= \epsilon\left(D_1 \frac{\mathrm{d}^2\psi_{01}}{\mathrm{d}x^2} + f_1(0)\psi_{01}\right) + \epsilon^2 g_1(\epsilon\psi_{01})\psi_{01}^2 \\ &= \epsilon\psi_{01}[\sigma_0 + \epsilon g_1(\epsilon\psi_{01})\psi_{01}] > 0. \end{aligned}$$

The same calculation applies on Ω_2.

Now we proceed as above. If $\underline{v}(x,t)$ is a solution of (3.2.3) with $\underline{v}(x,0) = \epsilon\psi_0 = \epsilon(\psi_{01}, \psi_{02})$, then $\underline{v}_t \mid_{t=0} > 0$ on $\Omega = \Omega_1 \cup \Omega_2$. Standard arguments of subsolution and supersolutions, together with monotonicity and regularity estimates, then imply that $\underline{v}(x,t)$ is increasing in t and, since it is also bounded above by (K_2, K_2) if ϵ is small enough, converging upwards to the minimal positive steady state. Since we showed above that the positive steady state is unique, $\underline{v}$ and $\bar{v}$ have to converge to the same steady state.

If v is the solution to any bounded, nonnegative, nonzero initial condition v_0, the maximum principle implies that there is a time t_0 such that $v(t_0) > 0$ on Ω. Hence, we can choose $\epsilon > 0$ small enough such that $\epsilon\psi_0 < v(t_0)$. Then, by the comparison principle, $v(t)$ has to also converge to that steady state. Hence, the unique positive steady state is globally stable among all nonnegative nonzero bounded solutions. ∎

3.3 Classifying the shapes of the positive steady state

We illustrate how the value of the composite parameter

$$k = \frac{p_1}{1-p_1}\frac{D_2}{D_1} \tag{3.3.1}$$

affects the steady state of the system. We choose patch preference (p_1) as our parameter of interest here. We discuss the influence of the diffusion rates in a different context in the next section.

For reference, we summarize the results from Section 3.2.2. To avoid confusion, we will use the notation from (3.2.2) with tildes. According to Theorem 3.2.1, there are three possible shapes of the positive steady-state solution.

a) If $\widetilde{K}_1 = \widetilde{K}_2$, then the solution is constant in space.

b) If $\widetilde{K}_1 < \widetilde{K}_2$, then the solution is increasing with $v_1 > \widetilde{K}_1$ and $v_2 < \widetilde{K}_2$.

c) If $\widetilde{K}_1 > \widetilde{K}_2$, then the solution is decreasing with $v_1 < \widetilde{K}_1$ and $v_2 > \widetilde{K}_2$.

A direct translation of these properties to the unscaled steady-state problem (3.1.9) gives the following possible shapes.

Lemma 3.3.1. *The positive solution of (3.1.9) has exactly one of the following shapes.*

a′) *If $K_1 = kK_2$, then the solution is constant on each patch.*

b′) *If $K_1 < kK_2$, then the solution is increasing on each patch with $u_1 > K_1$ and $u_2 < K_2$.*

c′) *If $K_1 > kK_2$, then the solution is decreasing on each patch with $u_1 < K_1$ and $u_2 > K_2$.*

Solutions of the unscaled model are not continuous at the interface, unless $k = 1$. Even if a solution is monotone on each patch, the jump at the interface may be in the "opposite" direction so that the solution may not be monotone over the entire landscape. We illustrate how the value of k affects the steady-state solution in general and the jump at the interface in particular. We fix all parameters, except for p_1, and choose $K_2 > K_1$, without loss of generality. As we decrease p_1, k also decreases. According to the three cases above, we find three cases for the value of k; see Figure 3.1. When $k > 1$, the solution is monotone increasing in each patch but jumps

down at the interface; see Figure 3.2(a). As k decreases, the jump at the interface decreases until the solution becomes continuous at $k = 1$; see Figure 3.2(b). As long as $k > K_1/K_2$, the solution remains increasing in each patch. Since the jump is now up, the solution is monotone on the entire landscape; see Figure 3.2(c). When $k = K_1/K_2$, the solution is piecewise constant, equal to the carrying capacity in each patch; see Figure 3.2(d). When $k < K_1/K_2$ the jump at the interface is larger than the jump in the carrying capacities. In this case, the solution is decreasing on each patch. Since the jump at the interface is up, the solution is not globally decreasing. In fact, the solution now exceeds the larger of the two carrying capacities; see Figure 3.2(e). Finally, we briefly illustrate the case where $K_1 = K_2$. In this case, we have $k > 1$ exactly when $k > K_1/K_2$, so that the three cases in Figure 3.1 collapse to only two. When $k > 1$, the solution is increasing in each patch and the jump is down, so that the solution is not globally monotone. Necessarily, the solution exceeds the maximum of the carrying capacity; see Figure 3.2(f).

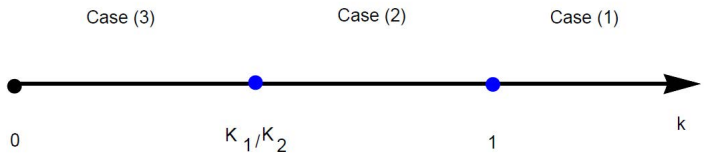

Figure 3.1: Three different cases for the parameter of discontinuity at the interface, k, where $K_2 > K_1$.

From a biological point of view, we see that when individuals have a high preference for Patch 1, they will pour into Patch 1 and thereby increase the steady-state density in Patch 1 near the interface above its carrying capacity. In fact, the density on the entire patch will then be above its carrying capacity. At the same time, individuals leave Patch 2, so that the density in that patch is decreased at the interface and therefore also in the entire patch. When the preference for Patch 1 is low, the situation is reversed.

To find the steady-state solutions, we should solve the boundary-value problem (3.2.4). However, we solved the time-dependent parabolic boundary problem until the solution reaches the steady state. We solved this time-dependent problem by the fully explicit finite scheme, the forward-time central-space scheme [67] and the plots in Figure 3.2 (and subsequent similar plots) were obtained by Matlab. Theorem 3.2.1 guarantees that the solution converges to the positive steady state.

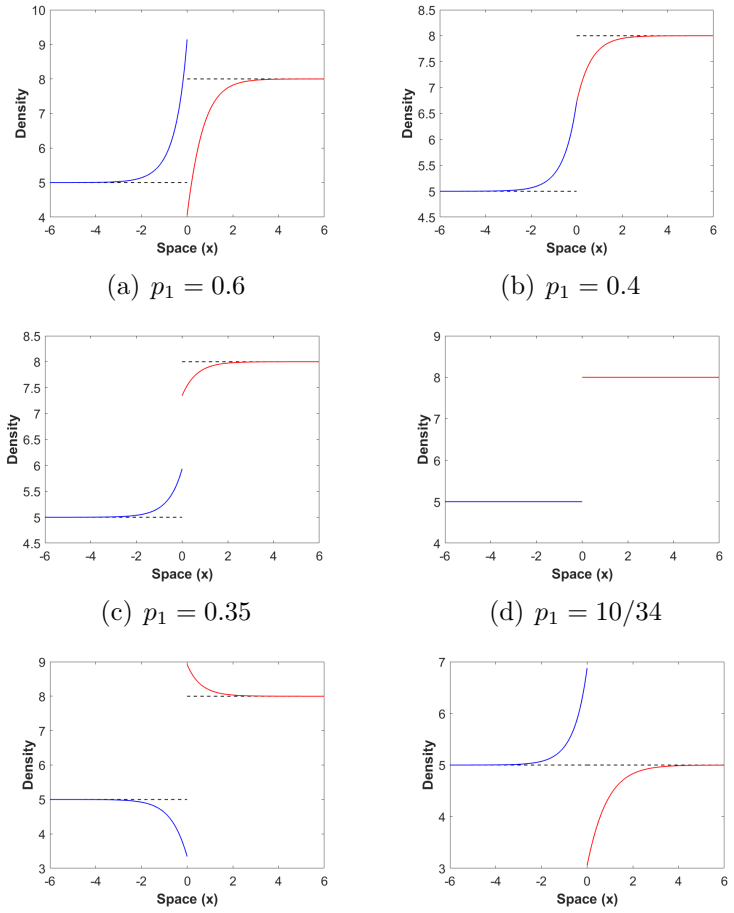

(a) $p_1 = 0.6$ (b) $p_1 = 0.4$

(c) $p_1 = 0.35$ (d) $p_1 = 10/34$

(e) $p_1 = 0.2$ (f) $K_1 = K_2$ and $p_1 = 0.6$

Figure 3.2: We illustrate how the shape of the steady-state solution of system (3.1.9) changes as the patch preference (p_1) changes. Top left: When $p_1 = 0.6$, we have Case 1 with $k = 2.25 > 1$. Top right: When $p_1 = 0.4$, we are exactly at the boundary of Cases 1 and 2 with $k = 1$. Middle left: When $p_1 = 0.35$, we have Case 2 with $K_1/K_2 = 0.625 < 0.8077 = k < 1$. Middle right: When $p_1 = 10/34$, we are exactly at the boundary of Cases 2 and 3 with $k = K_1/K_2 = 0.625$. Bottom left: When $p_1 = 0.2$, we have Case 3 with $k = 0.3750 < K_1/K_2$. Bottom right: When $K_1 = K_2$, the two threshold conditions for k are identical. When $p_1 = 0.6$, we are in Case 1 with $k = 2.25$. See text for detailed description. We chose the patches $\Omega_1 = [-6, 0]$, $\Omega_2 = [0, 6]$. Parameters are $K_1 = 5 = r_1$, $K_2 = 8 = r_2$, $D_1 = 2$ and $D_2 = 3$ unless otherwise indicated. The density in Patch 1 (Patch 2) is plotted in blue (red). The dashed lines correspond to the respective carrying capacities.

3.4 Role of movement in steady-state density

The illustrations in Figure 3.2 show that the steady-state density is greater than the local carrying capacity in one of the two patches and less than the local carrying capacity in the other patch. We are interested in whether the gain in population density over the carrying capacity in one patch exceeds the loss on the other patch or not. The magnitude of this effect depends on individual movement behaviour at the interface through the composite parameter k in (3.3.1). Hence, we ask whether individual movement behaviour benefits the population at steady state and what the underlying mechanisms are. It is clear that in the absence of any movement, the steady-state density equals carrying capacity everywhere.

As mentioned in Section 3.1, this question has been studied in the context of population dynamics in discrete habitat patches by Freedman and Waltman in [27]. The first such study in the context of reaction-diffusion equations that we are aware of is by Lou in [41]. Lou studied the steady-state density of (3.1.1) under the assumption that $r(x) = K(x)$ is not constant. He showed that inequality (3.1.2) holds for all $D > 0$. DeAngelis et al. [20] studied the same question in the case where $r(x) \neq K(x)$ is not constant. They found that inequality (3.1.2) holds under the additional assumption that r and K are positively correlated in space, at least when D is small. In both works, the authors assumed that $D > 0$ is independent of local conditions.

It turns out that the basic result in Lou [41] is still true when the diffusion term in (3.1.1) is replaced by spatially varying diffusion of Fickian type. The proof of this statement is only a slight generalization of the proof in Lou [41].

Lemma 3.4.1. *Consider the positive solution of*

$$\frac{\mathrm{d}}{\mathrm{d}x}\left(D(x)\frac{\mathrm{d}u}{\mathrm{d}x}\right) + u(K(x) - u) = 0, \tag{3.4.1}$$

on $[0, L]$ *with positive and sufficiently smooth functions* $D(\cdot)$ *and* $K(\cdot)$ *and no-flux boundary conditions*

$$D(0)\frac{\mathrm{d}u}{\mathrm{d}x}(0) = 0, \quad D(L)\frac{\mathrm{d}u}{\mathrm{d}x}(L) = 0.$$

Then

$$\int_0^L [u(x) - K(x)]dx > 0.$$

Proof: We assume that $u(x)$ is a positive solution of the steady-state equation

with Fickian diffusion term and no-flux boundary condition:

$$\begin{cases} \dfrac{\mathrm{d}}{\mathrm{d}x}\left(D(x)\dfrac{\mathrm{d}u(x)}{\mathrm{d}x}\right) + u(x)\left(K(x) - u(x)\right) = 0, \quad x \in [0, L], \\ \\ D(0)\dfrac{\mathrm{d}u(0)}{\mathrm{d}x} = 0, \quad D(L)\dfrac{\mathrm{d}u(L)}{\mathrm{d}x} = 0. \end{cases}$$

We assume that all functions are sufficiently smooth and positive.

First, we divide both sides of the equation by $u(x)$ and integrate by parts over the interval $[0, L]$. After applying the boundary conditions, we obtain:

$$\begin{aligned} \int_0^L \left(u(x) - K(x)\right)\mathrm{d}x &= \int_0^L \frac{1}{u(x)}\left(\frac{\mathrm{d}}{\mathrm{d}x}\left(D(x)\frac{\mathrm{d}u(x)}{\mathrm{d}x}\right)\right)\mathrm{d}x \\ &= \int_0^L D(x)\left(\frac{1}{u(x)}\frac{\mathrm{d}u(x)}{\mathrm{d}x}\right)^2\mathrm{d}x. \end{aligned}$$

Thus, the integral difference is positive, as claimed in the lemma. ∎

Next, we model spatial movement by using the ecological diffusion (forward Kolmogoroff) formulation for random movement in heterogeneous habitats [68]. The following calculations show that we cannot expect a similar result to hold in that case. In fact, we will see that there is no simple condition under which inequality (3.1.2) would hold in this case.

The equations are

$$\begin{cases} \dfrac{\mathrm{d}^2}{\mathrm{d}x^2}\left(D(x)u(x)\right) + u(x)\left(K(x) - u(x)\right) = 0, & x \in [0, L], \\ \\ \dfrac{\mathrm{d}}{\mathrm{d}x}(D(x)u(x))|_{x=0} = 0, \quad \dfrac{\mathrm{d}}{\mathrm{d}x}(D(x)u(x))|_{x=L} = 0. \end{cases}$$

We follow the same steps as above to find

$$\begin{aligned} \int_0^L (u(x) - K(x))\mathrm{d}x &= \int_0^L \frac{1}{u(x)}\frac{\mathrm{d}^2}{\mathrm{d}x^2}(D(x)u(x))\mathrm{d}x \\ &= \int_0^L \frac{\mathrm{d}}{\mathrm{d}x}D(x)\left(\frac{\mathrm{d}}{\mathrm{d}x}\ln(u(x))\right)\mathrm{d}x \\ &\quad + \int_0^L D(x)\left(\frac{1}{u(x)}\frac{\mathrm{d}u(x)}{\mathrm{d}x}\right)^2\mathrm{d}x. \end{aligned}$$

We see that the right-hand side is not necessarily positive. Instead, some conditions on slope or curvature need to be satisfied for positivity. Since the shape of u depends on the shape of K and D, it is not obvious what these conditions are.

As mentioned in Chapter 1, the assumption that movement behaviour is independent of local conditions is highly unrealistic in natural systems. Most organisms adjust their movement behaviour to the quality of the habitat that they are in and often also direct their movement to certain types of habitat. For a recent review of some empirical evidence, see Crone et al. [18]. In models with continuously varying landscape quality, such as (3.4.1), determining the form of $D(x)$ and/or estimating it from data is a complicated endeavour. Our modelling approach with piecewise constant functions and a single parameter at an interface offers a much more manageable alternative. In fact, empirical estimates of habitat preferences are quite common in the literature; see, for example, references in Maciel and Lutscher [46].

In our model, we calculated the difference between the total steady-state density and the total carrying capacity for the six plots in Figure 3.2; see Table 3.1. We find that inequality (3.1.2) holds only in two of the six cases. We will derive a sufficient condition for the inequality to hold.

Fig 3.2	$\int_\Omega u(x)\mathrm{d}x$	$\int_\Omega K(x)\mathrm{d}x$	$\int_\Omega [u(x)-K(x)]\mathrm{d}x$
(a)	77.686	78	−0.31417
(b)	78.221	78	0.22094
(c)	78.168	78	0.16754
(d)	78	78	0
(e)	77.442	78	−0.55800
(f)	59.505	60	−0.49502

Table 3.1: Numerical evaluation of the total population abundance at steady state, the total carrying capacity, and their difference for the six plots in Figure 3.2. Only in cases (b) and (c) is inequality (3.1.2) is satisfied.

3.4.1 Total population abundance at steady state

To derive a sufficient condition for inequality (3.1.2) to hold in our system, we consider the positive solution of our steady-state equations as usual

$$\begin{cases} D_1 \dfrac{\mathrm{d}^2 u_1(x)}{\mathrm{d}x^2} + u_1 f_1(u_1) = 0, & x \in \Omega_1 = [-L_1, 0], \\ D_2 \dfrac{\mathrm{d}^2 u_2(x)}{\mathrm{d}x^2} + u_2 f_2(u_2) = 0, & x \in \Omega_2 = [0, L_2], \\ D_1 \dfrac{\mathrm{d}u_1(0)}{\mathrm{d}x} = D_2 \dfrac{\mathrm{d}u_2(0)}{\mathrm{d}x}, \quad u_1(0) = k u_2(0), \\ \dfrac{\mathrm{d}u_1(-L_1)}{\mathrm{d}x} = 0, \quad \dfrac{\mathrm{d}u_2(L_2)}{\mathrm{d}x} = 0. \end{cases} \tag{3.4.2}$$

We divide the first equation by u_1 and integrate. We find

$$\frac{D_1}{u_1(0)} \frac{\mathrm{d}u_1(0)}{\mathrm{d}x} + D_1 \int_{-L_1}^{0} \frac{1}{u_1^2(x)} \Big(\frac{\mathrm{d}u_1(x)}{\mathrm{d}x} \Big)^2 \mathrm{d}x + \int_{-L_1}^{0} f_1(u_1(x)) \mathrm{d}x = 0. \tag{3.4.3}$$

Similarly, dividing the second equation in (3.4.2) by u_2 and integrating gives

$$-\frac{D_2}{u_2(0)} \frac{\mathrm{d}u_2(0)}{\mathrm{d}x} + D_2 \int_{0}^{L_2} \frac{1}{u_2^2(x)} \Big(\frac{\mathrm{d}u_2(x)}{\mathrm{d}x} \Big)^2 \mathrm{d}x + \int_{0}^{L_2} f_2(u_2(x)) \mathrm{d}x = 0. \tag{3.4.4}$$

Now we use $f_i(u) = r_i(1 - u/K_i) = r_i(K_i - u)/K_i$. We multiply (3.4.3) by K_1/r_1 and (3.4.4) by K_2/r_2 and add the two. We obtain

$$\int_{-L_1}^{0} [u_1(x) - K_1] \mathrm{d}x + \int_{0}^{L_2} [u_2(x) - K_2] \mathrm{d}x = I_1 + I_2, \tag{3.4.5}$$

where

$$I_1 = \frac{K_1 D_1}{r_1} \int_{-L_1}^{0} \frac{1}{u_1^2(x)} \Big(\frac{\mathrm{d}u_1(x)}{\mathrm{d}x} \Big)^2 \mathrm{d}x + \frac{K_2 D_2}{r_2} \int_{0}^{L_2} \frac{1}{u_2^2(x)} \Big(\frac{\mathrm{d}u_2(x)}{\mathrm{d}x} \Big)^2 \mathrm{d}x \tag{3.4.6}$$

and

$$I_2 = \frac{K_1}{r_1} \frac{D_1}{u_1(0)} \frac{\mathrm{d}u_1(0)}{\mathrm{d}x} - \frac{K_2}{r_2} \frac{D_2}{u_2(0)} \frac{\mathrm{d}u_2(0)}{\mathrm{d}x}. \tag{3.4.7}$$

The left-hand side in (3.4.5) is the quantity that we are interested in: the difference between the total population abundance and the total carrying capacity. The

first term on the right-hand side is clearly positive; see (3.4.6). Using the interface conditions, we simplify the second term into

$$I_2 = \frac{D_1}{u_1(0)} \frac{\mathrm{d}u_1(0)}{\mathrm{d}x} \left(\frac{K_1}{r_1} - k \frac{K_2}{r_2} \right), \tag{3.4.8}$$

with k as in (3.3.1). Hence, we have the following result.

Theorem 3.4.2. *Let u_1, u_2 be the positive solution of (3.4.2) with logistic growth terms $f_i(u) = r_i(1 - u/K_i)$. If*

$$\frac{\mathrm{d}u_1(0)}{\mathrm{d}x} \left(1 - \frac{p_1}{1-p_1} \frac{D_2}{D_1} \frac{K_2}{r_2} \frac{r_1}{K_1} \right) = \frac{\mathrm{d}u_1(0)}{\mathrm{d}x} \left(1 - k \frac{K_2}{K_1} \frac{r_1}{r_2} \right) > 0, \tag{3.4.9}$$

then

$$\int_{-L_1}^{0} [u_1(x) - K_1] \mathrm{d}x + \int_{0}^{L_2} [u_2(x) - K_2] \mathrm{d}x > 0; \tag{3.4.10}$$

i.e., the total population abundance is higher than the total carrying capacity.

The condition in the theorem simplifies significantly if we assume $r_i = K_i$, as was done in Lou [41], or, slightly more generally, if $K_2/K_1 = r_2/r_1$.

Corollary 3.4.3. *Assume that $K_2/K_1 = r_2/r_1$. If $K_2 > K_1$, then inequality (3.4.10) holds if $K_1/K_2 < k < 1$. Similarly, if $K_1 > K_2$ then inequality (3.4.10) holds if $K_1/K_2 > k > 1$.*

Proof: When $K_2/K_1 = r_2/r_1$, condition (3.4.9) holds if and only if $\mathrm{d}u_1(0)/\mathrm{d}x$ and $(1-k)$ have the same sign. Assume $K_2 > K_1$. According to Lemma 3.3.1, the solution is increasing on each patch if $k > K_1/K_2$. Hence, $\mathrm{d}u_1(0)/\mathrm{d}x > 0$. If also $k < 1$, then both factors of (3.4.9) are positive. The other case is similar. ∎

In the general case, Lemma 3.3.1 gives us the sign of $\mathrm{d}u_1/\mathrm{d}x > 0$ as a function of K_1, K_2 and k. Combined with Theorem 3.4.2, we find that inequality (3.4.10) holds in the following two cases:

$$1 < k \frac{K_2}{K_1} < \frac{r_2}{r_1} \quad \text{and} \quad 1 > k \frac{K_2}{K_1} > \frac{r_2}{r_1}.$$

To illustrate this result, we return to Figure 3.2. Parameters were chosen such that $r_i = K_i$ and $K_2 > K_1$. Hence, only plot (c) satisfies the conditions of the preceding corollary. However, we see from Table 3.1 that the integral inequality does not hold for just that case. It also holds for case (b), where the above condition is not

satisfied. This means that the bounds of this condition or at least the upper bound is not optimal.

To show that these conditions are sufficient but not necessary, we present another set of numerical results, this time with $r_i \neq K_i$. Instead of varying parameter p_1 (the probability that an individual at the interface chooses to move into Patch 1), we vary the diffusion coefficients in the two patches. The set-up is the same as in Figure 3.2, only the parameter values are different (see figure caption). The conditions from Theorem 3.4.2 are satisfied only in panel (b), yet inequality (3.4.10) is satisfied for (b) and (d) as Table 3.2 shows. In panels (a) and (c), the value of kK_2/K_1 is an order of magnitude smaller or larger than unity, respectively. In those cases, inequality (3.4.10) cannot be satisfied.

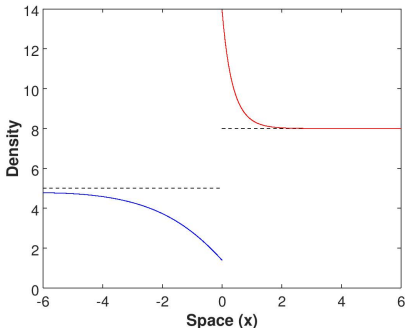

(a) $D_1 = 10$ and $D_2 = 1$

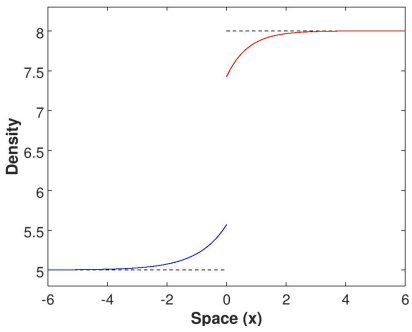

(b) $D_1 = 4$ and $D_2 = 3$

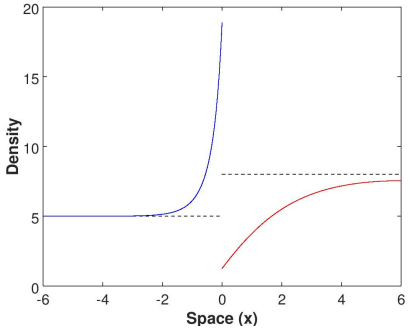

(c) $D_1 = 1$ and $D_2 = 15$

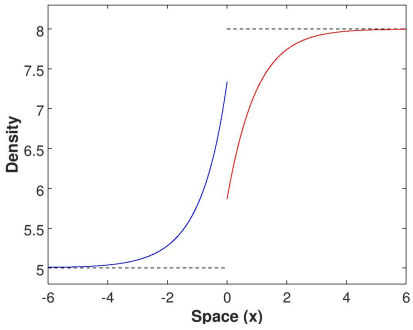

(d) $D_1 = 4$ and $D_2 = 5$

Figure 3.3: We illustrate how the shape of the steady-state solution of system (3.1.9) changes as diffusion coefficients change. Top left: $kK_2/K_1 = 0.16 < 1 < 1.5 = r_2/r_1$. Top right: $1 < kK_2/K_1 = 1.2 < 1.5 = r_2/r_1$. Bottom left: $kK_2/K_1 = 24 > 1.5 = r_2/r_1 > 1$. Bottom right: $kK_2/K_1 = 2 > 1.5 = r_2/r_1 > 1$. Common parameters are $r_1 = 4$, $r_2 = 6$, and $p_1 = 0.5$. Other parameters are as in Figure 3.2.

To further clarify the conditions under which inequality (3.4.10) can hold, we plot

Fig 3.3	$\int_\Omega u(x)\mathrm{d}x$	$\int_\Omega K(x)\mathrm{d}x$	$\int_\Omega (u(x)-K(x))\mathrm{d}x$
(a)	73.531	78	−4.4691
(b)	78.148	78	0.14769
(c)	70.292	78	−7.7085
(d)	78.136	78	0.13557

Table 3.2: Numerical evaluation of the total population abundance at steady state, the total carrying capacity, and their difference for the four plots in Figure 3.3. Inequality (3.1.2) is satisfied in cases (b) and (d) even though the sufficient conditions from Theorem 3.4.2 are satisfied only for (b).

the difference between the total steady-state density and the total carrying capacity as a function of parameter k; see Figure 3.4. We see that the inequality is satisfied for some intermediate range of k, but not for very small or very large k. We also see that the range in which the inequality holds (where the graph is positive) is larger than what the theorem predicts (between the two dashed vertical lines). In particular, while the lower bound, $k > K_1/K_2$, seems to be optimal, the upper bound, $k < K_1 r_2/(K_2 r_1)$, is clearly not optimal for the chosen parameters. We will return to this question later. When $k < K_1/K_2$, the steady state exceeds the higher of the two carrying capacities and is smaller than the lower of the two near the interface. In this case, the total population abundance is always below the total carrying capacity. On the other hand, if movement behaviour is such that the density exceeds the lower carrying capacity and remains below the higher of the two, then the total effect is positive for the population density, at least as long as the effect is not too large.

We can relate a special case of our results to those by DeAngelis et al. [20]. If we assume, as those authors did, that diffusion is constant throughout the two patches and that there is no preference for any of the patches, then we have $k = 1$. If we further assume (without loss of generality) that $K_2 > K_1$, then for inequality (3.4.10) to hold, we require $r_2/r_1 > K_2/K_1 > 1$. In particular, r_i and K_i have to be positively correlated, as was the case in DeAngelis et al. [20]. However, while those authors obtained their result only for a small enough diffusion coefficient, our reasoning applies without that restriction but for a much simpler landscape than theirs.

We conclude this section with another observation from Figure 3.3. When the two diffusion coefficients differ by an order of magnitude, there is a clearly visible difference in the maximum slope and curvature of the steady-state solution. For example, whenever D_i is small, the solution is close to the carrying capacity (and hence nearly constant) for much of the patch (e.g., the red curve in panel (a) and the blue curve in panel (c)). Whenever D_i is large, the maximum curvature is smaller, and the solution changes more gradually (e.g., the blue curve in panel (a) and the

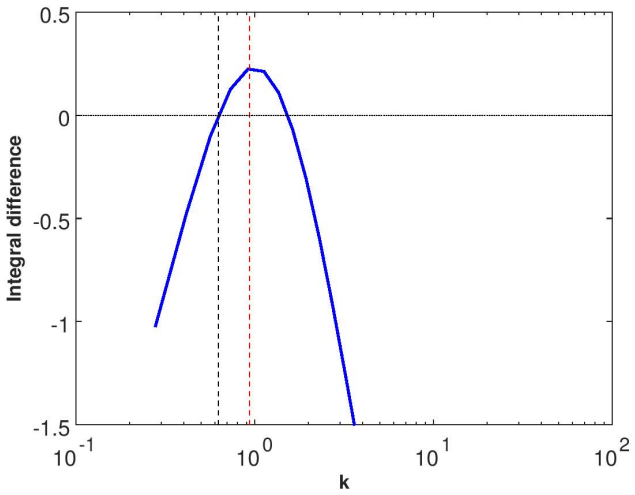

Figure 3.4: Plot of the integral difference $\int_\Omega (u(x) - K(x))\mathrm{d}x$ with respect to $\log(k)$. The black and red dashed lines indicate the sufficient conditions from the theorem, $\frac{K_1}{K_2} < k < \frac{K_1 r_2}{K_2 r_1}$.

red curve in panel (c)). In the next section, we study the shape of the steady-state density in the extreme cases where both diffusion coefficients become very small or both become very large.

3.4.2 The limits of fast and slow diffusion

So far, we have only examined one aspect of the results by Lou [41] in our two-patch model; namely, that if $r(x) = K(x)$ in the growth function of (3.1.1), then inequality (3.1.2) holds. We already found significant differences in our model that relate to individual movement behaviour. But Lou's results are much finer than inequality (3.1.2). He proves that as $D \to 0$, the steady-state density approaches the carrying capacity in the L^p-norm for all $p \geq 1$. He also proves that as $D \to \infty$, the steady-state density approaches a constant, given by the spatial average of the carrying capacity, in the $W^{2,p}$-norm for $p \geq 1$. In this final section, we formulate analogous questions for our two-patch model and give numerical and heuristic evidence that analogous results could hold.

The first question is how to formulate the problem, since the logistic growth function contains only one diffusion coefficient, but our two-patch model (1.1.13) contains two. We choose to vary $D_{1,2}$ in such a way that their ratio, $d = D_1/D_2$, remains constant. Then parameter k remains independent of D_i.

We present some numerical experiments. The plot in Figure 3.5 shows that as

$D_i \to 0$, the steady-state density approaches the carrying capacity on each patch with an increasingly steep transition zone near the interface. As $D_i \to \infty$, we see that the steady-state density approaches a constant on each patch. In contrast to the result by Lou, this constant is generally not the same throughout the entire domain, because the matching conditions at the interface need to be satisfied.

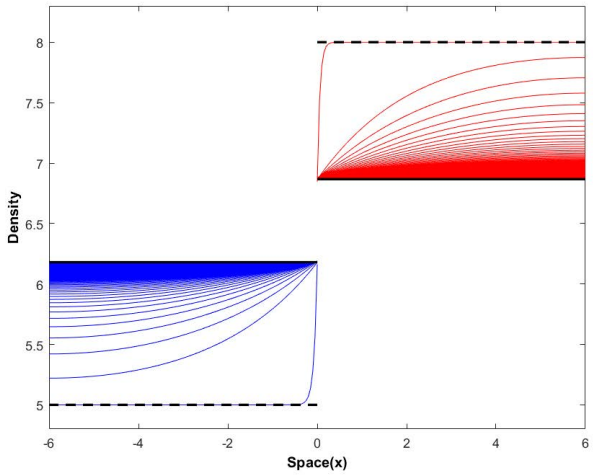

Figure 3.5: Steady-state profiles of the two-patch model for varying values of D_1 with constant ratio $D_2/D_1 = 0.9$. As D_1 approaches zero, the solution is close to the carrying capacity on each patch (indicated by the black dashed lines) and has a narrow but sharp transition zone near the interface (the lowest of the blue curves and the highest of the red curves correspond to the smallest value $D_1 = 0.1$). As D_1 gets large, the steady-state solution becomes increasingly flat and approaches the constant values u_i^* from (3.4.11) on Patch i (indicated by the black solid lines). Other parameters are as in Figure 3.3.

We can derive a heuristic expression for the densities in each patch in the limit as $D_i \to \infty$. We denote by u_i^* the spatially constant steady-state density on Patch i. Then we integrate the equations over both patches and find

$$L_1 r_1 u_1^* \left(1 - \frac{u_1^*}{K_1}\right) + L_2 r_2 u_2^* \left(1 - \frac{u_2^*}{K_2}\right) = 0.$$

Substituting the interface condition $u_1^* = k u_2^*$ gives the solution

$$u_2^* = \frac{L_1 r_1 k + L_2 r_2}{\frac{L_1 r_1 k}{K_1/k} + \frac{L_2 r_2}{K_2}}, \quad u_1^* = k u_2^*. \tag{3.4.11}$$

DeAngelis et al. derive several similar formulas for the limit of large diffusion [21]. Their formula (C.6) is a special case of our result when $L_1 = L_2 = 1$ and $k =$

1, as is formula (3.2) in Freedman and Waltman [27] for the case of two discrete patches. Upon closer inspection, we see that (3.4.11) is the harmonic mean of K_2 and K_1/k with weights $L_2 r_2$ and $L_1 r_1 k$. This result is closely related to the work on spatial averaging in [74]. Those authors considered population dynamics in an infinite landscape of periodically alternating patches of two types. They derived equations for the homogenization limit when the patch sizes $L_{1,2} \to 0$. In that limit, the carrying capacity turned out to be an appropriately weighted harmonic average of the patch-level carrying capacities. A steady-state solution of our model on just two patches is equivalent to a periodic solution of their model with twice the patch size because of the no-flux conditions at $-L_1$ and L_2; see also Maciel et al. [45] for a similar argument. Our assumption that $D_i \to \infty$ can be turned into the homogenization assumption that $L_i \to 0$ by a simple rescaling of space.

For the solution in (3.4.11), we can explicitly calculate exact conditions for the total population abundance to exceed the total carrying capacity. We have

$$L_1 u_1^* + L_2 u_2^* > L_1 K_1 + L_2 K_2,$$

if and only if

$$\frac{K_1}{K_2} < k < \frac{K_1}{K_2}\frac{r_2}{r_1}. \tag{3.4.12}$$

In other words, in the limit of fast diffusion, the upper bound that we found from Theorem 3.4.2 for inequality (3.4.9) to hold is sharp.

We show three possible behaviours illustrating the difference between the total steady-state density and the total carrying capacity as a function of diffusion rates in Figure 3.6. When $k < K_1/K_2$, the total steady-state density is below the total carrying capacity for all values of D_1 (dashed curve). The curve is monotone decreasing and approaches the value given by (3.4.11). When (3.4.12) is satisfied, the total steady-state density is above the total carrying capacity for all D_1 (solid curve). The curve has an intermediate maximum as in the case studied by Lou [41]. In the limit, however, we obtain again the values from (3.4.11), whereas Lou found that the total steady-state density equals the total carrying capacity in the limit. When $k > (K_1 r_2)/(K_2 r_1)$ is not too large, the curve increases initially but decreases below zero eventually (dashes and circles). As always, the limiting value for large D_i is given by (3.4.11). When $k \gg (K_1 r_2)/(K_2 r_1)$, the curve has the same shape as for small k: it is monotone decreasing (plot not shown).

3.5 Summary and open questions

Spatial population dynamics are often studied via reaction-diffusion equations [13]. There is, however, a certain disconnect: while spatially homogeneous models have

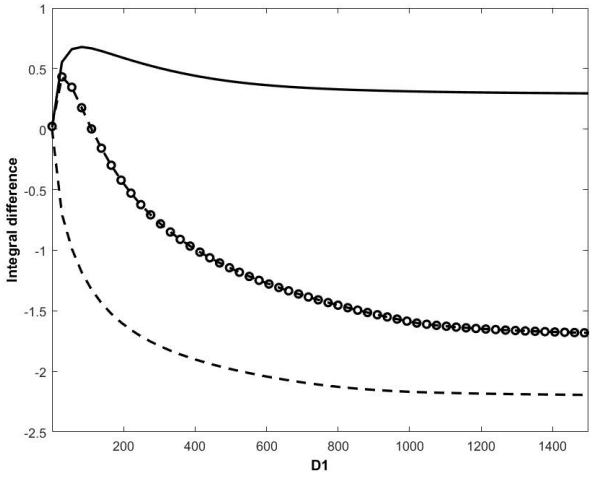

Figure 3.6: Plot of the integral difference $\int_\Omega (u(x) - K(x))\mathrm{d}x$ versus D_1 for three values of k. The ratio $d = D_1/D_2$ is fixed at $d = 1.1$, $d = 0.9$ and $d = 0.5$, corresponding to the circles, solid and dashed curves, respectively. Other parameters are the same as in Figure 3.3.

found many applications—e.g., for spread rates of biological invasions [4, 40] or for critical patch sizes in conservation biology [66]—spatially heterogeneous models are largely studied from an abstract analytical point of view. We speculate that among the reasons for this disconnect are that spatially heterogeneous models are almost prohibitively difficult to parametrize, since they require too many data points, and also that the available mathematical results are often too abstract and require numerical evaluation. One potential way forward was proposed by Shigesada et al. [65], who studied persistence and invasions in piecewise constant, periodic landscapes. This simplification not only significantly reduced the number of parameters in the model, it also allowed explicit analytical results that are easy to evaluate and apply. Maciel and Lutscher [46] extended their model framework by introducing individual movement behaviour at interfaces between different habitat types, based on earlier work by Ovaskainen and Cornell [55]. Many empirical studies collect the required data (see, for example, references in Crone et al. [18]), and the qualitative behaviour of the models with interface behaviour differs significantly from those without [2, 38, 44, 46, 47]. However, almost all conclusions about the resulting reaction-diffusion systems with interface matching conditions are based on linear analysis (but see Freedman [26] and Maciel et al. [45]). Our work here studies several aspects of steady states of these models and applies the results to the question of whether and how the total population abundance at steady state can exceed the total carrying capacity as a result of movement behaviour.

In this chapter, we first established the existence and uniqueness of steady states by adopting the method of Freedman et al. [26]. We then significantly extended their stability result by proving that this steady state was unconditionally stable, using monotonicity results. Then we showed that the steady-state density was always monotone on each patch, it is either increasing or decreasing on both patches. The density jump at the interface may, however, prevent the solution from being monotone on the entire landscape. We gave precise conditions, in terms of the composite parameter k, that classify the steady states into one of three cases (Figure 3.1). We are aware of only one other study of the qualitative behaviour of steady states for population dynamics in patchy landscapes: Cruywagen et al. used a perturbation expansion approach in the model without interface behaviour (i.e., with $k = 1$) [19] .

In the critical case where $k = K_1/K_2$, the steady-state solution is piecewise constant. This case has already shown significance in two ways elsewhere. Langebrake et al. studied a model for marine reserves and found that the critical value of k delineated the case where model behaviour matches empirical results from the case where it does not [38]; see also Alqawasmeh and Lutscher [3]. Maciel et al. studied the evolution of dispersal and patch preference in a two-patch landscape and showed that this special case was an evolutionarily steady strategy and a neighborhood invader strategy [45].

As an application, we studied the question of when the total steady-state density can exceed the total carrying capacity in the landscape. This question has a long tradition in ecology, starting with the work by Freedman and Waltman [27], who studied it in an ordinary differential equation model of two patches without explicit spatial location. The first treatment of this question with reaction-diffusion equations was by Lou [41] and later by DeAngelis et al. [20]. A typical result is the existence of a maximum of the total steady-state density at intermediate diffusion rates, and that maximum exceeds the total carrying capacity. Empirical results confirm the existence of such an intermediate maximum [78]. For a recent synthesis of this topic and its ecological importance, see Zhang et al. [77]. Our model is the first, based on reaction-diffusion equation, that considers differential movement rates and patch preference in this context. It is also the first that finds that the total population abundance for very large diffusion need not equal the total carrying capacity. Rather, we give precise conditions for when the total population abundance is above or below the total carrying capacity. Arditi et al. found the same qualitative behaviour in a two-patch model with linear dispersal [6]. In fact, their results also include the thresholds K_1/K_2 and $(r_2K_1)/(r_1K_2)$, but their movement behaviour does not include bias. With movement bias included, Arditi et al. found patterns of total population abundance that are very similar to ours, illustrated in their Figures 4 and 5 [7]. Since our model is spatially explicit within each patch, it makes additional predictions about the density profile within each patch while the patch models in the papers by

Arditi et al. [6, 7] cannot make. We expect that our results can be related to theirs via "patch averaging" [14]. This is a technique to turn reaction-diffusion systems in patchy landscapes into ordinary differential equation systems with appropriate movement terms between patches. We are curious whether experimental systems can be set up where the density within each patch can be resolved so that an increase or decrease at an interface could be measured.

Arguably the most obvious open question from our work is to find an analytical proof of the numerical and heuristic convergence results for the steady-state density as $D_1 = dD_2$ approach zero and infinity. The discontinuity condition at the interface requires the development of new techniques to prove this convergence. An ecologically more interesting task is to extend this model to more than two patches, each separated by interfaces with corresponding matching conditions, and to study the qualitative behaviour of steady states. The infinite periodic case with two patch types is equivalent to our two-patch case, but we are unaware of any study of three or more different patch types.

Chapter 4

Pattern formation in homogeneous landscapes

In this chapter, we introduce the concept of diffusion-driven instability (DDI), and we explore the impact of diffusion on the formation of spatial patterns in a general predator–prey system. Here, the concept of instability means that a uniform steady state becomes unstable to certain perturbations and the populations typically exhibit a periodic spatial pattern. The main process driving the spatially inhomogeneous instability is diffusion. More precisely, we show that, under certain conditions, the presence of diffusion can lead to the emergence of spatial patterns, which is however impossible under the same conditions when diffusion is absent. We derive the conditions for DDI of the steady state and the initiation of spatial patterns for a general predator–prey model in a one-dimensional homogeneous landscape, and we apply them to the May model. We perform numerical simulations to visualize the spatial patterns. Our exposition follows the general descriptions in the books by Keshet [36] and Murray [50].

4.1 A brief survey of Turing-pattern formation

Spatial patterns are ubiquitous in ecological systems and are widely investigated using reaction-diffusion equations that account for the random motion and population dynamics of targeted species. The pioneering work of pattern formation was conducted by Turing [70], who derived conditions under which a spatially homogeneous steady state is stable in the absence of diffusion but becomes unstable in the presence of diffusion. This mechanism determines the spatial pattern that evolves [36, 50]. The process is known as DDI, and the associated spatial pattern is usually called a Turing pattern. When Turing patterns arise, the reaction-diffusion system admits at least

one non-constant steady state [50].

The study of Turing patterns originated from modelling chemical reactions. Turing [70] showed that the key elements necessary for pattern formations are:

- There are two substances, an activator and an inhibitor. An activator is a substance that promotes or activates its own formation, and an inhibitor is a substance that inhibits its own rate of formation.
- There has to be a negative feedback loop between the activator and the inhibitor.
- The diffusion rate of the inhibitor must be one order of magnitude larger than that of the activator.

The basic pattern-formation mechanism is visualized in Figure 4.1. This mechanism shows that Turing patterns are generated by the interaction of two substances, an activator and inhibitor, with different diffusion rates. As we see in Figure 4.1, the activator promotes its own production and the production of the inhibitor, and the inhibitor only inhibits the production of the activator. In fact, this mechanism starts with a homogeneous equilibrium and then some perturbation arises. Next, the inhibitor spreads widely, whereas the activator remains localized, since the inhibitor diffuses faster than the activator. The activator can then use its activation to grow and becomes narrowly concentrated because of the inhibitory effect of inhibitor.

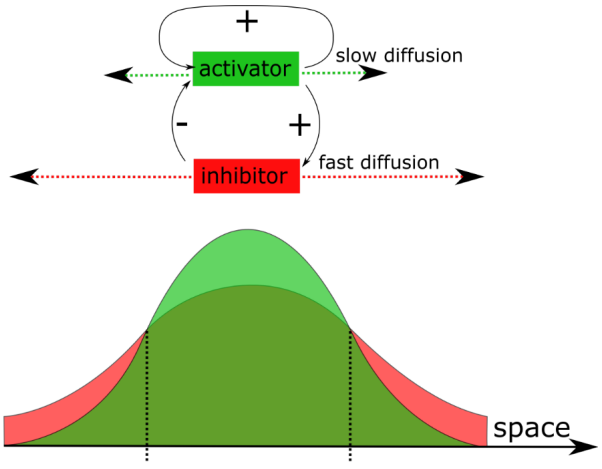

Figure 4.1: Schematic illustration of the basic Turing pattern mechanism. This figure is taken from www.commons.wikimedia.org.

To understand how this mechanism works and leads to Turing patterns, we provide an example from Murray [50]: "Consider a field of dry grass in which there is a large number of grasshoppers, which can generate a lot of moisture by sweating if

they get warm. Now suppose the grass is set alight at some point and a flame front starts to propagate. We can think of the grasshopper as an inhibitor and the fire as an activator. If there were no moisture to quench the flames, the fire would simply spread over the whole field, which would result in a uniform charred area. Suppose, however, that when the grasshoppers get warm enough they can generate enough moisture to dampen the grass so that when the flames reach such a premoistened area, the grass will not burn. The scenario for spatial pattern is then as follows. The fire starts to spread with its diffusion coefficient. When the grasshoppers ahead of the flame front feel it coming, they move quickly well ahead of it; that is, they have their diffusion coefficient, which is much larger than the diffusion coefficient of fire. The grasshoppers then sweat profusely and generate enough moisture to prevent the fire spreading into the moistened area. In this way, the charred area is restricted to a finite domain, which depends on the diffusion coefficients of the fire and grasshoppers and various parameters. If the grasshoppers and flame front diffused at the same speed no such spatial pattern could evolve." In this example, all this happens locally, whenever a fire starts. Then one observes a pattern.

Although Turing's study was originally proposed in chemistry, his idea has spread to developmental biology and animal-coat patterns [50]. Few applications to ecology exist, because some of the conditions seem quite restrictive for ecological system. For example, the Rosenzweig–MacArthur model, one of the most widely used predator–prey models, does not allow Turing-pattern formation [62].

We start the first part of this chapter with a general reaction-diffusion model to derive the DDI conditions. In the second part, we apply the theory to the May model.

4.2 Conditions for DDI

In this section, we define DDI in mathematical terms and derive necessary and sufficient conditions for the initiation of spatial patterns for the following general reaction-diffusion model in a one-dimensional homogeneous landscape:

$$\begin{cases} \dfrac{\partial u}{\partial t} = D^u \dfrac{\partial^2 u}{\partial x^2} + f(u,v), & (x,t) \in \Omega \times [0,\infty), \\ \dfrac{\partial v}{\partial t} = D^v \dfrac{\partial^2 v}{\partial x^2} + g(u,v), & (x,t) \in \Omega \times [0,\infty), \\ u(x,0) = u_0 > 0, \quad v(x,0) = v_0 > 0. \end{cases} \tag{4.2.1}$$

We assume that (4.2.1) has a spatially constant positive steady state, denoted

by (u^*, v^*). We say that this system exhibits DDI if the state is linearly stable to homogeneous perturbations and unstable to spatially varying perturbations. The conditions for DDI differ slightly between a bounded and an unbounded domain. So we consider general model (4.2.1) in two different types of domains:

1. A finite domain, $\Omega = [0, L]$, which requires boundary conditions. We consider system (4.2.1) with no-flux boundary conditions:

$$\frac{\partial u(0,t)}{\partial x} = \frac{\partial u(L,t)}{\partial x} = 0, \quad \frac{\partial v(0,t)}{\partial x} = \frac{\partial v(L,t)}{\partial x} = 0, \quad t \geqslant 0. \tag{4.2.2}$$

   We choose no-flux boundary conditions because we are interested in self-organisation of patterns. No-flux conditions imply no external input.

2. An infinite domain, $\Omega = \mathbb{R}$, without boundaries.

The derivation of the conditions for DDI in these two cases follows essentially the same steps except some small differences. We introduce the concept using a finite domain and no-flux boundary conditions, where all the calculations are easy to follow. Then we briefly discuss the differences that occur when we consider the infinite domain, which will be used in Chapter 5.

We start by linearizing the partial differential equations in system (4.2.1) about the steady state (u^*, v^*). We set $W = u - u^*$ and $Z = v - v^*$, where $|W| \ll 1$ and $|Z| \ll 1$. We expand the function

$$f(u,v) = f(W + u^*, Z + v^*) = f(u^*, v^*) + W f_u + Z f_v + \text{h.o.t.}, \tag{4.2.3}$$

and similarly for $g(u, v)$. Here, f_u and f_v denote the partial derivatives evaluated at the steady state. Therefore, the linearized equations about the steady state (u^*, v^*) are:

$$\begin{cases} \dfrac{\partial W}{\partial t} = D^u \dfrac{\partial^2 W}{\partial x^2} + W f_u + Z f_v, \\[2ex] \dfrac{\partial Z}{\partial t} = D^v \dfrac{\partial^2 Z}{\partial x^2} + W g_u + Z g_v. \end{cases} \tag{4.2.4}$$

To determine the stability of (u^*, v^*), we look for solutions of the following form, based on the method of separation of variables:

$$W(x,t) = \hat{u}(t)\cos(n\pi x/L), \qquad Z(x,t) = \hat{v}(t)\cos(n\pi x/L), \tag{4.2.5}$$

where n is an integer. This solution satisfies the no-flux boundary conditions at $x = 0$ and $x = L$. Here, $k = n\pi/L$ is called the wave number, and $1/k$ is proportional to

the wavelength $\omega = 2\pi/k = 2L/n$. With finite domains, there is a discrete set of possible wave numbers, since n is integer.

By substituting ansatz (4.2.5) into (4.2.4) and cancelling $\cos(kx)$, for each k, we get the system of ordinary differential equations

$$\begin{cases} \dfrac{\mathrm{d}\hat{u}}{\mathrm{d}t} = -D^u k^2 \hat{u} + f_u \hat{u} + f_v \hat{v}, \\ \dfrac{\mathrm{d}\hat{v}}{\mathrm{d}t} = -D^v k^2 \hat{v} + g_u \hat{u} + g_v \hat{v}, \end{cases} \tag{4.2.6}$$

with parameter k.

We are interested in the stability of $\hat{u} = \hat{v} = 0$. This trivial steady state for the linear model corresponds to the steady state (u^*, v^*) in the nonlinear model.

We formulate the DDI conditions for our transformed system (4.2.6) in terms of parameter k as follows:

1. $\hat{u} = \hat{v} = 0$ is stable to homogeneous perturbations; that is, $k = 0$.
2. $\hat{u} = \hat{v} = 0$ is unstable to some inhomogeneous perturbations; that is, $k \neq 0$.

System (4.2.6) can be written in matrix form as follows:

$$\begin{pmatrix} \dfrac{\mathrm{d}\hat{u}}{\mathrm{d}t} \\ \\ \dfrac{\mathrm{d}\hat{v}}{\mathrm{d}t} \end{pmatrix} = \begin{pmatrix} -D^u k^2 + f_u & f_v \\ \\ g_u & -D^v k^2 + g_v \end{pmatrix} \begin{pmatrix} \hat{u} \\ \\ \hat{v} \end{pmatrix} = J(k^2) \begin{pmatrix} \hat{u} \\ \\ \hat{v} \end{pmatrix}. \tag{4.2.7}$$

To study the stability of the system, we evaluate the trace and the determinant of $J(k^2)$, which are denoted by $\mathrm{tr}(J(k^2))$ and $\det(J(k^2))$, respectively. Their expressions are

$$\mathrm{tr}(J(k^2)) = -D^u k^2 + f_u - D^v k^2 + g_v = f_u + g_v - k^2(D^u + D^v), \tag{4.2.8}$$

and

$$\det J((k^2)) = (D^u D^v)(k^2)^2 - (D^u g_v + D^v f_u)k^2 + f_u g_v - f_v g_u. \tag{4.2.9}$$

From here on, we will refer to $\mathrm{tr}(J(k^2))$ and $\det(J(k^2))$ to emphasize the explicit dependence on k. For simplicity, we denote $\mathrm{tr}(J) = \mathrm{tr}(J(0))$ and $\det(J) = \det(J(0))$.

The above conditions for DDI are expressed as follows.

1. We require $\hat{u} = \hat{v} = 0$ to be stable for $k = 0$. Thus, we require

$$\mathrm{tr}(J) = f_u + g_v < 0, \qquad \text{(DDI 1)}$$
$$\det(J) = f_u g_v - f_v g_u > 0. \quad \text{(DDI 2)}$$

2. We require $\hat{u} = \hat{v} = 0$ to be unstable for some $k \neq 0$. This can happen if either $\mathrm{tr}(J(k^2)) > 0$ or $\det(J(k^2)) < 0$ for some $k \neq 0$. We see that $\mathrm{tr}(J(k^2))$ in (4.2.8) is always negative because we have $f_u + g_v < 0$ from condition DDI 1 and the term $-(D^u + D^v)k^2$ is also negative. Therefore, to get $\hat{u} = \hat{v} = 0$ to be unstable for some $k \neq 0$, we require $\det(J(k^2)) < 0$ for some $k \neq 0$.

   We observe that $\det(J(\cdot))$ is quadratic in k^2. For $\det(J(\cdot))$ to be negative for some nonzero k, the minimum $\det(J(k^2))_{\min}$ must be negative and $k^2_{\min}$ must be positive. Differentiating (4.2.9) with respect to k^2 gives

$$\frac{\mathrm{d}\det(J(k^2))}{\mathrm{d}k^2} = 2D^uD^vk^2 - \left(D^ug_v + D^vf_u\right). \tag{4.2.10}$$

   We find $k^2_{\min}$ by solving $\dfrac{\mathrm{d}\det(J(k^2))}{\mathrm{d}k^2} = 0$ for k^2. Hence, we obtain

$$k^2_{\min} = \frac{(D^ug_v + D^vf_u)}{2D^uD^v}. \tag{4.2.11}$$

   Since $k^2_{\min}$ must be positive, we get the third condition for DDI as

$$D^ug_v + D^vf_u > 0. \qquad \text{(DDI 3)}$$

   Finally, we need $\det(J(k^2_{\min})) = \det(J(k^2))_{\min} < 0$. Substituting $k^2_{\min}$ from (4.2.11) into (4.2.9), we get

$$\begin{aligned}\det(J(k^2))_{\min} = \det(J(k^2_{\min})) &= -\frac{\left(D^ug_v + D^vf_u\right)^2}{4D^uD^v} + f_ug_v - f_vg_u \\ &= -\frac{\left(D^ug_v + D^vf_u\right)^2}{4D^uD^v} + \det(J).\end{aligned} \tag{4.2.12}$$

   Thus, the condition that $\det(J(k^2)) < 0$ for some $k^2 \neq 0$ is

$$\frac{\left(D^ug_v + D^vf_u\right)^2}{4D^uD^v} > \det(J), \tag{4.2.13}$$

   which is the last condition for DDI, and it is obtained by requiring

$$\left(f_ug_v - f_vg_u\right)4D^uD^v < \left(D^ug_v + D^vf_u\right)^2. \qquad \text{(DDI 4)}$$

In summary, the conditions for spatial pattern formation are

$$\begin{aligned}\mathrm{tr}(J) = f_u + g_v < 0, &\qquad \text{(DDI 1)}\\ \det(J) = f_ug_v - f_vg_u > 0, &\qquad \text{(DDI 2)}\end{aligned}$$

$$D^u g_v + D^v f_u > 0, \qquad \text{(DDI 3)}$$

$$(D^u g_v + D^v f_u)^2 - (f_u g_v - f_v g_u)\, 4D^u D^v > 0. \qquad \text{(DDI 4)}$$

Under the assumption that the first two conditions are satisfied, we now aim to find ranges for the diffusion coefficients to ensure that DDI 3 and DDI 4 are satisfied. For this purpose, we divide DDI 3 and DDI 4 by D^u and set $D = \frac{D^v}{D^u}$. Since these two conditions depend only on the ratio D, by assuming that condition DDI 3 is satisfied, we study condition DDI 4 by looking at the stability boundary, which is given when DDI 4 is an equality. We can express the stability boundary as

$$\det(J) = \frac{(Df_u + g_v)^2}{4D}. \tag{4.2.14}$$

For fixed parameters, the above expression defines a critical diffusion-coefficient ratio, D_c, as the appropriate root of (4.2.14), or equivalently

$$(f_u)^2 D_c^2 + 2\,(2f_v g_u - f_u g_v)\, D_c + (g_v)^2 = 0, \tag{4.2.15}$$

where $D_c > 1$; see Lemma 4.3.1.

The critical wave number, which is denoted by k_c^2, is given (using (4.2.13)) by

$$k_c^2 = \frac{D_c f_u + g_v}{2D_c} = \left[\frac{\det(J)}{D_c}\right]^{1/2} = \left[\frac{f_u g_v - f_v g_u}{D_c}\right]^{1/2}. \tag{4.2.16}$$

The corresponding critical wavelength, w_c, is

$$\omega_c = \frac{2\pi}{k_c} = 2\pi \left(\frac{D_c f_u + g_v}{2D_c}\right)^{-1/2}. \tag{4.2.17}$$

From (4.2.9), for any $D > D_c$ the range of unstable wave numbers $k_1^2 < k^2 < k_2^2$ is given by the zeros k_1^2 and k_2^2 of $\det(J(k^2)) = 0$; namely,

$$k_1^2 = \frac{1}{2D^v}\left[(Df_u + g_v) - \left((Df_u + g_v)^2 - 4D\det(J)\right)^{1/2}\right], \tag{4.2.18}$$

$$k_2^2 = \frac{1}{2D^v}\left[(Df_u + g_v) + \left((Df_u + g_v)^2 - 4D\det(J)\right)^{1/2}\right]. \tag{4.2.19}$$

Now we have all the required ingredients to study Turing patterns in bounded domains.

For the second case, when we have an infinite domain, the steps that we need to follow to find the DDI conditions are basically the same as for DDI in finite domains, except that in infinite domains, the possible wave numbers and corresponding spatial wavelengths of allowable patterns are continuous. Furthermore, our domain in Chapter 5 will be an infinite domain. For this case, we start with linearized system (4.2.4)

and look for solutions of the following form, based on the method of separation of variables:

$$W(x,t) = \hat{u}(t)e^{ikx}, \qquad Z(x,t) = \hat{v}(t)e^{ikx}, \tag{4.2.20}$$

where $k \geq 0$ denotes the wave number, and the corresponding wavelength can be found by $\omega = 2\pi/k$. The next steps in this case are exactly the same as in the first case to find the conditions for DDI in a finite domain. As we mentioned earlier, the crucial difference between the situation here and that for a finite domain is that now there is always an unstable wave number if, in (4.2.18) and (4.2.19), $0 < k_1^2 < k_2^2$ since we are not restricted to a discrete set of k^2. So, when k_c^2, given by (4.2.16), causes the system to be linearly unstable, the mechanism may evolve to a spatial pattern with the critical wavelength $\omega_c = 2\pi/k_c$.

4.3 Biological explanations of Turing-pattern formation

In this section, we interpret the biological meaning of the DDI conditions that we derived in Section 4.2. We start by giving general biological explanations and characteristics of the main substances of Turing-pattern formation: activator and inhibitor. Next, we define the range of activation and inhibition, then we show how to derive the formula to calculate these ranges. These ranges, which come from DDI 3, give more information about the formation of Turing patterns; namely, the requirement to have a short range of activation and a long range of inhibition.

The biological meaning of the DDI conditions can be interpreted as follows:

1. By condition DDI 1, at least one of the two coefficients f_u or g_v is negative. Without loss of generality, we will from here on suppose that g_v is negative. This means that species v has to inhibit its own rate of formation. This species is typically called an inhibitor.

2. From conditions DDI 3 and DDI 4, f_u and g_v cannot be both zero. Hence, f_u must be positive. It means that species u has to promote its own formation. This species is typically called an activator.

3. The first two steps together imply that $f_u g_v < 0$.

4. From Step 3, it follows that inequality DDI 2 can only be met if $f_v g_u < 0$. This means that f_v and g_u have to have opposite signs. There are two possibilities, each giving a distinct sign pattern to the Jacobi matrix $J(k^2)$ when $k = 0$ ($J = J(0)$):

- Activator–inhibitor:

$$f_v < 0, \quad g_u > 0, \qquad J = \begin{pmatrix} + & - \\ + & - \end{pmatrix}. \tag{4.3.1}$$

  The sign structure of the Jacobi J for this case shows that u increases v and itself but v decreases u and itself.

- Positive feedback:

$$f_v > 0, \quad g_u < 0, \qquad J = \begin{pmatrix} + & + \\ - & - \end{pmatrix}. \tag{4.3.2}$$

  In this case, the sign structure of J shows that v increases u and u increases itself. Also, u decreases v and v decreases itself.

For applications in ecology, since f_v and g_u have to have opposite signs, the corresponding species must have a predator–prey relationship. We will denote the prey by u and the predator by v so that the sign pattern is that of the activator–inhibitor case.

We provide an important consequence of DDI 1 and DDI 3 in the following lemma, which is a fundamental condition to get Turing patterns.

Lemma 4.3.1. *If $f_u > 0$ and $g_v < 0$, then* DDI 3 *requires $D^v > D^u$.*

Proof: By using DDI 1, which shows $f_u < -g_v$, we get $D^u f_u < -D^u g_v$. On the other hand, from DDI 3, we have $D^u g_v + D^v f_u > 0$. So, we get $D^v f_u > -D^u g_v$. As a result, we find $D^u f_u < -D^u g_v < D^v f_u$. Comparing the first and last terms of this inequality gives the desired result, $D^v > D^u$. ∎

Remark 4.3.2. *If $f_u < 0$ and $g_v > 0$, then the reverse inequality is required.*

A formulation of Lemma 4.3.1 in words is that the diffusion coefficient of predator (inhibitor) should be greater than the diffusion coefficient of prey (activator) to get Turing patterns; see Figure 4.1.

The next and last goal of this section is to define the range of activation and inhibition.

Lemma 4.3.3. *Let $\tau^u = 1/|f_u|$ and $\tau^v = 1/|g_v|$. These are time constants associated with activation and inhibition, respectively. Then one can deduce from* DDI 3 *that $D^u\tau^u < D^v\tau^v$.*

Proof: From condition DDI 3, we have $D^v f_u > -D^u g_v = |g_v| D^u$. So, we obtain $\frac{D^v}{|g_v|} > \frac{D^u}{|f_u|}$, which shows that we get our desired result, $D^v \tau^v > D^u \tau^u$. ∎

The quantities $\sqrt{D^u \tau^u}$ and $\sqrt{D^v \tau^v}$ have units of length and are referred to as the range of activation and inhibition, respectively. Based on Lemma 4.3.3, we can conclude that we may get Turing patterns only if the range of inhibition is larger than the range of activation.

4.4 Turing-pattern formation for the May model

In this section, we study the nondimensional May model as an example for DDI. First, we provide explicit calculations of the DDI conditions, then we illustrate the behaviour with numerical simulations. We explain our numerical methods in Section 4.4.2.

4.4.1 Analysis of the DDI conditions

We consider the May predator–prey model [48]

$$\frac{\mathrm{d}u}{\mathrm{d}t} = u(1-u) - \frac{uv}{b+u}, \quad \frac{\mathrm{d}v}{\mathrm{d}t} = sv\left(1 - \frac{v}{qu}\right), \tag{4.4.1}$$

where b denotes the half-saturation constant of the Holling type II functional response [33, 34]. The functional response, here $\frac{u}{b+u}$, is the rate at which each predator captures prey. Predator dynamics are modeled by a logistic equation with intrinsic growth rate s and carrying capacity qu. Parameters b, q and s are positive.

Here, we study the spatial form of the May model with no-flux boundary conditions on $\Omega = [0, L]$:

$$\begin{cases} \dfrac{\partial u}{\partial t} = D^u \dfrac{\partial^2 u}{\partial x^2} + u(1-u) - \dfrac{uv}{b+u}, & (x,t) \in \Omega \times [0,\infty), \\[2ex] \dfrac{\partial v}{\partial t} = D^v \dfrac{\partial^2 v}{\partial x^2} + sv\left(1 - \dfrac{v}{qu}\right), & (x,t) \in \Omega \times [0,\infty), \\[2ex] \dfrac{\partial u(0,t)}{\partial x} = \dfrac{\partial u(L,t)}{\partial x} = 0, \quad \dfrac{\partial v(0,t)}{\partial x} = \dfrac{\partial v(L,t)}{\partial x} = 0, & t \geqslant 0, \\[2ex] u(x,0) = u_0 > 0, \quad v(x,0) = v_0 > 0. \end{cases} \tag{4.4.2}$$

A complete analysis of all the dynamic behaviour of the spatial May model is given in Mukhopadhyay and Bhattacharyya [49].

System (4.4.1) has a unique positive steady state, given by

$$u^* = \frac{1}{2}\left(1 - b - q + \sqrt{(1-b-q)^2 + 4b}\right), \qquad v^* = qu^*. \tag{4.4.3}$$

The Jacobi matrix at this steady state is

$$J = \begin{pmatrix} f_u & f_v \\ g_u & g_v \end{pmatrix} = \begin{pmatrix} 1 - 2u^* - \frac{b(1-u^*)}{b+u^*} & -\frac{u^*}{b+u^*} \\ sq & -s \end{pmatrix}. \tag{4.4.4}$$

We check the sign pattern, which is a necessary condition for DDI. The sign pattern of the matrix for the activator–inhibitor case in this model holds if f_u is positive. The other entries have already the correct signs. This partial derivative depends on parameters b and q. Since we are not interested in a complete qualitative analysis of this model but rather in giving an example for Turing-pattern formation, we fix parameter b and express f_u in terms of q as a function of b. To provide the range where f_u is positive, we first find the critical value for parameter q so that $f_u = 0$. We denote this critical value by q_A, and we obtain it as follows

$$q_A = -\frac{(b+1)^2}{2(b-1)}. \tag{4.4.5}$$

When $q > q_A$, f_u is positive; so that we have the sign pattern for the activator–inhibitor case.

The determinant of (4.4.4) at the steady state, is

$$\det(J) = \frac{su^*(b+q+2u^*-1)}{b+u^*} = \frac{su^*\sqrt{4b+(1-b-q)^2}}{b+u^*}. \tag{4.4.6}$$

Since the steady state and parameters are positive, the above expression is positive; as a result, DDI 2 is satisfied.

Condition DDI 1 depends on all three population dynamic parameters. As before, we are not interested in a complete qualitative analysis of the model but only in giving an example for Turing-pattern formation. So, we fix parameters s and b and express condition DDI 1 in terms of q as a function of s and b. To find the range for parameter q that satisfies this condition, first we obtain the critical value when the trace of the Jacobi matrix at the steady state is zero. Hence, we get

$$1 - 2u^* - b\frac{1-u^*}{b+u^*} = s, \tag{4.4.7}$$

where u^* is given in (4.4.3). At a critical value, which we denote by q_H, the stability behaviour of the steady state changes from stable to unstable.

If parameter s is large, then equation (4.4.7) has no solution and the steady state is stable. If s is small enough, there are two critical values $q_{H,1} < q_{H,2}$ given by

$$\begin{aligned} q_{H,1} &= \frac{-1}{4s}\Big[2b - s + 2\sqrt{b^2 - 6bs - 2b + s^2 - 2s + 1} + 3bs - s^2 \\ &\qquad + s\Big(\sqrt{b^2 - 6bs - 2b + s^2 - 2s + 1}\Big) - 2\Big], \\ q_{H,2} &= \frac{1}{4s}\Big[- 2b + s + 2\sqrt{b^2 - 6bs - 2b + s^2 - 2s + 1} - 3bs + s^2 \\ &\qquad + s(\sqrt{b^2 - 6bs - 2b + s^2 - 2s + 1}\Big) + 2\Big]. \end{aligned} \tag{4.4.8}$$

Condition DDI 1 is satisfied for $q < q_{H,1}$ and $q > q_{H,2}$. Hence, for given parameters b and s, we find ranges of parameter q (namely, $q_A < q < q_{H,1}$ and $q > q_{H,2}$), so that we can guarantee that the Jacobi matrix has an activator–inhibitor sign pattern and that the positive steady state is stable in the absence of diffusion.

Finally, the last two DDI conditions should be also satisfied to make sure that we have all the requirements to get Turing patterns. Since these two conditions depend on the critical diffusion rate, we obtain this value by finding the root of quadratic equation (4.2.15), where the partial derivatives are given in (4.4.4). This equation is

$$\left(1 - 2u^* - \frac{b(1-u^*)}{b+u^*}\right)^2 D_c^2 + 2\left(-2sq\frac{u^*}{b+u^*} + s\left(1 - 2u^* - \frac{b(1-u^*)}{b+u^*}\right)\right) D_c + s^2 = 0, \tag{4.4.9}$$

where u^* is given in (4.4.3). This quadratic equation has two roots. Only one root is greater than unity. We know from Lemma 4.3.1 that we require $D_c > 1$. Hence, the larger root of (4.4.9) is the critical diffusion. For all $D > D_c$, conditions DDI 3 and DDI 4 are satisfied and we expect to get Turing-pattern formation.

4.4.2 Numerical methods and simulation

We simulate (4.4.2) with initial conditions, which are given by a small random perturbation of the spatially constant steady state. If this steady state is unstable and the DDI conditions are satisfied, Turing patterns will eventually arise. We simulate the time-dependent parabolic boundary-value problem (4.4.2) with a fully discrete explicit finite difference scheme. We choose the Crank–Nicolson scheme [67], which is unconditionally stable. We implemented this scheme in Matlab. We compared the accuracy of our program with the built-in `pdepe` program in Matlab. `pdepe` solves a system of partial differential equations with one spatial variable x and time t. The ordinary differential equations resulting from discretization in space are integrated

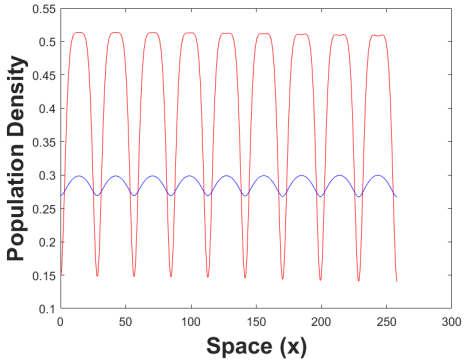

Figure 4.2: We see a periodic spatial pattern in the steady-state profile of (4.4.2) for the prey (red) and the predator (blue). The figure was obtained using the Crank–Nicolson scheme with the final time $T = 3000$, spatial step size $\mathrm{d}x = 0.05$ and time step size $\mathrm{d}t = 0.1$. Parameters are $b = 0.1$, $s = 0.2$, $q = 0.8$, $D^u = 1$, $D^v = 40$, and the domain length $L = 10w_c = 258$. The initial conditions are a small perturbation of the steady state. Here, a small perturbation was obtained by the random number generator with a maximal absolute value of 0.01.

with an ODE solver, more precisely by using the `ode15s` solver, to obtain approximate solutions at the times specified in the discretization.

We choose $b = 0.1$ and $s = 0.2$. We calculate $q_A \approx 0.672$ and $q_{H,1} \approx 0.895$. Then we fix $q = 0.8 \in (q_A, q_{H,1})$. With these parameter values, the steady state is given by $(u^*, v^*) \approx (0.3701, 0.2961)$. The critical diffusion ratio is $D_c \approx 28.6 > 1$. We pick $D = 40$ for our simulations. Figure 4.2 shows a periodic spatial pattern as the steady-state profile of (4.4.2) for both densities. From it, we calculate $w_c \approx 25.79$ as the critical wavelength. We also see these patterns by using the `pdepe` program in Figures 4.3(a) and 4.3(b).

Remark 4.4.1. *The numerical parameters in the Crank–Nicolson scheme and in* `pdepe` *(i.e., the parameters that determine the numerical aspects,* $\mathrm{d}x = 0.05$, $\mathrm{d}t = 0.1$ *and* $T = 3000$*) will be the same for all simulation throughout the thesis unless otherwise noted.*

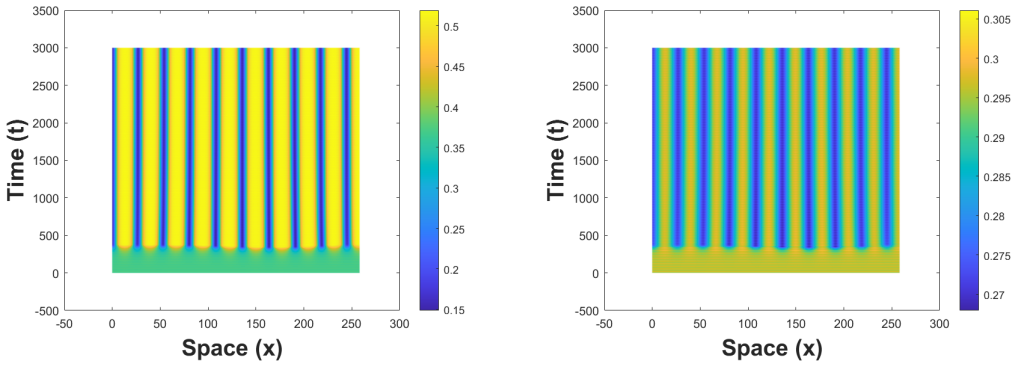

(a) (b)

Figure 4.3: The temporal development of patterns for system (4.4.2) for both densities: (a) the prey density and (b) the predator density. Plots were obtained by the `pdepe` program. Parameters and initial values are the same as in Figure 4.2.

Chapter 5

Pattern formation in patchy landscapes

In Chapter 4, we studied Turing-pattern formation by deriving the conditions for diffusion-driven instability (DDI) in a homogeneous environment. Here, we combine this idea with the idea of patchy landscapes from Chapter 3 to study DDI in a heterogeneous landscape. To analyze the DDI conditions in a periodic patchy landscape, we assume that the period is small and use homogenization theory to derive spatially homogeneous equations that we then analyze according to the theory from Chapter 4.

5.1 Introduction

One of the most challenging problems in ecology is to explore and explain the mechanisms that generate spatial patterns of population densities. Here, we study spatial patterns that arise in a predator–prey system in a heterogeneous landscape from species interaction and dispersal through DDI. The study of Turing patterns originated in chemistry [70] and has since also been applied in the context of developmental biology and animal coat patterns [50]; see Chapter 4.

Segel and Jackson [63] were the first to call attention to the fact that DDI can appear in an ecological context. They presented an example of a predator–prey interaction, where the addition of random dispersal results in an instability of the homogeneous steady-state distribution to perturbations of a certain wavelength. In particular, they chose the Lotka–Volterra predator–prey model with Allee effect for

the prey and self limitation for the predator. They used the following model

$$\begin{cases} \dfrac{\partial u}{\partial t} = uR(u) - auv + D^u \left[\dfrac{\partial^2 u}{\partial x^2} + \dfrac{\partial^2 u}{\partial y^2} \right], \\ \\ \dfrac{\partial v}{\partial t} = buv - dv - cv^2 + D^v \left[\dfrac{\partial^2 v}{\partial x^2} + \dfrac{\partial^2 v}{\partial y^2} \right], \end{cases} \tag{5.1.1}$$

where u and v denote the prey and predator densities, respectively. The corresponding diffusion coefficients are denoted by D^u and D^v, respectively. The prey's reproduction rate is defined as $R(u) = \kappa_0 + \kappa_1 u - \kappa_2 u^2$. All parameters are positive constants. For a certain range of parameters, the sign structure of the Jacobi matrix at the positive steady state for this model has an activator–inhibitor structure (4.3.1) with the prey as an activator. As a result, this model can give rise to Turing patterns if the prey disperse sufficiently less than the predator.

Turing's mechanism was also studied by Levin and Segel [39] to explain the emergence of patchy population distributions of oceanic plankton. If biological interactions between phytoplankton and herbivores reduce the efficiency of herbivory as phytoplankton density increases and if differential dispersal rates favour higher herbivore mortality, such patterns arise.

The Rosenzweig–MacArthur model is the most prominent predator–prey model [62]. Its spatially extended version is

$$\begin{cases} \dfrac{\partial u}{\partial t} = \left[r\left(1 - \dfrac{u}{K}\right) - \dfrac{av}{1+ahu} \right] u + D^u \dfrac{\partial^2 u}{\partial x^2}, \\ \\ \dfrac{\partial v}{\partial t} = \left[e\dfrac{au}{1+ahu} - d \right] v + D^v \dfrac{\partial^2 v}{\partial x^2}, \end{cases} \tag{5.1.2}$$

where u, v, D^u and D^v are as in the model by Segel and Jackson (5.1.1). Parameters r and K are prey net growth rate and carrying capacity. Parameters a, h, e and d are the predator attack rate, handling time, efficiency and death rate, respectively. The sign pattern of the Jacobi matrix at the positive steady state for this model is

$$J = \begin{pmatrix} - & - \\ \\ + & 0 \end{pmatrix}. \tag{5.1.3}$$

Hence, there is no activator, and therefore this model does not support pattern formation [53]. In fact, the $(2,2)$-entry is zero because the predator equation is linear in the predator, which implies that we do not get an activator–inhibitor sign pattern. This prevents Turing-pattern formation.

While the Rosenzweig–MacArthur model in a homogeneous landscape does not lead to Turing patterns, there are several different predator–prey models that do. For example, pattern formation has been studied in the Beddington–DeAngelis model [8], the ratio–dependent model [5] and the May model [48]. More precisely, if we add diffusion to these models, they can give rise to DDI [1, 49, 72]. The spatially extended May model has been discussed in Chapter 4. The spatial Beddington–DeAngelis and ratio-dependent models are given by:

$$\begin{cases} \dfrac{\partial u}{\partial t} = r\left(1-\dfrac{u}{K}\right)u - \dfrac{buv}{B+\beta v+u} + D^u\dfrac{\partial^2 u}{\partial x^2}, \\ \\ \dfrac{\partial v}{\partial t} = e\dfrac{buv}{B+\beta v+u} - \mu v + D^v\dfrac{\partial^2 v}{\partial x^2}, \end{cases} \tag{5.1.4}$$

and

$$\begin{cases} \dfrac{\partial u}{\partial t} = r\left(1-\dfrac{u}{K}\right)u - \dfrac{buv}{\beta v+u} + D^u\dfrac{\partial^2 u}{\partial x^2}, \\ \\ \dfrac{\partial v}{\partial t} = e\dfrac{buv}{\beta v+u} - \mu v + D^v\dfrac{\partial^2 v}{\partial x^2}, \end{cases} \tag{5.1.5}$$

respectively. As before, u and v are the densities of prey and predator, and D^u and D^v are their diffusion coefficients. Parameter b is the maximum consumption rate, β represents predator interference, and B is a saturation constant. For both models, the Jacobi matrix has an activator–inhibitor structure (4.3.1) for appropriate parameter ranges with the prey as an activator. These models will form Turing patterns if the prey disperse sufficiently less than the predator.

In a different approach, Fasani and Rinaldi studied spatial-pattern formation mechanisms by modifying the Rosenzweig–MacArthur model [23]. They chose to include several additional factors for the predator that were not considered in the original model and studied which of these factors could lead to pattern formation. They chose small perturbations so that the coexistence equilibrium remained positive and stable and that the $(1,1)$-entry of the Jacobi matrix remained negative. Hence, the prey is an inhibitor in their model. For several of the factors that they added, the $(2,2)$-entry of the Jacobi matrix became positive; for example in the case of a nonlinear predator harvesting term. Then the predator became an activator and the Jacobi matrix had a positive feedback structure (4.3.2). Hence, Turing-pattern formation is possible when the predator disperses sufficiently less than the prey.

In this chapter, we study Turing-pattern formation by considering a general predator–prey model in a periodic heterogeneous landscape. Several authors studied Turing-pattern formation in heterogeneous landscapes that consist of only two patches [10, 11, 57, 58].

Benson et al. [11] considered Turing-pattern formation in embryological and ecological contexts with a general two species reaction-diffusion model in one space dimension, where the domain is composed of two parts. They required that solutions are continuous at the interface and that the flux is continuous as well. In particular, they considered the Segel–Jackson model with only the diffusion coefficient of the predator differing between the two patches. They derived the DDI conditions by extending the theory that we presented in Chapter 4. Their analysis in this simple case provides an understanding of the way in which environmental heterogeneities can modulate the pattern-forming capabilities of reaction-diffusion systems. A similar way to study Turing patterns with constant kinetics parameters and spatially varying diffusion coefficients can be found in Benson et al. [10].

Page et al. investigated the patterns near the interface between two patches, where population dynamics parameters but not diffusion rates differ between patches [57]. They showed that a step-function heterogeneity in a kinetic parameter of a reaction–diffusion system can lead to spatial pattern formation outside the classical Turing parameter regime for patterning. In particular, in this paper, they simulated the nondimensional Gierer–Meinhardt activator–inhibitor model [31] numerically with parameter values that are outside the Turing space but within the range of stability of the uniform steady state to homogeneous perturbations. Their simulations then showed that no patterns evolve for the system with constant parameters. However, when they imposed a step function spatial variation in one of the parameters, a stable spatially nonuniform pattern formed. Then they derived results for a linearized version of the Gierer–Meinhardt model system and showed that the analytical solutions of the linearized system can be used to predict many features of the full nonlinear system. They also showed that the resulting patterns are spatially localised around the parameter discontinuity because the discontinuity in the steady state values acts like a local perturbation and can induce pattern formation if the homogeneous steady state on either side of the boundary is unstable.

Page et al. in [58] extended their model in [57] with kinetic parameters changing smoothly, either spatially monotone and periodically. By spatially varying parameters individually, they explored the patterning capabilities of this model system to determine how the variation of each parameter in the model affects the steady-state patterns formed. They used analytical expressions and model simulations to compare the widths, heights and separations of the peaks. They showed that the form of the resulting complex pattern depends on which parameter is modulated by the control species and that various parameters in this model control different aspects of the pattern.

Some authors studied Turing-pattern formation in a heterogeneous landscape with more than two patches. Spatial patterns in species densities can emerge for two reasons: variation in habitat quality in a heterogeneous landscape or species

interaction and DDI. Sheffer et al. studied the interaction between these mechanisms in terms of both theoretical and empirical approaches in the formation of patterned vegetation in semi-arid regions [64]. They were the first authors who showed that both mechanisms significantly affect the pattern-formation process with their relative contribution depending on water availability. They introduced a conceptual model to link the structure of the physical template to self-organisation processes to explore the effect of spatial scales on pattern formation by comparing the length scale of the spatial extent of landscape feature to the length scale on which biological feedbacks operate.

Cobbold et al. developed a theoretical framework to study how extrinsic factors, environmental variation and intrinsic interaction can lead to spatial patterns in a predator–prey model in a heterogeneous landscape [15]. The landscape consists of discrete patches, and movement is modeled by a discrete diffusion process with periodic boundary conditions when they have finitely many patches. The heterogeneous landscape consists of a series of periodically alternating patches of two types. Population dynamics on each patch are described by a system of differential equations. Cobbold et al. explored emergent patterns with two different approaches: (i) when the number of patches is finite, they found a large number of patterns, often stably coexisting, and complex bifurcation diagrams through a numerical bifurcation analysis; (ii) when the number of patches is infinite, they used linear stability analysis to derive the dispersion relation of the spatially homogeneous steady state and the corresponding pattern formation conditions.

Our study is closest to the one by Cobbold et al. [15]. In fact, it is a continuous-space version of their model. We also investigate spatial patterns in a predator–prey system on a heterogeneous landscape with infinitely many patches: patches of Type 1 (good patches, suitable for prey growth) and patches of Type 2 (bad patches, unsuitable for prey growth) are periodically alternating. At patch boundaries, we use the interface conditions that were derived by Ovaskainen and Cornell [55] and studied further by Maciel and Lutscher [46]. We study Turing-pattern formation in a partial-differential equation context. We use the method of homogenization to simplify the model by deriving the homogenized model under the assumption that the landscape period is small [74, 75]. We derive the DDI conditions for this homogenized model. We use numerical evaluation to analyze and visualize the DDI conditions. We also simulate the homogenized model to test the prediction of the DDI conditions. In Sections 5.3–5.5, we render illustrations of our results in Turing-pattern formation for three different scenarios.

5.2 The model set-up and method

We present a general predator–prey model in a one-dimensional heterogeneous landscape that contains infinitely many patches: patches of Type 1, or "good patches", and patches of Type 2, or "bad patches", which are periodically alternating. We denote by L_1 and L_2 the length of good and bad patches, respectively, and by $L = L_1+L_2$ the spatial period. We also denote $l_1 = \frac{L_1}{L}$ as the ratio of good patches and $l_2 = \frac{L_2}{L}$ as the ratio of bad patches, so that $l_1 + l_2 = 1$. Without loss of generality, we choose a good patch to be located at $(-L_1, 0)$ and other good patches L-periodic from thereon. Accordingly, bad patches are located at $(0, L_2)$ and L-periodic from thereon. The population densities for prey and predator are denoted by $u_i(x,t)$ and $v_i(x,t)$, respectively. Then we describe the population dynamics and individual movement in our predator–prey model with reaction diffusion equations for each species on each patch as follows:

$$\begin{cases} \dfrac{\partial u_1(x,t)}{\partial t} = D_1^u \dfrac{\partial^2 u_1(x,t)}{\partial x^2} + f_1(u_1, v_1), & t \geqslant 0, \\ \dfrac{\partial v_1(x,t)}{\partial t} = D_1^v \dfrac{\partial^2 v_1(x,t)}{\partial x^2} + g_1(u_1, v_1), & t \geqslant 0, \\ \dfrac{\partial u_2(x,t)}{\partial t} = D_2^u \dfrac{\partial^2 u_2(x,t)}{\partial x^2} + f_2(u_2, v_2), & t \geqslant 0, \\ \dfrac{\partial v_2(x,t)}{\partial t} = D_2^v \dfrac{\partial^2 v_2(x,t)}{\partial x^2} + g_2(u_2, v_2), & t \geqslant 0. \end{cases} \tag{5.2.1}$$

Here, we set $x = 0$ to be the interface between patches $(-L_1, 0)$ and $(0, L_2)$. We also set the other interface on the right side of $x = 0$ at $x = L_2$, which is located between patches $(0, L_2)$ and $(L_2, L_1 + L_2)$. Then we impose the matching conditions for population density and flux that were derived from a random-walk model by Ovaskainen and Cornell [55] and studied further by Maciel and Lutscher [46]. At these two interfaces, we have the following matching conditions:

$$\begin{cases} u_1(0,t) = k_u u_2(0,t), \quad v_1(0,t) = k_v v_2(0,t), & t \geqslant 0, \\ D_1^u \dfrac{\partial u_1(0,t)}{\partial x} = D_2^u \dfrac{\partial u_2(0,t)}{\partial x}, \quad D_1^v \dfrac{\partial v_1(0,t)}{\partial x} = D_2^v \dfrac{\partial v_2(0,t)}{\partial x}, & t \geqslant 0, \\ u_1(L_2,t) = k_u^{-1} u_2(L_2,t), \quad v_1(L_2,t) = k_v^{-1} v_2(L_2,t), & t \geqslant 0, \\ D_1^u \dfrac{\partial u_1(L_2,t)}{\partial x} = D_2^u \dfrac{\partial u_2(L_2,t)}{\partial x}, \quad D_1^v \dfrac{\partial v_1(L_2,t)}{\partial x} = D_2^v \dfrac{\partial v_2(L_2,t)}{\partial x}, & t \geqslant 0. \end{cases} \tag{5.2.2}$$

We similarly set the interface conditions for the remaining of the interfaces, which are located L-periodic from thereon. Parameters D_i^u and D_i^v are the diffusion rates for prey and predator on Patch i, respectively. We have $k_u = \frac{p_1^u}{p_2^u}\frac{D_2^u}{D_1^u}$ and $k_v = \frac{p_1^v}{p_2^v}\frac{D_2^v}{D_1^v}$ as the discontinuity parameters for prey and predator, respectively, which are defined based on their corresponding diffusion coefficients and patch preferences. Parameters p_i^u and p_i^v are probabilities for prey and predator, respectively, that an individual at the interface moves to patch of Type i; see Chapter 1.

To study Turing-pattern formation, we assume that the period L is small, apply homogenization to equations (5.2.1) and then use the theory from Chapter 4 to determine DDI conditions for the homogenized equations.

The homogenized model is given by

$$\begin{cases} \dfrac{\partial U(x,t)}{\partial t} = \hat{D}^u \dfrac{\partial^2 U(x,t)}{\partial x^2} + \hat{f}(U,V), \\ \dfrac{\partial V(x,t)}{\partial t} = \hat{D}^v \dfrac{\partial^2 V(x,t)}{\partial x^2} + \hat{g}(U,V), \end{cases} \tag{5.2.3}$$

where $x \in \mathbb{R}$. The derivation follows Yurk et al. [75] and is quite lengthy and technical. We give details in Appendix A. In this model, the population densities for prey and predator are denoted by $U(x,t)$ and $V(x,t)$ and $\hat{D}^u$ and $\hat{D}^v$ represent the homogenized diffusion coefficients for prey and predator, given by

$$\hat{D}^u = \left(\frac{(1-p^u)l_1 + p^u l_2}{l_1+l_2}\right)^{-1}\left(\frac{r_1^u l_1 + r_2^u l_2}{l_1+l_2}\right)^{-1}, \tag{5.2.4}$$

and

$$\hat{D}^v = \left(\frac{(1-p^v)l_1 + p^v l_2}{l_1+l_2}\right)^{-1}\left(\frac{r_1^v l_1 + r_2^v l_2}{l_1+l_2}\right)^{-1}, \tag{5.2.5}$$

respectively. Here, r_i^u and r_i^v are the residence indices [68] for prey and predator on patches of Type i, given by

$$r_1^u = \frac{1}{D_1^u(1-p^u)}, \qquad r_2^u = \frac{1}{D_2^u p^u}, \tag{5.2.6}$$

and

$$r_1^v = \frac{1}{D_1^v(1-p^v)}, \qquad r_2^v = \frac{1}{D_2^v p^v}, \tag{5.2.7}$$

respectively.

In homogenized model (5.2.3), $\hat{f}(U,V)$ and $\hat{g}(U,V)$ are the homogenized reaction terms for prey and predator, whose expressions are

$$\hat{f}(U,V) = \frac{f_1\left(\frac{r_1^u U}{\langle r^u\rangle}, \frac{r_1^v V}{\langle r^v\rangle}\right) l_1 + f_2\left(\frac{r_2^u U}{\langle r^u\rangle}, \frac{r_2^v V}{\langle r^v\rangle}\right) l_2}{l_1+l_2}, \tag{5.2.8}$$

and

$$\hat{g}(U,V) = \frac{g_1\left(\frac{r_1^u U}{\langle r^u\rangle}, \frac{r_1^v V}{\langle r^v\rangle}\right) l_1 + g_2\left(\frac{r_2^u U}{\langle r^u\rangle}, \frac{r_2^v V}{\langle r^v\rangle}\right) l_2}{l_1 + l_2}, \tag{5.2.9}$$

respectively. Here, $\langle r^u\rangle$ and $\langle r^v\rangle$ denote the average residence indices for prey and predator, given by

$$\langle r^u\rangle = \frac{l_1 r_1^u + l_2 r_2^u}{l_1 + l_2} = \frac{\frac{l_1}{(1-p^u)D_1^u} + \frac{l_2}{p^u D_2^u}}{l_1 + l_2}, \tag{5.2.10}$$

and

$$\langle r^v\rangle = \frac{l_1 r_1^v + l_2 r_2^v}{l_1 + l_2} = \frac{\frac{l_1}{(1-p^v)D_1^v} + \frac{l_2}{p^v D_2^v}}{l_1 + l_2}, \tag{5.2.11}$$

respectively.

Then the conditions for DDI are derived based on linear stability analysis of a positive steady state of system (5.2.3). We assume that our system has a spatially constant positive steady state, which we denote by (U^*, V^*). In the absence of spatial variation, the homogenized steady state must be linearly stable, but its state must be unstable to certain spatially varying perturbations; see Chapter 4. The DDI conditions for general homogenized model (5.2.3) are given as follows:

$$\begin{aligned} \hat{f}_U + \hat{g}_V &< 0, \quad \text{(DDI 1)} \\ \hat{f}_U\hat{g}_V - \hat{f}_V\hat{g}_U &> 0, \quad \text{(DDI 2)} \\ \hat{D}^u\hat{g}_V + \hat{D}^v\hat{f}_U &> 0, \quad \text{(DDI 3)} \\ \left(\hat{D}^u\hat{g}_V + \hat{D}^v\hat{f}_U\right)^2 - \left(\hat{f}_U\hat{g}_V - \hat{f}_V\hat{g}_U\right) 4\hat{D}^u\hat{D}^v &> 0. \quad \text{(DDI 4)} \end{aligned} \tag{5.2.12}$$

If these conditions are satisfied, the homogenized model will exhibit Turing patters; see Chapter 4. In Appendix B, we give the expressions of these DDI conditions in terms of the patch-level quantities.

Lemma 5.2.1. *If function $g_i(u_i, v_i)$ is linear in v_i on both patches, then it is impossible to get Turing-pattern formation in the homogenized model.*

Proof: Since $g_i(u_i, v_i)$ is linear in v_i on both patches, in homogenized model (5.2.3), $\hat{g}(U,V)$ is linear in V. Thus, the $(2,2)$-entry of the Jacobi matrix will be zero, which shows that we do not have the required activator–inhibitor structure in the model to support the existence of DDI. ∎

In Chapter 4, we saw that there is a critical ratio of the diffusion coefficients, below which no patterns form. This critical value is obtained from quadratic equation (4.2.15). The corresponding expression for our homogenized model is

$$\hat{D}_c = \frac{-(2\hat{f}_V\hat{g}_U - \hat{f}_U\hat{g}_V) + \sqrt{(2\hat{f}_V\hat{g}_U - \hat{f}_U\hat{g}_V)^2 - (\hat{f}_U\hat{g}_V)^2}}{(\hat{f}_U)^2}. \tag{5.2.13}$$

We recall that $\hat{D}_c$ must be greater than one for patterns to form; see Lemma 4.3.1. In Chapter 4, Condition DDI 4 was satisfied if we had $D > D_c$. In a homogeneous landscape, D_c depends only on the population kinetic parameters and not on the diffusion coefficients. Therefore, one can choose diffusion coefficients for prey and predator so that their ratio exceeds D_c and patterns can form; see Chapter 4. However, in the homogenized version (5.2.13), $\hat{D}_c$ depends on all model parameters, including diffusion coefficients of both species in both patch types. Hence, we cannot vary those diffusion coefficients independently in order to achieve the necessary condition $\frac{\hat{D}^v}{\hat{D}^u} > \hat{D}_c$.

The critical wave number k_c^2, is given by

$$k_c^2 = \frac{\hat{D}_c \hat{f}_U + \hat{g}_V}{2\hat{D}_c}, \tag{5.2.14}$$

and the corresponding critical wavelength, w_c, is

$$\omega_c = \frac{2\pi}{k_c} = 2\pi \left(\frac{\hat{D}_c \hat{f}_U + \hat{g}_V}{2\hat{D}_c} \right)^{-1/2}. \tag{5.2.15}$$

For our particular application, we use the May model [48] as the reaction term on good patches and a simple death term for the prey in bad patches. Then the model is given by (5.2.1) and (5.2.2), where

$$\begin{aligned} f_1 &= u_1(1-u_1) - \frac{u_1 v_1}{b+u_1}, \quad g_1 = s v_1 \left(1 - \frac{v_1}{q u_1}\right), \\ f_2 &= -m u_2 - \frac{u_2 v_2}{b+u_2}, \qquad\quad g_2 = s v_2 \left(1 - \frac{v_2}{q u_2}\right). \end{aligned} \tag{5.2.16}$$

Here, b denotes the half-saturation constant of the Holling type II functional response [33, 34], m denotes the prey's mortality rate on bad patches and $D_i^u(D_i^v)$ denotes the prey (predator) diffusion coefficient. The functional response, here $\frac{u_i}{b+u_i}$, is the rate at which each predator captures prey. Predator growth is modeled by the logistic equation with intrinsic growth rate s and carrying capacity qu_i. This formulation is given by Turchin [69].

If the landscape was homogeneous and the reaction terms were f_1 and g_1, we could choose parameter values so that the DDI conditions were satisfied and Turing patterns would form; see Chapter 4. If the landscape was homogeneous and the reaction terms were f_2 and g_2, no patterns could possibly form because the only spatially homogeneous steady state of the model would be the trivial state $(0,0)$.

The homogenized reaction terms for the May model are explicitly given by

$$\hat{f}(U,V) = \frac{1}{l_1+l_2}\left[l_1 \left(\frac{r_1^u U}{\langle r^u \rangle}\left(1 - \frac{r_1^u U}{\langle r^u \rangle}\right) - \frac{\frac{r_1^u U}{\langle r^u \rangle}\frac{r_1^v V}{\langle r^v \rangle}}{b + \frac{r_1^u U}{\langle r^u \rangle}} \right) - l_2 \left(m\frac{r_2^u U}{\langle r^u \rangle} + \frac{\frac{r_2^u U}{\langle r^u \rangle}\frac{r_2^v V}{\langle r^v \rangle}}{b + \frac{r_2^u U}{\langle r^u \rangle}} \right) \right], \tag{5.2.17}$$

and

$$\hat{g}(U,V)=\frac{1}{l_1+l_2}\left[l_1 s\frac{r_1^v V}{\langle r^v\rangle}\left(1-\frac{\frac{r_1^v V}{\langle r^v\rangle}}{q\frac{r_1^u U}{\langle r^u\rangle}}\right)+l_2 s\frac{r_2^v V}{\langle r^v\rangle}\left(1-\frac{\frac{r_2^v V}{\langle r^v\rangle}}{q\frac{r_2^u U}{\langle r^u\rangle}}\right)\right]. \tag{5.2.18}$$

A spatially constant positive steady state, (U^*,V^*), is given by

$$\left(\frac{l_1 r_1^v+l_2 r_2^v}{\frac{l_1(r_1^v)^2\langle r^u\rangle}{q r_1^u\langle r^v\rangle}+\frac{l_2(r_2^v)^2\langle r^u\rangle}{q r_2^u\langle r^v\rangle}}\right)U=\frac{l_1 r_1^u-l_1\frac{(r_1^u)^2}{\langle r^u\rangle}U-l_2 r_2^u m}{\frac{l_1 r_1^u r_1^v(b+\frac{r_2^u U}{\langle r^u\rangle})+l_2 r_2^u r_2^v(b+\frac{r_1^u U}{\langle r^u\rangle})}{\langle r^v\rangle(b+\frac{r_1^u U}{\langle r^u\rangle})(b+\frac{r_2^u U}{\langle r^u\rangle})}}, \tag{5.2.19}$$

and

$$V=\frac{l_1 r_1^u(1+\frac{r_1^u U}{\langle r^u\rangle})-l_2 r_2^u m}{\frac{l_1 r_1^u r_1^v}{\langle r^v\rangle(b+\frac{r_1^u U}{\langle r^u\rangle})}+\frac{l_2 r_2^u r_2^v}{\langle r^v\rangle(b+\frac{r_2^u U}{\langle r^u\rangle})}}. \tag{5.2.20}$$

The equation for U is a cubic. While there are explicit solution formulas for the cubic, it would still be impossible to evaluate the DDI conditions explicitly. We therefore revert to numerical evaluation of the equations and DDI conditions. We also simulate reaction-diffusion system (5.2.3) to test the prediction of the DDI conditions. We use the Crank–Nicolson scheme [67] and Matlab's `pdepe` program for all our simulations; see Chapter 4.

We consider the following scenarios in our exploration.

Scenario 1: We choose parameters on patches of Type 1 such that all DDI conditions are satisfied on a homogeneous landscape of Type 1. As we mentioned above, no patterns can form on a homogeneous landscape of Type 2. We then expect that patterns may emerge or disappear as we change the proportion of the two types of patches in the landscape.

Scenario 2: We choose parameters such that the DDI conditions are not satisfied on patches of Type 1. Since no pattern formation is possible on patches of Type 2, there is no obvious reason to believe that patterns could form on a landscape with both patch types mixed. However, we shall show that patterns are possible on some mixed landscapes. We consider two subcases, depending on which pattern formation conditions are violated on patches of Type 1.

Scenario 2a: Here, we assume that the Jacobi matrix has an activator–inhibitor sign pattern but the ratio of the diffusion coefficients is below the critical ratio in patches of Type 1.

Scenario 2b: Here, we assume that both diagonal entries of the Jacobi matrix are negative on patches of Type 1 so that there is no activator-inhibitor sign pattern.

We study those scenarios for three different aspects of heterogeneity: (i) only population dynamics vary between patches; (ii) population dynamics and movement behaviour vary between patches but there is no preference for a particular type of patch; (iii) population dynamics vary between patches and there is preference for a patch type, but movement behaviour does not vary.

5.3 Analysis of Scenario 1

We choose population dynamics parameter such that on patches of Type 1 (good patches), we have an activator–inhibitor sign-pattern (see Section 4.3), whereas on patches of Type 2 (bad patches), we have no positive coexistence state. Then, we can choose diffusion coefficients in patches of Type 1, such that Turing patterns would form on an infinite homogeneous landscape ($l_2 = 0$) of this type. No Turing patterns are possible on an infinite homogeneous landscape of Type 2 ($l_2 = 1$). By continuity, we expect that there is some threshold value of l_2, below which Turing patterns can form in homogenized equations (5.2.3), where $\hat{f}(U, V)$ and $\hat{g}(U, V)$ are defined in (5.2.17) and (5.2.18), respectively. This threshold value will depend on the other model parameters.

For this section, we choose the population dynamics parameters to be $b = 0.1$, $s = 0.2$ and $q = 0.8$, so that an activator–inhibitor sign pattern is satisfied in patches of Type 1 (see Section 4.4.2). On patches of Type 2, we choose $m = 0.6$. In the following section, we set the movement parameters equal in both patches; in later sections, we consider spatially varying movement and patch preferences.

5.3.1 Patchiness in terms of population dynamics

In this section, only population dynamics but not movement behaviour change between patch types. For the population dynamics parameters in patches of Type 1, we calculate the critical diffusion ratio for pattern formation on an infinite landscape of this type to be $D_c \approx 28.6$ (see Section 4.4.2). We choose diffusion rates for prey and predator on patches of Type 1 such that their ratio exceeds this critical ratio. Since the movement behaviour does not change between patches, we choose the same values for diffusion coefficients in patches of Type 2. Specifically, for simulations we set $D_1^v = D_2^v = 40$ and $D_1^u = D_2^u = 1$. We assume that there is no patch preference for either species, so that $p_1^u = p_1^v = 0.5$.

A minimum requirement for pattern formation is that there will be a coexistence state. Explicitly evaluating the steady-state expressions in (5.2.19)–(5.2.20) is tedious if not impossible. A weaker, necessary condition is that the prey can persist in the system. The prey can persist if it can grow at low density. To evaluate this condition,

we linearize system (5.2.3) at the trivial equilibrium and derive conditions for which $\hat{f}_U$ is positive. We find that $\hat{f}_U > 0$ if and only if

$$l_2 < \frac{1}{1 + m\frac{D_1^u}{D_2^u}(\frac{p_2^u}{p_1^u})}. \tag{5.3.1}$$

This value serves as an upper bound for the threshold that we are looking for.

To find the actual range of values for l_2 where pattern formation is possible, we evaluate conditions DDI 3 and DDI 4 numerically as functions of l_2 in the range where DDI 1 and DDI 2 are satisfied. We plot the left-hand side of DDI 3 in (5.2.12) as a function of l_2 (red curve in Figure 5.1). Hence, DDI 3 is satisfied wherever the curve is positive. For DDI 4, we plot the critical value of (5.2.13) of the homogenized diffusion coefficients, $\hat{D}_c$, as a function of l_2 (black solid in Figure 5.1). We also plot the actual ratio of the homogenized diffusion coefficients, $\frac{\hat{D}^v}{\hat{D}^u}$, as a function of l_2 (black dashed in Figure 5.1). Since the movement rates are identical between patches, this value is constant with respect to l_2. Then DDI 4 is satisfied when the black solid curve is below the black dashed line. The threshold value of l_2 for pattern formation is the smaller of the two values; in this case, it is the value where DDI 4 turns into an equality.

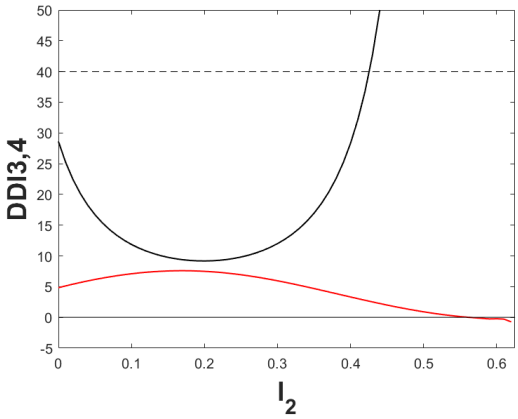

Figure 5.1: Illustrating the pattern formation conditions for Scenario 1 when movement rates are constant in space. The left-hand side of DDI 3 is plotted in red hence, DDI 3 is satisfied when the red curve is positive. The black curve is the critical ratio of the homogenized diffusion coefficients, $\hat{D}_c$, whereas the dashed line is the actual value of that ratio, $\frac{\hat{D}^v}{\hat{D}^u}$. Condition DDI 4 is satisfied where $\frac{\hat{D}^v}{\hat{D}^u} > \hat{D}_c$. The DDI conditions hold for the actual range of values $l_2 \in [0, 0.43]$.

We check this result by simulating homogenized model (5.2.3) using the Crank–Nicolson scheme. We fix all parameters as above. According to Figure 5.1, pat-

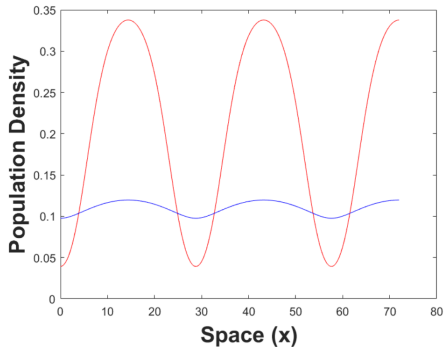

Figure 5.2: The periodic spatial pattern is the steady-state profile of (5.2.3) in Scenario 1, where $\hat{f}(U,V)$ and $\hat{g}(U,V)$ are defined in (5.2.17) and (5.2.18), respectively, for the prey (red) and predator (blue). The figure was obtained using the Crank–Nicolson scheme with the same numerical parameters as in Remark 4.4.1. Parameters are $b = 0.1$, $s = 0.2$, $q = 0.8$, $m = 0.6$, $D_1^u = D_2^u = 1$, $D_1^v = D_2^v = 40$, $p_1^u = p_2^u = 0.5$ and the domain length $L = 3w_c \approx 72$. The initial conditions are a small perturbation of the steady state. Here, a small perturbation was obtained by the random number generator with a maximal absolute value of 0.01.

tern formation can occur for $l_2 < 0.43$. We choose the specific value $l_2 = 0.3$ and simulate the system. With these parameter values, the steady state is given by $(U^*, V^*) \approx (0.1198, 0.0958)$ and the critical value of (5.2.13) of the homogenized diffusion coefficient is $\hat{D}_c \approx 12$. Figure 5.2 shows a periodic spatial pattern as the steady-state profile of our system. From it, we calculate $w_c \approx 24$ as the critical wavelength.

Now we investigate how the characteristics of the patterns depend on the size of bad patches, l_2. More precisely, we compare how the critical wave number and wavelength that arise from DDI 4 (when all other conditions are satisfied) depend on l_2. Since we have chosen the diffusion coefficients independent of patch type and the patch preferences to equal 1/2 (i.e., there is no patch preference), neither the diffusion coefficients not the patch preferences affect the averaged reaction terms $\hat{f}$ and $\hat{g}$. Also, the averaged diffusion coefficients equal the actual diffusion coefficients. Hence, the diffusion coefficients are independent parameters in the DDI conditions (just as they were in Chapter 4), and we can find the critical values. The situation will change in later sections.

We plot the critical wave number and wavelength as the red and blue curves, respectively, in Figure 5.3. For easier comparison, we include the critical values for a homogeneous landscape of Type 1 as the black dashed and solid lines. We observe that the critical wavelength is a concave up function of l_2. Compared to a homogeneous

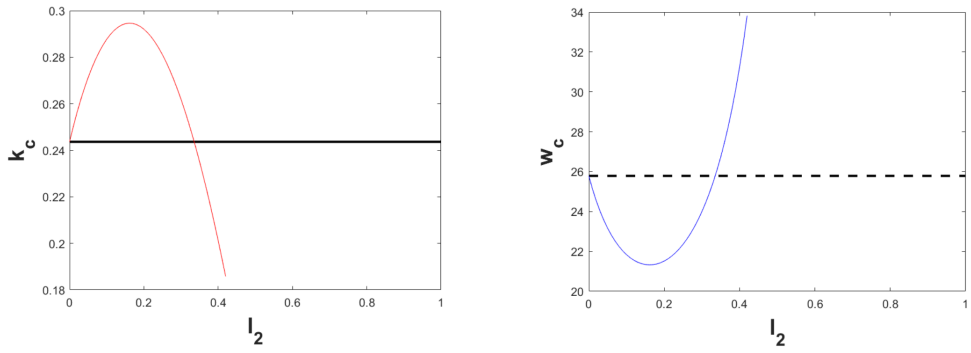

(a) (b)

Figure 5.3: The critical wave number (a) and critical wavelength (b) as a function of the size of bad patches. The black solid and dashed lines are the corresponding values in a homogeneous Type 1 landscape for comparison. Parameters are the same as in Figure 5.2.

Type 1 landscape, the critical wavelength first decreases as the size of Type 2 patches increases. Then there is a minimal value, and when bad patches become even larger, the critical wavelength of the pattern increases. It appears that patterns are lost when the critical wavelength approaches infinity.

5.3.2 Patchiness in terms of movement rates

In the previous section, movement behaviour was identical between the two patch types and there was no patch preference. Therefore, the homogenized diffusion coefficients were independent of the size of the two habitat types. There is ample evidence that individuals adjust their movement behaviour to their environment and do show preference for certain habitat types [18]. In this section, we explore how differences in movement rate affect pattern formation, in particular through conditions DDI 3 and DDI 4. In the next section, we study the effect of patch preference. Similar considerations in a discrete-patch model showed that spatially varying movement rates can significantly affect parameter ranges for DDI [15].

For the population dynamics parameters in patches of Type 1, the critical diffusion ratio for pattern formation on an infinite landscape of this type is $D_c \approx 28.6$ (see Section 4.4.2). We choose diffusion coefficients for both species in patches of Type 1 to be the same as Section 5.3.1. In our first scenario, we vary only the diffusion coefficient of species v on patches of Type 2. We set $D_1^v = 40$ and $D_1^u = D_2^u = 1$ as above and evaluate DDI conditions in the two-parameter plane of D_2^v and l_2. Our second scenario is the same, except that we vary the diffusion coefficient of species u

on patches of Type 2. For both scenarios, we assume that there is no patch preference for either species, so that $p_1^u = p_1^v = 0.5$.

The two plots in Figure 5.4 show the regions in parameter space where the four DDI conditions are or are not satisfied. As in the previous section, there is a threshold value of l_2, above which the prey cannot persist. This threshold is indicated as the 'Extinction Boundary' in pink. In the left plot, this threshold is a vertical line, because the critical value in (5.3.1) does not depend on D_2^v. In the right plot, it is a curve, since the threshold does depend on D_2^u. To the right of the extinction boundary, no patterns can form, because the prey cannot even persist. To the left of the boundary, all pattern-formation conditions are satisfied in the red area. Patterns cease to exist because DDI 4 is not satisfied (blue area). In the white area, conditions DDI 3 and 4 are both not satisfied, whereas in the green area, only DDI 3 is violated. Conditions DDI 1 and 2 are satisfied throughout the region where the prey can persist in the left plot, but there is a tiny region (orange) in the right plot, where DDI 1 is violated. Hence, there are (at least) two unstable modes in this case: the zero mode of a spatially constant perturbation with a pair of complex conjugate eigenvalues with positive real part, and a nonzero mode with positive real part for the usual diffusion-driven instability.

We simulated the non-spatial system in this region of parameter space and found that, indeed, the coexistence state was unstable and temporally oscillating solutions emerged (Figure 5.5(a)). These solutions correspond to spatially constant, time-periodic solutions of the reaction-diffusion system (5.2.3), because of the no-flux boundary conditions. We also simulated the reaction-diffusion system for the same parameter values with the initial condition a small random perturbation of the spatially constant coexistence state. Those simulations show the emergence of spatial patterns (Figure 5.5(b)).

Finally, we take a closer look at the region where pattern formation occurs by including information about the critical wavelength, similar to Figure 5.3. In Figure 5.6 and similar figures to follow, the white curve delineates the region where all DDI conditions are satisfied (blue to yellow colours) from where they are not (uniform blue colour). Where the DDI conditions are satisfied, colours indicate the level sets of the critical wavelength with lighter colours indicating longer wavelengths (see side bar). The critical wavelength was computed as follows: for a given set of parameters, the homogeneous steady state was calculated and the Jacobi matrix was evaluated there. The critical wavelength is then computed from the critical wave number, where condition DDI 4 becomes an equality. We emphasize that this value generally depends on the diffusion coefficients and the patch preferences through the averaging process. In particular, even if the Jacobi matrix has the required sign pattern, the choice of movement parameters may lead to DDI 4 not being satisfied. This is in contrast to the spatially homogeneous theory, where the Jacobi matrix is independent of the

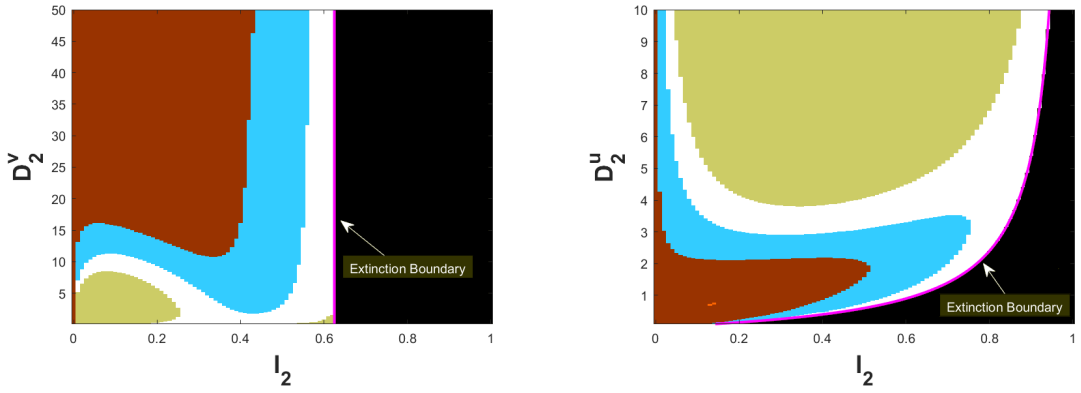

(a) (b)

Figure 5.4: Regions where DDI conditions do and do not hold when a diffusion coefficient depends on patch type. See text for color scheme. The pink curve shows the extinction boundary of the prey according to (5.3.1). Parameters are as in Figure 5.2 unless otherwise noted.

diffusion coefficients. In that case, as long as the Jacobi matrix has an appropriate sign pattern, one can always choose movement parameters so that condition DDI 4 is satisfied.

We see from Figure 5.6 that the pattern in Figure 5.3 is quite common: along a horizontal transect, the critical wavelength is a concave up function of l_2: it decreases for small l_2 and increases for larger l_2. The largest wavelengths occur as one approaches the boundary where pattern formation is possible. For the left plot in Figure 5.6, we note that there is an interval for D_2^v where pattern formation occurs for very small values of l_2 and again for intermediate values, but not in between. For the right plot in Figure 5.6, we note that the small region where the homogeneous steady state is unstable is shown with the white boundary.

From Figures 5.4 and 5.6, we see that it is possible to get patterns even for small values of D_2^v and for larger values of D_2^u. As long as patches of Type 2 are small enough, the homogenized diffusion coefficient is still large enough so that the DDI conditions are satisfied.

5.3.3 Patchiness in terms of patch preferences

In this section, we study the second aspect of movement behaviour in a patchy landscape: patch preference. We keep the diffusion coefficients constant in space. While it seems more reasonable to assume that organisms who can adjust their movement behaviour to local habitat conditions would adjust movement rate *and* patch preference,

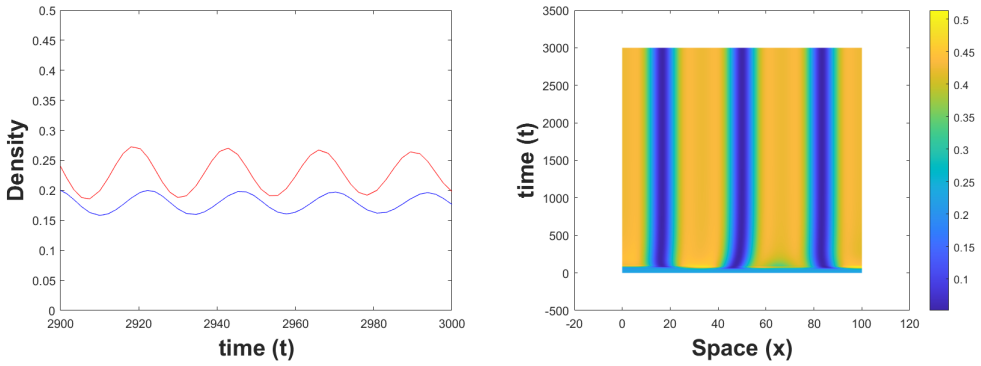

(a) (b)

Figure 5.5: Plot (a) shows a periodic orbit of the non-spatial system when DDI 1 is violated (orange area in Figure 5.4(b)). Densities of prey (red) and predator (blue) are plotted as functions of time. Plot (b) shows that a spatially periodic, temporally constant pattern emerges for the same parameter values in the reaction-diffusion system when the initial conditions are small perturbations of the (unstable) coexistence steady state. Only the prey density is shown. Parameters chosen from the orange region are (l_2, D_2^u)=(0.13, 0.72). Other parameters are as in Figure 5.4(b). Plot (b) was obtained with the Matlab's `pdepe` program with the same numerical parameters as in Remark 4.4.1. The domain length is $L = 100$.

we consider each aspect separately to disentangle the different effects.

For the population dynamics parameters in patches of Type 1, the critical diffusion ratio for pattern formation on an infinite landscape of this type remains the same as previous two sections, $D_c \approx 28.6$ (see Section 4.4.2). We choose diffusion rates for prey and predator on patches of Type 1 such that their ratio exceeds this critical ratio. Since the movement behaviour does not change between patches, we choose the same values for the diffusion coefficients in both patches. Specifically, for simulations, we set $D_1^v = D_2^v = 40$, $D_1^u = D_2^u = 1$. In our first scenario, we vary only the patch preference of the prey species (u) and set $p_1^v = 0.5$ as above. In the second scenario, we vary patch preference for the predator (v) but not for the prey ($p_1^u = 0.5$). We evaluate the DDI conditions and illustrate our results in two-parameter planes of the preference of Type 1 patches of prey (see Figure 5.7(a) with $p_1^u = 1 - p_2^u$) and predator (see Figure 5.7(b) with $p_1^v = 1 - p_2^v$).

Several conclusions that can be drawn from this figure are similar to those in the preceding figure. For example, for a fixed value of p_1^u or p_1^v, the critical wavelength is typically a concave-up function of l_2, and patterns disappear as the wavelength becomes large. At the boundary (white curve), condition DDI 4 becomes an equality

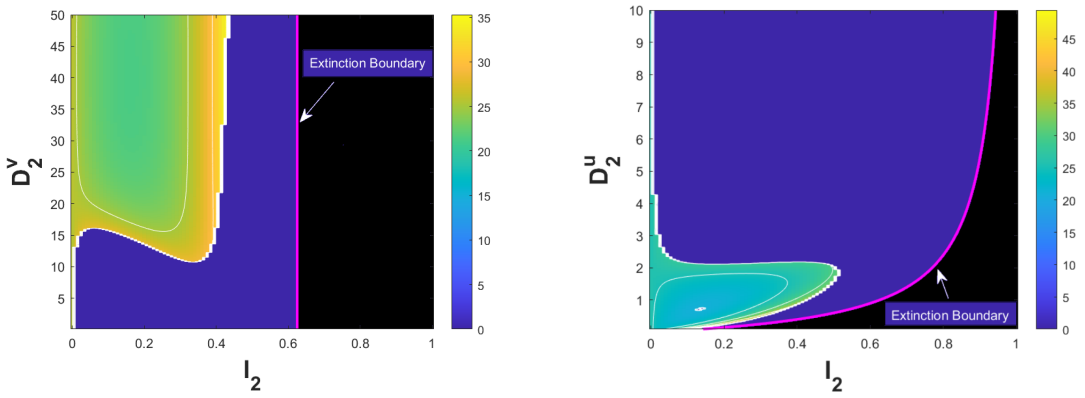

(a) (b)

Figure 5.6: Level sets of the critical wavelength as a function of l_2 and D_2^v (left plot) or D_2^u (right plot) for Scenario 1. Parameters, the black region and the extinction boundary are as in Figure 5.4.

and then fails to hold so that no patterns form. Also, pattern formation is possible for quite a wide range of parameter values. Interestingly, the pattern formation boundary is almost a horizontal line in plot (a): the critical value of p_1^u is nearly constant for a range of l_2 between 0.1 and 0.5. In plot (b), on the other hand, the boundary is nearly vertical near $l_2 \approx 0.45$ where p_1^v can range from around 0.3 to around 0.7 with no visible change in the pattern formation boundary.

In the middle of the turquoise region of Figure 5.7(a), we see a small white region. This occurs as before where condition DDI 1 is violated and the non-spatial system has a periodic orbit. The situation here is the same as in the corresponding situation in the previous section.

5.4 Analysis of Scenario 2a

In Scenario 1, the two patch types were chosen such that pattern formation occurred in a homogeneous landscape of Type 1 but not of Type 2. By shifting parameter l_2, which controls the relative size of the patch types, we could obtain patterns or have them disappear. In Scenario 2, we choose both patch types such that no patterns form on the corresponding homogeneous landscapes. Yet we will find that patterns can form for intermediate ratios of the two patch types in a heterogeneous landscape. We split this scenario into two cases: (a), we assume that the Jacobi matrix on Patch Type 1 has the correct sign pattern (activator–inhibitor), but the ratio of the diffusion rates is too small to generate patterns; (b) we assume that the sign pattern of the

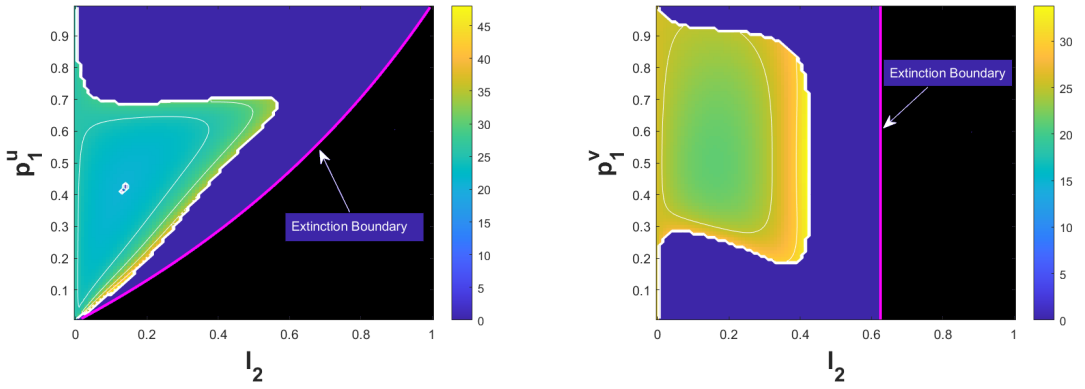

(a) (b)

Figure 5.7: Level sets of the critical wavelength as a function of l_2 and p_1^u (left plot) or p_1^v (right plot) for Scenario 1. The pink extinction boundary and the black region to the right of it are defined as in the preceding figures. Parameters are the same as in Figure 5.2 unless otherwise noted.

Jacobi matrix does not allow pattern formation on either patch type in isolation.

In this section, we choose parameters for population dynamics such that on patches of Type 1 (good patches), we have an activator–inhibitor sign-pattern (see Section 4.3) and conditions DDI 1 and DDI 2 are satisfied, whereas on patches of Type 2 (bad patches), we have no positive coexistence state. Then we calculate the critical diffusion ratio on patches of Type 1, where conditions DDI 3 and DDI 4 are satisfied, and choose a ratio smaller than that so that no patterns can form on an infinite homogeneous Type 1 landscape. Obviously, pattern formation is impossible on a homogeneous Type 2 landscape. We conduct the same numerical experiments as in the preceding section.

5.4.1 Patchiness in terms of population dynamics

We begin with the case where only population dynamics but not movement behaviour change between patch types. With the same population-dynamic parameters as in the preceding section, conditions DDI 1 and DDI 2 are satisfied on Type 1 patches, and the critical diffusion ratio is $D_c \approx 28.6$ as before (see also Section 4.4.2). We choose diffusion coefficients with a ratio smaller than that. Specifically, for simulations, we set $D_1^v = D_2^v = 15$ and $D_1^u = D_2^u = 1$, which gives a ratio of just over half of the critical ratio. We assume that there is no patch preference for either species, so that $p_1^u = p_1^v = 0.5$. As in Section 5.3, an upper bound for the threshold of l_2, above which the prey cannot persist, is given in (5.3.1).

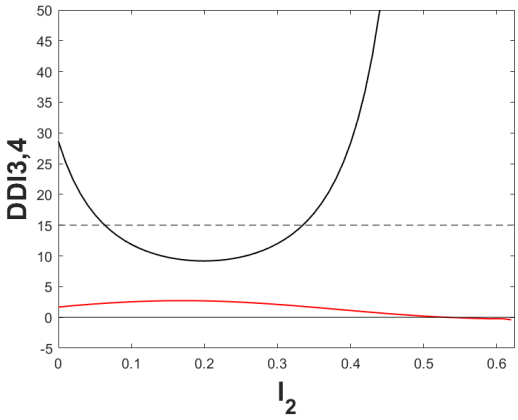

Figure 5.8: Illustrating the pattern-formation conditions for Scenario 2a when movement rates are constant in space. DDI 3 is satisfied when the red curve is positive. DDI 4 is satisfied when the black curve is below the black dashed line. The DDI conditions hold for the range $l_2 \in [0.06, 0.33]$.

To see whether pattern formation is possible for the homogenized model, we evaluate conditions DDI 3 and DDI 4 numerically as functions of l_2 in the range where DDI 1 and DDI 2 are satisfied. While condition DDI 3 is satisfied for all l_2 below some threshold (red curve in Figure 5.8), DDI 4 is satisfied only for intermediate values of l_2 but not as l_2 approaches zero (black curve in Figure 5.8). This behaviour, of course, reflects our choice of condition DDI 4 not being satisfied on a homogeneous Type 1 landscape. We compare and contrast this with Figure 5.1, where condition DDI 4 holds for all small enough l_2 because condition DDI 4 holds on a homogeneous Type 1 landscape there.

As before, we check whether and which patterns actually form by simulating homogenized model (5.2.3), where $\hat{f}(U, V)$ and $\hat{g}(U, V)$ are given by (5.2.17) and (5.2.18), respectively. We use the Crank–Nicolson scheme. We choose a specific value for l_2 in the range where the preceding analysis predicts pattern formation (here $l_2 = 0.1$), and we fix the other parameters as mentioned above. With these parameter values, the steady state is given by $(U^*, V^*) \approx (0.279, 0.223)$, and the critical value of (5.2.13) for the homogenized diffusion coefficient is $\hat{D}_c \approx 11.86$. Figure 5.9 shows a spatially periodic pattern as the steady-state profile of our system. From it, we calculate $w_c \approx 21.84$ as the critical wavelength.

5.4.2 Patchiness in terms of movement rates

We continue our investigation of Scenario 2a by choosing the movement rates to vary as we did in Scenario 1, Section 5.3.2. While keeping population dynamics parameters

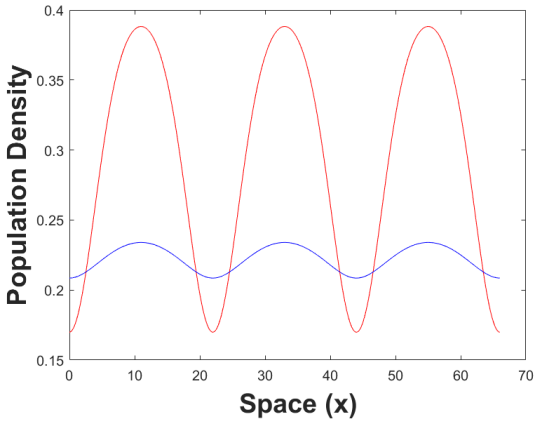

Figure 5.9: The periodic spatial pattern is the steady-state profile of (5.2.3) in Scenario 2a for the prey (red) and predator (blue). The figure was obtained using the Crank–Nicolson scheme with the same numerical and population dynamics parameters as in Figure 5.8, except that here $D_1^v = D_2^v = 15$. The domain length is $L = 3w_c \approx 66$.

as in the first part of Scenario 2a, we now choose $D_1^v = 15$ and $D_1^u = D_2^u = 1$ and evaluate DDI conditions in the two-parameter plane of D_2^v and l_2; see Figure 5.10(a). We also vary the diffusion coefficient of species u on patches of Type 2 see Figure 5.10(b). For both scenarios, we assume that there is no patch preference for either species, so that $p_1^u = p_1^v = 0.5$.

In Figure 5.10, the white curve delineates the region where all DDI conditions are satisfied (blue to yellow colours) from where they are not all satisfied (uniform blue colour). Where the DDI conditions are satisfied, the colours indicate the level sets of the wavelength of emerging patterns with lighter colours indicating longer wavelengths (see side bar). As in the previous section, there is a threshold of l_2, the 'Extinction Boundary' (pink), above which the prey cannot persist.

Figure 5.10 shares many similarities with Figure 5.6 but also shows some crucial differences. The most important is that pattern formation is impossible for very small *and* large values of l_2 by our choice of Scenario 2a. Nonetheless, we see that pattern formation is possible for a large range of intermediate parameter values. Patterns are more likely to form when D_2^v is large or D_2^u is small, since then the ratio of the homogenized diffusion coefficients is larger, and we know that this ratio typically needs to be large for patterns to form.

Similar to Figure 5.6, Figure 5.10(a) also shows that for fixed values of D_2^v, the critical wavelength is a concave up function of l_2. Patterns cease to exist when the wavelength approaches infinity. The situation is similar in Figure 5.10(b) where the

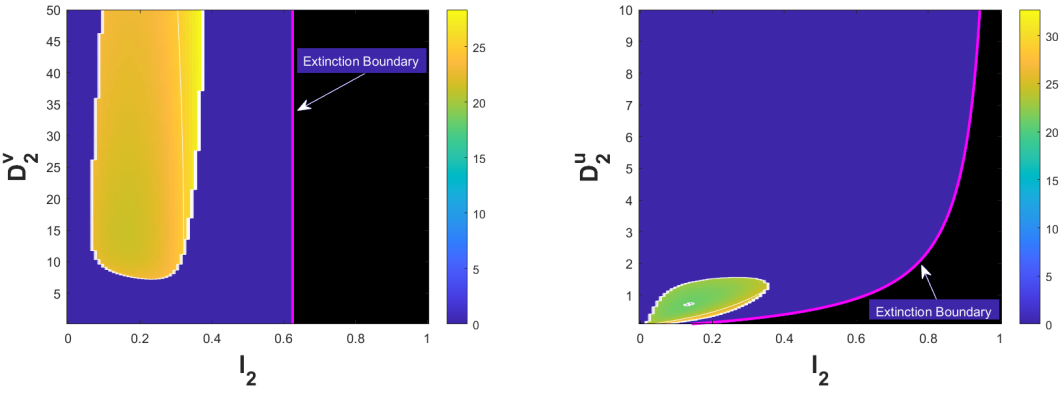

(a) (b)

Figure 5.10: Level sets of the critical wavelength as a function of l_2 and D_2^v (left plot) or D_2^u (right plot) for Scenario 2a. Parameters, the black region and the extinction boundary are as in Figure 5.9.

critical wavelength is concave up with respect to l_2 for any fixed D_2^u. In that Figure, we also see again a small spot where condition DDI 1 is violated in the turquoise region. As in the scenarios before, there is a periodic orbit in the non-spatial system.

5.4.3 Patchiness in terms of patch preferences

We conclude our investigation of Scenario 2a by varying the patch preferences of the two species while keeping other parameters fixed, similar to what we did in Scenario 1, Section 5.3.3. Parameters other than patch preferences are set exactly as in Section 5.4.1. As in Figure 5.7, we vary the patch preference of the predator and prey species separately and evaluate the corresponding DDI conditions. We present and illustrate our results as contours of critical wave lengths in the corresponding two-parameter planes of $p_1^u = 1 - p_2^u$ or $p_1^v = 1 - p_2^v$ and l_2; see Figure 5.11.

The plots in Figure 5.11 should be compared to those in Figure 5.7. They show a number of similarities, but their biggest difference is that pattern formation is not possible for $l_2 = 0$ by the setting of Scenario 2. Hence, there is a region without pattern formation near $l_2 = 0$. Interestingly, when p_1^u is very small, pattern formation is possible for very small values of l_2. There seems to be a trade-off: when l_2 is small, bad patches are small, but when the preference for these bad patches is high, their effect appears larger. As before, for fixed values of patch preferences, the critical wavelength is a concave-up function of l_2.

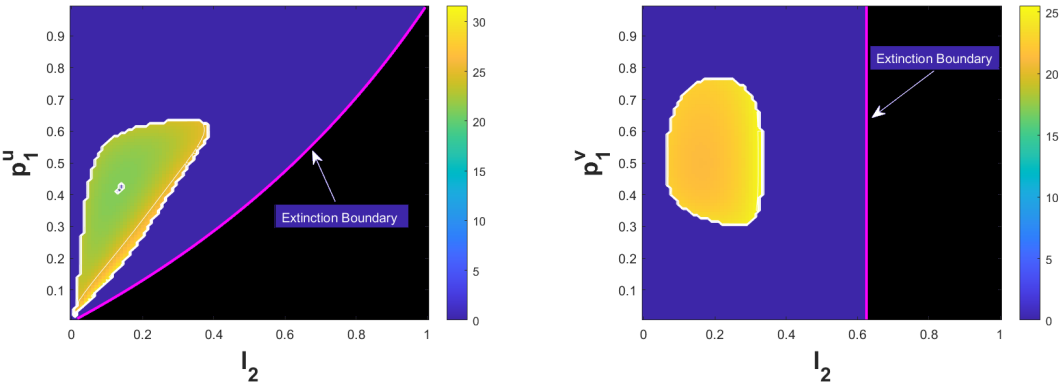

(a) (b)

Figure 5.11: Level sets of the critical wavelength as a function of l_2 and p_1^u (left plot) or p_1^v (right plot) for Scenario 2a. The pink extinction boundary and the black region to the right of it are defined as in the preceding figures. Parameters are the same as in Figure 5.8 unless otherwise noted.

5.5 Analysis of Scenario 2b

In contrast to the last two sections, we now choose population dynamics parameters such that on patches of Type 1 (good patches), we do not have an activator–inhibitor sign-pattern (see Section 4.3). It is therefore impossible to get Turing patterns on a homogeneous Type 1 landscape. More precisely, by choosing parameter q to be less than q_A (see Section 4.4.1), the (1,1)-entry in the Jacobi matrix is negative. This means that condition DDI 3 cannot be satisfied for any values of the diffusion coefficients, even though conditions DDI 1 and DDI 2 can be. Patches of Type 2 (bad patches) remain the same as before, where we have no positive coexistence state, so that no Turing patterns are possible on an infinite homogeneous landscape on Type 2.

For numerical simulations, we choose the population dynamics parameters $b = 0.1$, $s = 0.2$ and $q = 0.5 < q_A \approx 0.672$. This ensures that the Jacobi matrix on Type 1 patches does not have an activator–inhibitor pattern. On patches of Type 2, we choose $m = 0.6$ as before. As in the previous scenarios, we first set the movement parameters equal in both patches; later, we consider spatially varying movement and patch preferences.

5.5.1 Patchiness in terms of population dynamics

As in the previous scenarios, we begin our investigation of Scenario 2b with the case where only population dynamics but not movement behaviour changes between patch types. Set $D_1^v = D_2^v = 40$, and $D_1^u = D_2^u = 1$. We assume that there is no patch preference for either species, so that $p_1^u = p_2^v = 0.5$. As before, (5.3.1) defines a threshold of l_2, above which the prey cannot persist.

We begin with the analogue of Figures 5.1 and 5.8; i.e., we visualize conditions DDI 3 and DDI 4 as a function of l_2. We checked that conditions DDI 1 and DDI 2 are satisfied in the range $l_2 \in [0, 0.6]$. The plot in Figure 5.12 shows that condition DDI 4 is satisfied for l_2 near zero, but DDI 3 is not. This is in contrast to Scenario 1, where both were satisfied near zero, and Scenario 2a, where DDI 3 was satisfied near zero but DDI 4 was not. As l_2 is increased, DDI 4 is violated before DDI 3 holds. Then there is an intermediate range of l_2 where both conditions hold (approximately for $l_2 \in [0.29, 0.44]$) before both are violated for larger values of l_2.

We can explain the emergence of an activator–inhibitor sign pattern for intermediate values of l_2 mathematically and biologically. Mathematically, we note that the prey density at the coexistence state decreases as l_2 increases. Furthermore, the derivative of $\hat{f}$ with respect to U, the (1,1)-entry of the Jacobi matrix, is a decreasing function of U. Hence, there can be a range of l_2 where U is small enough to make this entry positive and give the required sign pattern. Biologically speaking, the productivity of a population (its rate of change) is typically the highest at intermediate population densities. At low density, there are not enough individuals around; at high density, there are too many. When there are bad patches into which some individuals are moving, the steady state density is decreased, and productivity is increased. If productivity is high enough, we have an activator.

As in the last two scenarios, we illustrate pattern formation by simulating homogenized model (5.2.3), using the Crank–Nicolson scheme. We fix all parameters as above and choose $l_2 = 0.4$. Then the steady state is given by $(U^*, V^*) \approx (0.1296, 0.0648)$, and the critical value of (5.2.13) of the homogenized diffusion coefficient is $\hat{D}_c \approx 28.84$. Figure 5.13 shows a periodic spatial pattern as the steady-state profile of our system. From it, we calculate $w_c \approx 32.53$ as the critical wavelength.

5.5.2 Patchiness in terms of movement rates

In the previous section, movement behaviour was identical between the two patch types, so that the homogenized diffusion coefficients were independent of the sizes of the two habitat types. Similar to Sections 5.3.2 and 5.4.2, we now explore how differences in movement rate affect pattern formation, in particular through conditions DDI 3 and DDI 4. As before, we vary D_2^v and D_2^u as well as l_2 and visualize the

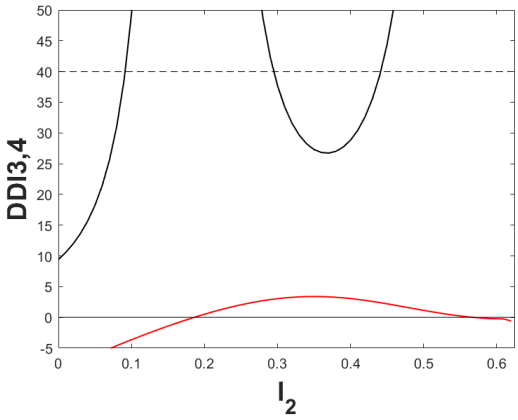

Figure 5.12: Illustrating the pattern formation conditions in Scenario 2b when movement rates are constant in space. DDI 3 is satisfied when the red curve is positive. DDI 4 is satisfied when the black curve is below the black dashed line. The DDI conditions hold for the range $l_2 \in [0.29, 0.44]$.

critical wavelength in the corresponding parameter planes. Unless otherwise noted, all parameters are as in Section 5.5.1.

In Figure 5.14, the colour coding, the extinction boundary and the white curve that delineates the regions where pattern formation is possible are exactly the same as in previous figures; e.g., Figure 5.3. No pattern formation is possible near $l_2 = 0$. Figure 5.14(a) shows the intermediate range of l_2 where pattern formation is possible provided D_2^v is large enough. Similarly, Figure 5.14(b) shows the intermediate range of l_2 where patterns can form when D_2^u is small enough. We note that pattern formation is possible very close to the extinction boundary here. As we have seen in all previous plots of this kind, the largest wavelengths occur as one approaches the boundary where pattern formation is possible.

5.5.3 Patchiness in terms of patch preferences

We conclude our investigation of Scenario 2b by allowing patch preferences to vary while keeping movement rates constant in space, as we did in Sections 5.3.3 and 5.4.3. Population dynamics parameters and diffusion coefficients are as in Section 5.5.1. We evaluate the DDI conditions and illustrate our results in two-parameter planes of the preference of Type 1 patches of prey (see Figure 5.15(a) with $p_1^u = 1 - p_2^u$) and predator (see Figure 5.15(b) with $p_1^v = 1 - p_2^v$).

Several conclusions that can be drawn from this figure are similar to those in the corresponding preceding figures. For example, at the boundary (white curve),

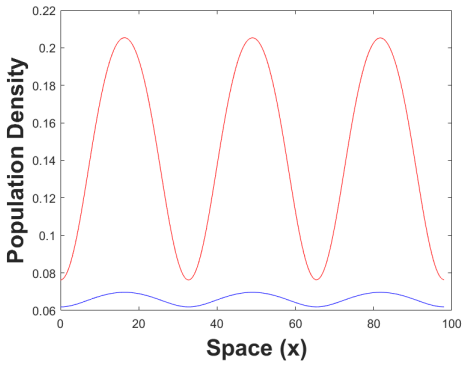

Figure 5.13: The periodic spatial pattern is the steady-state profile of (5.2.3) in Scenario 2b for the prey (red) and predator (blue). The figure was obtained using the Crank–Nicolson scheme with the same numerical and population dynamics parameters as in Figure 5.2, except that here $q = 0.5$. The domain length is $L = 3w_c \approx 98$.

condition DDI 4 becomes an equality and then fails to hold so that no patterns form. Pattern formation is not possible for quite a wide range of parameter values, especially in plot (b). When the preference of the prey for patches of Type 1 is large, no patterns can form. When the preference is low, in particular when prey prefer patches of Type 2, patterns can form for intermediate values of l_2. The biological explanation behind this mathematical observation is again in the question of release from intraspecific competition. When prey have a preference for Type 1 patches, not many leave for Type 2 patches; hence, there is no relief from this competition. When the preference is for Type 2 patches and those patches are large enough, the release from competition is strong enough so that an activator–inhibitor sign pattern exists and patterns can form. If, however, the Type 2 patches are too long, the overall population density will be too small for pattern formation.

In plot (a), as the preference of prey for patches of Type 1 (p_1^u) increases, we get Turing patterns for the larger value and wider range of l_2. Moreover, in this plot, we can see that when p_1^u exceeds 0.5, l_2 needs to be large enough for patterns to form. The reason is again that a large enough bad patch will provide release from intraspecific competition in patches of Type 1. Finally, in contrast to plots (a) in Figures 5.7 and 5.11, in this plot, we do not have any hole in the region where we get patterns. In plot (b), we observe that it is possible to get patterns when p_1^v varies approximately between 0.3 and 0.7, but only when Type 2 patches are long enough.

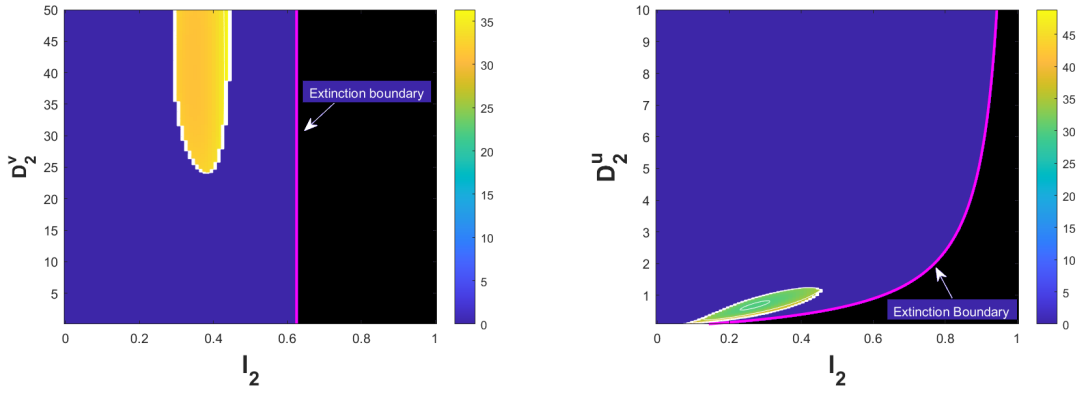

(a) (b)

Figure 5.14: Level sets of the critical wavelength as a function of l_2 and D_2^v (left plot) or D_2^u (right plot) for Scenario 2b. Parameters, the black region and the extinction boundary are as in Figure 5.13.

5.6 Conclusion and discussion

Spatial patterns are ubiquitous in ecological systems and are widely investigated using reaction-diffusion equations that account for the random motion and population dynamics of the species involved. The pioneering work of pattern formation was conducted by Turing [70], who discovered pattern formation through DDI by deriving conditions under which a spatially homogeneous steady state that is stable in the absence of diffusion becomes unstable in the presence of diffusion. This mechanism determines the spatial pattern that evolves [36, 50]. Although Turing's study was originally proposed in chemistry, his idea spread to biology; e.g., developmental biology and animal-coat patterns [50]. Turing patterns are generated by the interaction of two substances, an activator and an inhibitor, with different diffusion rates: the inhibitor must diffuse faster than the activator.

We specialize the general Turing pattern idea to ecological population dynamics and predator–prey interactions. A few authors explored the application of DDI to population dynamics in ecology. The model by Segel and Jackson [63], the Beddington–DeAngelis model [8], the ratio-dependent model [5] and the May model [48] show that the simple interactions of prey and predator can support DDI to get pattern formation in a homogeneous landscape. In these models, the prey is an activator and the predator is an inhibitor [1, 49, 72]. However, the Rosenzweig–MacArthur model [62], one of the most prominent predator–prey models, does not support DDI to get Turing patterns [53]. Fasani and Rinaldi found ways to include additional mechanisms in the Rosenzweig–MacArthur model, some of which lead to DDI. In their model, however,

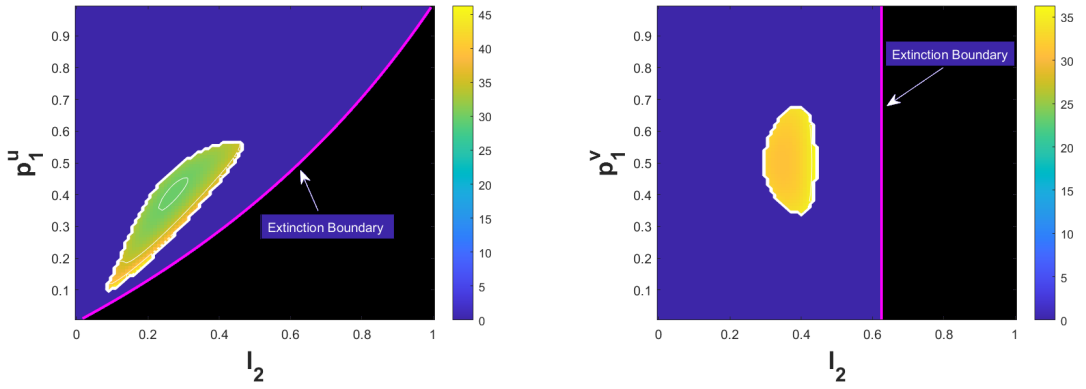

(a) (b)

Figure 5.15: Level sets of the critical wavelength as a function of l_2 and p_1^u (left plot) or p_1^v (right plot) for Scenario 2b. The pink extinction boundary and the black region to the right of it are defined as in the preceding figures. Parameters are the same as in Figure 5.12 unless otherwise noted.

the prey is an inhibitor and the predator is an activator. In contrast to the previous predator–prey models, which had an activator-inhibitor structure, this one gives rise to a positive feedback structure (see (4.3.2)). Accordingly, pattern formation can occur if the prey disperses far and the predator does not.

In this chapter, we studied Turing-pattern formation in three different scenarios for three important aspects of heterogeneity for our predator–prey model. Since we assumed that our landscape period is small, we could study pattern formation in a patchy landscape by applying the homogenization technique to derive the homogenized model. Then we used the same approach as in Chapter 4 to derive DDI conditions for this simplified model to explore DDI for our scenarios in Sections 5.3–5.5. We used numerical evaluation to analyze and visualize the DDI conditions because the expressions are too complex for analytical insights; see expressions (5.2.19)–(5.2.20). We also simulated the homogenized model to test the prediction of the DDI conditions. In most plots of this chapter, we explored the patterning capabilities of our model with spatially varying parameters l_2, the size of bad patches. The main result of this chapter showed that, even if it is impossible to get patterns in a homogeneous landscape, by adding bad patches to obtain a patchy landscape, heterogeneity could generate pattern formation. In particular, in Scenario 2b, we showed how spatial heterogeneity could turn a system without an activator–inhibitor sign structure into the system that has one to generate patterns.

There are a number of similarities and differences between our approach and the ones by Benson et al. and Page et al. to study spatial patterns [10, 11, 57]. In the

model by Benson et al., only the diffusion coefficients depend on space. Hence, the steady state is constant in space. They chose diffusion coefficients such that pattern formation is possible on one side of the two-patch domain but not on the other. Under appropriate conditions, they found that patterns can emerge on the entire domain through DDI. In the model by Page et al., only the population dynamics change in space but not the diffusion terms. They showed that, under some conditions, the mismatch of the steady state at the interface can generate patterns that are centred around this discontinuity and then decay away from it to the boundaries of the domain. Our mechanism of pattern formation is different from one in Benson et al. and Page et al. We assumed that we have a large landscape with many small patches and applied homogenization theory to study spatial patterns. The resulting patterns occur across the entire domain over several patch lengths, and they are generated by Turing instability rather than the discontinuity at the interface. Benson et al. and Page et al. considered the length of patches to be larger than the length of the patterns and saw a variation of the densities in one patch. Instead, we assumed that the pattern wavelength is much larger than the length of patches. There is currently no theory in place to study the case when the pattern wavelength and patch length are comparable.

Our study in this chapter was closest to the one by Cobbold et al. [15], but there are some differences as well. Since our study is a continuous-space version of their model, the first difference is that Cobbold et al. used the discrete patches in terms of space, while we had continuous patches. The other main difference is related to the approaches that were used to study pattern formation. We explored spatial patterns by using the homogenization technique, whereas Cobbold et al. used two different approaches: (i) a numerical bifurcation analysis with a finite number of patches; (ii) linear stability analysis with an infinite number of patches. Several of our results are similar to those of Cobbold et al. For example, they found that no patterns form when prey movement was heavily biased toward good patches. Similar behaviour results can be found in our work, as seen in Figures 5.11(a) and 5.15(a). Cobbold et al. also compared the range of pattern formation in a homogeneous landscape with a heterogeneous landscape. They showed that the range of parameter q that leads to pattern formation in a homogeneous landscape is much smaller than in a heterogeneous landscape. We reached a similar conclusion when we compared our result in Chapter 4 with Chapter 5, specially in Scenario 2b by comparing parameter q in two different landscapes.

In this chapter, we studied the effect of heterogeneity on Turing patterns in a framework of partial differential equations with specific functional responses for each of patch-types. We chose the May model on good patches and the no-growth model for prey on bad patches. We showed that, over some range of parameters, we can get patterns. If we replace the May model by the Beddington–DeAngelis functional

response, we also observe that it is possible to get Turing patterns for some range of the size of bad patches (l_2). Hence, an interesting task is to replace the May model on Type 1 patches with different functional responses such as the ratio-dependent model [5] and the modified Rosenzweig–MacArthur model that was introduced by Fasani and Rinaldi [23]. Then we can study how heterogeneity may affect Turing patterns for each of these models in terms of how the characteristics of the patterns such as the wavelength etc. depend on the size of bad patches, l_2. Another interesting question is to explore spatial patterns when we have no more strict bad and good type of patches; e.g., a heterogeneous landscape consists of two different type of patches, with the same functional form of the model, say the May model, but different values for our model parameters. More generally, the question is how robust our results are, for example, with respect to other modelling assumptions or the arrangement of patches.

In this chapter, we only simulated our homogenized predator–prey model. Another obvious question is to simulate our model in a heterogeneous landscape, including the discontinuity conditions at the interface, to explore how close the results of our patterns in a patchy landscape are to its homogenized model. This also can be done with a finite difference scheme. We leave this for future work.

Chapter 6

Summary and discussion

Problems related to population dynamics, population persistence and spatial spread rates are fundamental to spatial ecology. Spatial population dynamics are often studied via reaction-diffusion equations [13], which have not only generated a number of important ecological insights but also some deep mathematical results. There are a lot of spatially explicit ecological theories for homogeneous environments. The study of spatial spread phenomena which has many applications to spatially homogeneous models, started with Fisher [24]. These include spread rates of biological invasions by Andow et al. [4] and Lewis et al. [40] or critical patch sizes in conservation biology by Skellam [66]. While spatially homogeneous models have been studied in detail with their applications, spatially heterogeneous models are largely studied from an abstract analytical point of view. We used mathematical models to study some aspects of spatial ecology in a heterogeneous landscape, especially to explore how heterogeneity affects different characteristics of steady-state solutions (see Chapter 3) and Turing-pattern formation (see Chapter 5).

A heterogeneous landscape means that population dynamics and individual movements change spatially. In general, spatially heterogeneous models are almost prohibitively difficult to parameterize, since they require too many data points. Also, the available mathematical results are often too abstract and require numerical evaluation. One potential way forward was proposed by Shigesada et al. [65], who studied persistence and invasions in piecewise constant, periodic landscapes. This simplification not only significantly reduced the number of parameters in the model, it also allowed explicit analytical results that are easy to evaluate and apply. Maciel and Lutscher [46] extended their model framework by introducing individual movement behaviour at interfaces between different habitat types, based on earlier work by Ovaskainen and Cornell [55]. Many empirical studies collect the required data (see, for example, references in Crone et al. [18]), and the qualitative behaviour of the models with interface behaviour differs significantly from those without [2, 38, 44, 46, 47].

However, almost all results on the resulting reaction-diffusion systems with interface matching conditions are based on linear analysis (but see Freedman [26] and Maciel et al. [45]).

We studied several applications of reaction-diffusion equations as the mathematical modelling framework for population dynamics in a heterogeneous landscape with the interface conditions to represent movement behaviour. The results fall into two categories:

(i) How the total population abundance at steady state can exceed the total carrying capacity; see Chapter 3.

(ii) How heterogeneity affects Turing-pattern formation; see Chapter 5.

We addressed these questions by starting our studies with Chapter 2, where we provided all the necessary analytical background on semigroup theory and other analytical aspects. We then proved the existence and uniqueness of solutions for the simplest meaningful patchy reaction-diffusion equation by applying semigroup theory. In Chapter 3, we proved the existence, uniqueness and global stability of steady states, and we classified their qualitative shape depending on movement behaviour. We then applied our results to study the question of why and under which conditions the total population abundance at steady state may exceed the total carrying capacity of the landscape. In Chapter 4, we gave some background on the concept of DDI and Turing patterns on a homogeneous environment. We then explored the impacts of diffusion coefficients on the formation of spatial patterns in a general predator–prey system by analyzing the DDI conditions at the steady state in a one-dimensional homogeneous landscape. We illustrated the general conditions using the May model, and we performed numerical simulations to visualize the results of spatial patterns. In Chapter 5, we studied Turing-pattern formation on patchy landscapes, where we had an infinite landscape divided into periodically alternating patches, patches of Type 1 and Type 2, with appropriate interface conditions. On Type 1 patches, we considered the May model, and on Type 2 patches, we replaced logistic growth for the prey by a simple death term. We then derived its corresponding homogenized model by the homogenization technique as the practical tool to investigate Turing patterns. In fact, we performed these studies by analyzing the DDI conditions for the homogenized model at the steady state. Finally, we illustrated our results with numerical simulations.

A real landscape is not necessarily homogeneous but is almost always heterogeneous. By adding heterogeneity in our model, we had more complexity to study analytical and numerical aspects of steady state and Turing patterns. However, we showed in Chapter 5 that heterogeneity could bring some advantages for our model to promote spatial patterns. For example, changes in a landscape that increase heterogeneity could lead to emergent patterns where there were none to begin with. In

particular, in Scenario 2b, we showed that spatial heterogeneity could turn a system without an activator–inhibitor sign structure into a system that has one to generate patterns. This is an interesting result, especially from the viewpoint of biologists.

In Chapter 3, we proved the existence and uniqueness of a steady state in our model for two patches. We can relate our Chapter 5 to Chapter 3 by posing the question of uniqueness with more than two patches. For example, with four good patches and four bad patches, do we still have uniqueness of the steady state? We leave this as future work.

In Chapter 5, we explored Turing-pattern formation in a heterogeneous landscape with infinitely many alternatively good and bad patches by finding the homogeneous steady state and evaluating the DDI conditions for the homogenized model. Another task to explore is: if we cut the landscape with enough periodic patches, is it still possible to see patterns?

Appendix A

Homogenization technique

Homogenization is a technique that can proficiently accommodate small-scale variation in environmental heterogeneity for large-scale movement patterns [73]. This process is an efficient tool to predict large-scale dynamics for populations with individuals moving differently in different habitat types.

Homogenization techniques have been applied to partial differential equations with Fickian diffusion terms [54] and with ecological diffusion [29, 30] in order to determine the impact of small-scale habitat variation on large-scale movement and to explore the asymptotic spread speed. Yurk and Cobbold used homogenization techniques to find the wave speed for unstructured populations [74], and Cobbold et al. used homogenization techniques to find the speed of a predator invading a prey [75]. In this appendix, which is extracted and extended from the paper by Cobbold et al. [75], we show how to apply homogenization to the patchy landscape model to obtain the homogenized model, for which we study pattern formation in Chapter 5.

A.1 The model and the homogenization ansatz

We consider a predator–prey model in the same set-up as system (5.2.1) with interface conditions (5.2.2). In patches of Type i, the differential equations are

$$\frac{\partial u_i(x,t)}{\partial t} = D_i^u \frac{\partial^2 u_i(x,t)}{\partial x^2} + f_i\left(u_i, v_i\right), \tag{A.1.1}$$

$$\frac{\partial v_i(x,t)}{\partial t} = D_i^v \frac{\partial^2 v_i(x,t)}{\partial x^2} + g_i\left(u_i, v_i\right), \tag{A.1.2}$$

where $x \in (x_{i-1}, x_i)$, $i = 0, \pm 1, \pm 2, \ldots$ are the interface points and D_i^u (D_i^v) denotes the prey (predator) diffusion coefficient. Functions f_i and g_i denote the prey and predator growth functions, respectively.

The interface conditions are:

$$(1-\beta_i^u)D_{i+1}^u u_{i+1}(x_i^+,t) = \beta_i^u D_i^u u_i(x_i^-,t), \tag{A.1.3}$$

$$D_{i+1}^u \frac{\partial u_{i+1}(x_i^+,t)}{\partial x} = D_i^u \frac{\partial u_i(x_i^-,t)}{\partial x}, \tag{A.1.4}$$

$$(1-\beta_i^v)D_{i+1}^v v_{i+1}(x_i^+,t) = \beta_i^v D_i^v v_i(x_i^-,t), \tag{A.1.5}$$

$$D_{i+1}^v \frac{\partial v_{i+1}(x_i^+,t)}{\partial x} = D_i^v \frac{\partial v_i(x_i^-,t)}{\partial x}, \tag{A.1.6}$$

where

$$\beta_i^u = \begin{cases} 1-p^u, & \text{for } i \text{ odd}, \\ p^u, & \text{for } i \text{ even}, \end{cases}$$

and similarly for β_i^v. Parameter p^u (p^v) denotes the probability that the prey (predator) moves to the patch of Type 1. We denote the length of Type i patches on the landscape as L_i. Here, the period $\epsilon = L = L_1 + L_2 \ll 1$ is chosen to be small with respect to x, and we introduce $y = \frac{x}{\epsilon}$ as a new variable. The notation $l_i = \frac{L_i}{\epsilon}$ is used here to denote the patch length on the small scale so that they satisfy $l_1 + l_2 = 1$.

In this homogenization method, we use the residence index as described in [68]. For patches of Types 1 and 2, the residence indices for the prey are given by

$$r_1^u = \frac{1}{D_1^u(1-p^u)} \quad \text{and} \quad r_2^u = \frac{1}{D_2^u p^u}, \tag{A.1.7}$$

respectively. The residence index for predator on patches of Types 1 and 2 can be similarly defined. The residence index is used to approximate the patch equilibrium population density that would arise solely through the dispersal process. For notational convenience, the piecewise-constant periodic functions $r^u(y)$ and $r^v(y)$ are defined as the values r_i^u and r_i^v on patches of Type i, respectively. Here, $\langle\cdot\rangle$ is applied to denote the average of a function over one spatial period. In particular, the average residence index for prey is

$$\langle r^u \rangle = \frac{l_1 r_1^u + l_2 r_2^u}{l_1 + l_2} = \frac{\frac{l_1}{(1-p^u)D_1^u} + \frac{l_2}{p^u D_2^u}}{l_1 + l_2}, \tag{A.1.8}$$

and similarly for predator.

Assume that the diffusion coefficients and the density functions change accordingly to the variable y inside all patches and that the density functions of prey and predator depend on both scales x and y. Treating the two spatial scales, x and y, as independent induces a change in the spatial derivatives, $\partial x \to \partial x + \epsilon^{-1}\partial y$. This formula may be viewed as a consequence of the chain rule for differentiation. As a result, equations (A.1.1) and (A.1.2) become

$$\frac{\partial u(x,y,t)}{\partial t} = D_i^u(\partial x + \epsilon^{-1}\partial y)^2 u(x,y,t) + f_i\left(u,v\right), \tag{A.1.9}$$

$$\frac{\partial v(x,y,t)}{\partial t} = D_i^v(\partial x + \epsilon^{-1}\partial y)^2 v(x,y,t) + g_i\left(u,v\right). \tag{A.1.10}$$

For the interface conditions (A.1.3)–(A.1.6), we obtain

$$(1-\beta_i^u)D_{i+1}^u u(x,y_i^+,t) = \beta_i^u D_i^u u(x,y_i^-,t), \tag{A.1.11}$$

$$D_{i+1}^u\left(\frac{\partial}{\partial x} + \epsilon^{-1}\frac{\partial}{\partial y}\right)u(x,y_i^+,t) = D_i^u\left(\frac{\partial}{\partial x} + \epsilon^{-1}\frac{\partial}{\partial y}\right)u(x,y_i^-,t), \tag{A.1.12}$$

$$(1-\beta_i^v)D_{i+1}^v v(x,y_i^+,t) = \beta_i^v D_i^v v(x,y_i^-,t), \tag{A.1.13}$$

$$D_{i+1}^v\left(\frac{\partial}{\partial x} + \epsilon^{-1}\frac{\partial}{\partial y}\right)v(x,y_i^+,t) = D_i^v\left(\frac{\partial}{\partial x} + \epsilon^{-1}\frac{\partial}{\partial y}\right)v(x,y_i^-,t). \tag{A.1.14}$$

By expanding the density functions in formal power series in ϵ, we get

$$u(x,y,t) = u_0(x,y,t) + \epsilon u_1(x,y,t) + \epsilon^2 u_2(x,y,t) + \cdots, \tag{A.1.15}$$

$$v(x,y,t) = v_0(x,y,t) + \epsilon v_1(x,y,t) + \epsilon^2 v_2(x,y,t) + \cdots. \tag{A.1.16}$$

The goal is to find an approximation to the solution that is valid as $\epsilon \to 0$. In particular, we seek the leading-order solutions $u_0(x,y,t)$ and $v_0(x,y,t)$. We note that as $\epsilon \to 0$, $y = \frac{x}{\epsilon} \to \infty$, even for finite x. Thus, we must be concerned about the behaviour of the $u_i(x,y,t)$ functions as $y \to \infty$ for all i.

We rewrite the two-scale model (A.1.9)–(A.1.14) in a more convenient form by using the residence index [68] and the dynamical level [66]. For convenience, the piecewise constant functions are defined as $\beta^u(y) = \beta_i^u$ and $\beta^v(y) = \beta_i^v$, for $y \in (y_{i-1}, y_i)$ in a similar way as we defined for the residence index in equation (A.1.7).

Finally, Cobbold et al. defined $\tilde{\Gamma}^u(x,y,t)$ and $\tilde{\Gamma}^v(x,y,t)$ corresponding to the dynamic level for the population density [66, 68], which are given by

$$\tilde{\Gamma}^u(x,y,t) = \frac{u(x,y,t)}{r^u(y)} \quad \text{and} \quad \tilde{\Gamma}^v(x,y,t) = \frac{v(x,y,t)}{r^v(y)}. \tag{A.1.17}$$

If the system of equations (A.1.9)–(A.1.14) evolves toward the equilibrium solution $r^u(y)$ and $r^v(y)$ in the absence of population dynamics ($f_i, g_i = 0$), then the dynamic level evolves to become spatially uniform. In this way, we obtain the following formulation that is different from Yurk and Cobbold [74].

The multi-scale model (A.1.9)–(A.1.14) can be written in terms of the dynamic level as

$$\frac{\partial \tilde{\Gamma}^u(x,y,t)}{\partial t} = D_i^u(\partial x + \epsilon^{-1}\partial y)^2\tilde{\Gamma}^u(x,y,t) + D_i^u F_i\left(\tilde{\Gamma}^u(x,y,t), \tilde{\Gamma}^v(x,y,t)\right), \tag{A.1.18}$$

$$\frac{\partial \tilde{\Gamma}^v(x,y,t)}{\partial t} = D_i^v(\partial x + \epsilon^{-1}\partial y)^2\tilde{\Gamma}^v(x,y,t) + D_i^v G_i\left(\tilde{\Gamma}^u(x,y,t), \tilde{\Gamma}^v(x,y,t)\right), \tag{A.1.19}$$

with the following interface conditions:

$$\tilde{\Gamma}^u(x, y_i^+, t) = \tilde{\Gamma}^u(x, y_i^-, t), \tag{A.1.20}$$

$$(\beta_{i+1}^u)^{-1}(\partial x + \epsilon^{-1}\partial y)\tilde{\Gamma}^u(x, y_i^+, t) = (\beta_i^u)^{-1}(\partial x + \epsilon^{-1}\partial y)\tilde{\Gamma}^u(x, y_i^-, t), \tag{A.1.21}$$

$$\tilde{\Gamma}^v(x, y_i^+, t) = \tilde{\Gamma}^v(x, y_i^-, t), \tag{A.1.22}$$

$$(\beta_{i+1}^v)^{-1}(\partial x + \epsilon^{-1}\partial y)\tilde{\Gamma}^v(x, y_i^+, t) = (\beta_i^v)^{-1}(\partial x + \epsilon^{-1}\partial y)\tilde{\Gamma}^v(x, y_i^-, t). \tag{A.1.23}$$

We also get

$$F_i(\tilde{\Gamma}^u, \tilde{\Gamma}^v) = \beta_i^u f_i(r_i^u\tilde{\Gamma}^u, r_i^v\tilde{\Gamma}^v) \qquad \text{and} \qquad G_i(\tilde{\Gamma}^u, \tilde{\Gamma}^v) = \beta_i^v g_i(r_i^u\tilde{\Gamma}^u, r_i^v\tilde{\Gamma}^v). \tag{A.1.24}$$

Note that conditions (A.1.20) and (A.1.22) imply that the dynamical levels are continuous at each y_i if we define

$$\tilde{\Gamma}^u(x, y_i, t) = \tilde{\Gamma}^u(x, y_i^+, t) = \tilde{\Gamma}^u(x, y_i^-, t), \quad \text{and} \quad \tilde{\Gamma}^v(x, y_i, t) = \tilde{\Gamma}^v(x, y_i^+, t) = \tilde{\Gamma}^v(x, y_i^-, t). \tag{A.1.25}$$

The perturbation ansatz (A.1.15) and (A.1.16) may also be written in terms of the dynamical levels as

$$\tilde{\Gamma}^u \sim \tilde{\Gamma}_0^u(x, y, t) + \epsilon\tilde{\Gamma}_1^u(x, y, t) + \epsilon^2\tilde{\Gamma}_2^u(x, y, t) + \cdots, \tag{A.1.26}$$

and

$$\tilde{\Gamma}^v \sim \tilde{\Gamma}_0^v(x, y, t) + \epsilon\tilde{\Gamma}_1^v(x, y, t) + \epsilon^2\tilde{\Gamma}_2^v(x, y, t) + \cdots, \tag{A.1.27}$$

respectively, where $\tilde{\Gamma}_i^u = \frac{u_i(x,y,t)}{r^u(y)}$ $\left(\tilde{\Gamma}_i^v = \frac{v_i(x,y,t)}{r^v(y)}\right)$. We denote $\tilde{\Gamma}_0^u = \tilde{U}$ and $\tilde{\Gamma}_0^v = \tilde{V}$.

We assume that F_i and G_i in equation (A.1.24) satisfy the relationship

$$F_i(\tilde{\Gamma}^u, \tilde{\Gamma}^v) = F_i(\tilde{U}, \tilde{V}) + O(\epsilon) \quad \text{and} \quad G_i(\tilde{\Gamma}^u, \tilde{\Gamma}^v) = G_i(\tilde{U}, \tilde{V}) + O(\epsilon), \tag{A.1.28}$$

respectively, which is true for many commonly used reaction terms.

We apply the method of homogenization to find a leading order solution $\tilde{\Gamma}_0^u(x, y, t)$ by inserting the perturbation ansatz (A.1.26) into model (A.1.18) with interface conditions (A.1.20) and (A.1.21), to get

$$\begin{aligned}
\frac{\partial}{\partial t}\left(\tilde{\Gamma}_0^u + \epsilon\tilde{\Gamma}_1^u + \epsilon^2\tilde{\Gamma}_2^u + \cdots\right) &= D_i^u(\partial x + \epsilon^{-1}\partial y)^2\left(\tilde{\Gamma}_0^u + \epsilon\tilde{\Gamma}_1^u + \epsilon^2\tilde{\Gamma}_2^u + \cdots\right) \\
&\quad + D_i^u\Big(F_i(\tilde{U}, \tilde{V}) + \mathcal{O}(\epsilon)\Big), \\
\left(\tilde{\Gamma}_0^u + \epsilon\tilde{\Gamma}_1^u + \epsilon^2\tilde{\Gamma}_2^u + \cdots\right)(x, y_i^+, t) &= \left(\tilde{\Gamma}_0^u + \epsilon\tilde{\Gamma}_1^u + \epsilon^2\tilde{\Gamma}_2^u + \cdots\right)(x, y_i^-, t),
\end{aligned} \tag{A.1.29}$$

$$\begin{aligned}
(\beta_{i+1}^u)^{-1}(\partial x + \epsilon^{-1}\partial y)\left(\tilde{\Gamma}_0^u + \epsilon\tilde{\Gamma}_1^u + \epsilon^2\tilde{\Gamma}_2^u + \cdots\right)(x, y_i^+, t) = \\
(\beta_i^u)^{-1}(\partial x + \epsilon^{-1}\partial y)\left(\tilde{\Gamma}_0^u + \epsilon\tilde{\Gamma}_1^u + \epsilon^2\tilde{\Gamma}_2^u + \cdots\right)(x, y_i^-, t),
\end{aligned}$$

and similarly for v.

A.1.1 Equation of order ϵ^{-2}

We refer to (A.1.29) to write the system of order ϵ^{-2} as

$$D_i^u \frac{\partial^2 \tilde{\Gamma}_0^u(x,y,t)}{\partial y^2} = 0, \quad \text{for } y \in (y_{i-1}, y_i),\ i = 0, \pm 1, \pm 2, \ldots, \tag{A.1.30}$$

where

$$\tilde{\Gamma}_0^u(x, y_i^+, t) = \tilde{\Gamma}_0^u(x, y_i^-, t), \tag{A.1.31}$$

$$(\beta_{i+1}^u)^{-1} \frac{\partial \tilde{\Gamma}_0^u(x, y_i^+, t)}{\partial y} = (\beta_i^u)^{-1} \frac{\partial \tilde{\Gamma}_0^u(x, y_i^-, t)}{\partial y}, \tag{A.1.32}$$

We multiply equation (A.1.30) by $r^u(y)$ and integrate to obtain

$$\int_{y_0^+}^{y} \beta^u(s)^{-1} \frac{\partial^2 \tilde{\Gamma}_0^u(x,s,t)}{\partial y^2} \mathrm{d}s = 0. \tag{A.1.33}$$

Then we write the above integral as

$$\int_{y_{j-1}^+}^{y} \beta^u(s)^{-1} \frac{\partial^2 \tilde{\Gamma}_0^u(x,s,t)}{\partial y^2} \mathrm{d}s + \sum_{i=1}^{j-1} \int_{y_{i-1}^+}^{y_i^-} \beta^u(s)^{-1} \frac{\partial^2 \tilde{\Gamma}_0^u(x,s,t)}{\partial y^2} \mathrm{d}s = 0, \tag{A.1.34}$$

where $y \in (y_{j-1}, y_j)$ for some $j \in \mathbb{Z}$, and we adopt the convention that if $j = 1$, then the sum on the right is 0. We note that $\beta^u(y)$ is constant within each patch and integrate (A.1.34) to obtain

$$\begin{aligned}(\beta_j^u)^{-1} \left(\frac{\partial \tilde{\Gamma}_0^u(x,y,t)}{\partial y} - \frac{\partial \tilde{\Gamma}_0^u(x, y_{j-1}^+, t)}{\partial y} \right) \\ + \sum_{i=1}^{j-1} (\beta_i^u)^{-1} \left(\frac{\partial \tilde{\Gamma}_0^u(x, y_i^-, t)}{\partial y} - \frac{\partial \tilde{\Gamma}_0^u(x, y_{i-1}^+, t)}{\partial y} \right) = 0.\end{aligned} \tag{A.1.35}$$

We then use interface condition (A.1.32), which causes the sum to telescope to simplify (A.1.35) and obtain

$$\frac{\partial \tilde{\Gamma}_0^u(x,y,t)}{\partial y} = \beta^u(y) a_0(x,t), \tag{A.1.36}$$

where $a_0(x,t) = (\beta_1^u)^{-1} \frac{\partial \tilde{\Gamma}_0^u(x, y_0^+, t)}{\partial y}$.

Next, we integrate equation (A.1.36) and then apply interface condition (A.1.31) to obtain

$$\tilde{\Gamma}_0^u(x,y,t) = \tilde{\Gamma}_0^u(x,y_0,t) + a_0(x,t) \int_{y_0}^{y} \beta^u(s) \mathrm{d}s. \tag{A.1.37}$$

We need $\tilde{\Gamma}_0^u(x,y,t)$ to be bounded as $y \to \infty$. Hence, we require $a_0(x,t) = 0$. Thus, $\tilde{\Gamma}_0^u(x,y,t) = \tilde{\Gamma}_0^u(x,y_0,t)$ for all $y \geq y_0$, or, more simply,

$$\tilde{\Gamma}_0^u(x,y,t) = \tilde{U}(x,t). \tag{A.1.38}$$

Remark A.1.1. *By applying the same procedure to (A.1.19), we find that* $\tilde{\Gamma}_0^v(x,y,t) = \tilde{\Gamma}_0^v(x,y_0,t)$ *for all* $y \geq y_0$*, or, more simply,*

$$\tilde{\Gamma}_0^v(x,y,t) = \tilde{V}(x,t).$$

A.1.2 Equation of order ϵ^{-1}

We refer again to (A.1.29) and write the equation of order ϵ^{-1}:

$$D_i^u \left(2\frac{\partial^2 \tilde{U}}{\partial y \partial x} + \frac{\partial^2 \tilde{\Gamma}_1^u}{\partial y^2} \right)(x,y,t) = 0, \quad \text{for } y \in (y_{i-1}, y_i),\ i = 0, \pm 1, \pm 2, \ldots, \tag{A.1.39}$$

where

$$\tilde{\Gamma}_1^u(x, y_i^+, t) = \tilde{\Gamma}_1^u(x, y_i^-, t), \tag{A.1.40}$$

$$(\beta_{i+1}^u)^{-1} \left(\frac{\partial \tilde{U}(x,t)}{\partial x} + \frac{\partial \tilde{\Gamma}_1^u(x, y_i^+, t)}{\partial y} \right) = (\beta_i^u)^{-1} \left(\frac{\partial \tilde{U}(x,t)}{\partial x} + \frac{\partial \tilde{\Gamma}_1^u(x, y_i^-, t)}{\partial y} \right), \tag{A.1.41}$$

Since $\tilde{U}(x,t)$ is independent of y, we may write $2\dfrac{\partial^2 \tilde{U}(x,t)}{\partial y \partial x} = \dfrac{\partial^2 \tilde{U}(x,t)}{\partial y \partial x}$. Then we multiply equation (A.1.39) by $r^u(y)$ and integrate to obtain

$$\int_{y_0^+}^{y} \beta^u(s)^{-1} \left(\frac{\partial^2 \tilde{U}}{\partial y \partial x} + \frac{\partial^2 \tilde{\Gamma}_1^u}{\partial y^2} \right)(x,s,t) \mathrm{d}s = 0. \tag{A.1.42}$$

In the same procedure to how equation (A.1.36) was obtained, equation (A.1.42) may be written as

$$\begin{aligned} \int_{y_{j-1}^+}^{y} \beta^u(s)^{-1} \left(\frac{\partial^2 \tilde{U}}{\partial y \partial x} + \frac{\partial^2 \tilde{\Gamma}_1^u}{\partial y^2} \right)(x,s,t) \mathrm{d}s \\ + \sum_{i=1}^{j-1} \int_{y_{i-1}^+}^{y_i^-} \beta^u(s)^{-1} \left(\frac{\partial^2 \tilde{U}}{\partial y \partial x} + \frac{\partial^2 \tilde{\Gamma}_1^u}{\partial y^2} \right)(x,s,t) \mathrm{d}s = 0, \end{aligned} \tag{A.1.43}$$

where $y \in (y_{j-1}, y_j)$ for some $j \in \mathbb{Z}$. We may express the integral on the right-hand side as a sum that telescopes by applying interface condition (A.1.41). After simplification, we obtain

$$\left(\frac{\partial \tilde{U}}{\partial x} + \frac{\partial \tilde{\Gamma}_1^u}{\partial y}\right)(x, y, t) = \beta^u(y) a_1(x, t), \tag{A.1.44}$$

where $a_1(x,t) = (\beta_1^u)\left(\frac{\partial \tilde{U}}{\partial x} + \frac{\partial \tilde{\Gamma}_1^u}{\partial y}\right)(x, y_0^+, t)$. Then by integrating equation (A.1.44) and applying interface condition (A.1.40), we get

$$\tilde{\Gamma}_1^u(x, y, t) = a_1(x, t) \int_{y_0^+}^{y} \beta^u(s) \mathrm{d}s - y \frac{\partial \tilde{U}(x, t)}{\partial x} + b_1(x, t), \tag{A.1.45}$$

where $b_1(x,t) = y_0 \frac{\partial \tilde{U}(x,t)}{\partial x} + \tilde{\Gamma}_1^u(x, y_0^+, t)$. We need $\tilde{\Gamma}_1^u(x, y, t)$ to be bounded as $y \to \infty$. Thus, we require the first two terms on the right-hand side of equation (A.1.45) to be balanced in the limit, and then we get

$$a_1(x, t) = \langle \beta^u \rangle^{-1} \frac{\partial \tilde{U}(x, t)}{\partial x}, \tag{A.1.46}$$

where $\langle \beta^u \rangle$ is the arithmetic average of β^u over a period

$$\langle \beta^u \rangle = \frac{\int_{y_0}^{y} \beta^u(s) ds}{y} = \frac{\beta_1^u l_1 + \beta_2^u l_2}{l_1 + l_2} = \frac{(1 - p^u) l_1 + p^u l_2}{l_1 + l_2}. \tag{A.1.47}$$

By substituting (A.1.46) into (A.1.45), we find

$$\tilde{\Gamma}_1^u(x, y, t) = \left(\langle \beta^u \rangle^{-1} \int_{y_0^+}^{y} \beta^u(s) \mathrm{d}s - y\right) \frac{\partial \tilde{U}(x, t)}{\partial x} + b_1(x, t). \tag{A.1.48}$$

Remark A.1.2. *By applying the same procedure to (A.1.19), we obtain*

$$\tilde{\Gamma}_1^v(x, y, t) = \left(\langle \beta^v \rangle^{-1} \int_{y_0^+}^{y} \beta^v(s) \mathrm{d}s - y\right) \frac{\partial \tilde{V}(x, t)}{\partial x} + b_1'(x, t), \tag{A.1.49}$$

where $b_1'(x,t) = y_0 \frac{\partial \tilde{V}(x,t)}{\partial x} + \tilde{\Gamma}_1^v(x, y_0^+, t)$ *and* $\tilde{\Gamma}_1^v(x, y_0^+, t) = \tilde{\Gamma}_1^v(x, y_0^-, t)$.

A.1.3 Equation of order ϵ^0

We refer to (A.1.29) and write the equation of order ϵ^0:

$$\frac{\partial \tilde{U}}{\partial t} = D_i^u \left(\frac{\partial^2 \tilde{U}}{\partial x^2} + 2\frac{\partial^2 \tilde{\Gamma}_1^u}{\partial y \partial x} + \frac{\partial^2 \tilde{\Gamma}_2^u}{\partial y^2}\right) + D_i^u F_i(\tilde{U}, \tilde{V}), \quad \text{for } y \in (y_{i-1}, y_i),\ i = 0, \pm 1, \pm 2, \ldots, \tag{A.1.50}$$

where

$$\tilde{\Gamma}_2^u(x, y_i^+, t) = \tilde{\Gamma}_2^u(x, y_i^-, t), \tag{A.1.51}$$

$$(\beta_{i+1}^u)^{-1}\left(\frac{\partial\tilde{\Gamma}_1^u}{\partial x} + \frac{\partial\tilde{\Gamma}_2^u}{\partial y}\right)(x, y_i^+, t) = (\beta_i^u)^{-1}\left(\frac{\partial\tilde{\Gamma}_1^u}{\partial x} + \frac{\partial\tilde{\Gamma}_2^u}{\partial y}\right)(x, y_i^-, t), \tag{A.1.52}$$

In equation (A.1.50), we applied the assumption (A.1.28). We multiply equation (A.1.50) by $r^u(y)$ and integrate to obtain

$$\begin{aligned}\frac{\partial\tilde{U}}{\partial t}\int_{y_0^+}^{y} r^u(y)\mathrm{d}s = &\int_{y_0^+}^{y}\beta^u(s)^{-1}\frac{\partial}{\partial y}\left(\frac{\partial\tilde{\Gamma}_2^u}{\partial y} + \frac{\partial\tilde{\Gamma}_1^u}{\partial x}\right)(x, s, t)\mathrm{d}s \\ &+ \int_{y_0^+}^{y}\beta^u(s)^{-1}\frac{\partial}{\partial x}\left(\frac{\partial\tilde{\Gamma}_1^u}{\partial y} + \frac{\partial\tilde{U}}{\partial x}\right)(x, s, t)\mathrm{d}s \\ &+ \int_{y_0^+}^{y}\beta^u(s)^{-1}F(\tilde{U}, \tilde{V}, s)\mathrm{d}s.\end{aligned} \tag{A.1.53}$$

By applying interface equation (A.1.52), the first integral on the right-hand side of the above equation telescopes to become

$$\int_{y_0^+}^{y}\beta^u(s)^{-1}\frac{\partial}{\partial y}\left(\frac{\partial\tilde{\Gamma}_2^u}{\partial y} + \frac{\partial\tilde{\Gamma}_1^u}{\partial x}\right)(x, s, t)\mathrm{d}s = \beta^u(y)^{-1}\left(\frac{\partial\tilde{\Gamma}_2^u}{\partial y} + \frac{\partial\tilde{\Gamma}_1^u}{\partial x}\right)(x, y, t) - a_2(x, t), \tag{A.1.54}$$

where $a_2(x,t) = (\beta_1^u)^{-1}\left(\frac{\partial\tilde{\Gamma}_2^u}{\partial y} + \frac{\partial\tilde{\Gamma}_1^u}{\partial x}\right)(x, y_0^+, t)$. We may also substitute (A.1.48) into equation (A.1.54) to obtain

$$\begin{aligned}\int_{y_0^+}^{y}\beta^u(s)^{-1}\frac{\partial}{\partial y}\left(\frac{\partial\tilde{\Gamma}_2^u}{\partial y} + \frac{\partial\tilde{\Gamma}_1^u}{\partial x}\right)(x, s, t)\mathrm{d}s = &\beta^u(y)^{-1}\frac{\partial\tilde{\Gamma}_2^u}{\partial y} \\ &+\beta^u(y)^{-1}\left(\langle\beta^u\rangle^{-1}\int_{y_0^+}^{y}\beta^u(s)\mathrm{d}s - y\right)\frac{\partial^2\tilde{U}}{\partial x^2} - a_2(x, t) + \beta^u(y)^{-1}\frac{\partial b_1(x, t)}{\partial x}.\end{aligned} \tag{A.1.55}$$

By applying equation (A.1.44), the second integral on the right-hand side of (A.1.53) can be simplified to

$$\int_{y_0^+}^{y}\beta^u(s)^{-1}\frac{\partial}{\partial x}\left(\frac{\partial\tilde{\Gamma}_1^u}{\partial y} + \frac{\partial\tilde{U}}{\partial x}\right)(x, s, t)\mathrm{d}s = \frac{\partial a_1(x, t)}{\partial x}(y - y_0). \tag{A.1.56}$$

Substituting (A.1.46) into equation (A.1.56), and substituting the result along with (A.1.55) into equation (A.1.53), we obtain

$$\frac{\partial\tilde{U}}{\partial t}\int_{y_0^+}^{y} r^u(y)\mathrm{d}s = \left(\beta^u(y)^{-1}\left(\langle\beta^u\rangle^{-1}\int_{y_0^+}^{y}\beta^u(s)\mathrm{d}s - y\right) + (y - y_0)\langle\beta^u\rangle^{-1}\right)\frac{\partial^2\tilde{U}}{\partial x^2}$$

$$-a_2(x,t)+\beta^u(y)^{-1}\frac{\partial b_1(x,t)}{\partial x}+\int_{y_0^+}^{y}\beta^u(s)^{-1}F(\tilde{U},\tilde{V},s)\mathrm{d}s$$
$$+\beta^u(y)^{-1}\frac{\partial\tilde{\Gamma}_2^u}{\partial y}. \tag{A.1.57}$$

Then we solve equation (A.1.57) for $\frac{\partial\tilde{\Gamma}_2^u}{\partial y}$ and integrate, applying interface condition (A.1.51), to obtain

$$\begin{aligned}\tilde{\Gamma}_2^u(x,y,t)-\tilde{\Gamma}_2^u(x,y_0,t)=-\Bigg[&\left(\langle\beta^u\rangle^{-1}\int_{y_0^+}^{y}\left(\int_{y_0^+}^{s}\beta^u(w)\mathrm{d}w\right)\mathrm{d}s-\frac{y^2}{2}-\frac{y_0^2}{2}\right)\\&+\langle\beta^u\rangle^{-1}\int_{y_0^+}^{y}s\beta^u(s)\mathrm{d}s-\langle\beta^u\rangle^{-1}y_0\int_{y_0^+}^{y}\beta^u(s)\mathrm{d}s\Bigg]\frac{\partial^2\tilde{U}}{\partial x^2}\\&+a_2(x,t)\int_{y_0^+}^{y}\beta^u(s)\mathrm{d}s-(y-y_0)\frac{\partial b_1(x,t)}{\partial x}\\&-\int_{y_0^+}^{y}\beta^u(s)\left(\int_{y_0^+}^{s}(\beta^u(w))^{-1}F(\tilde{U},\tilde{V},w)\mathrm{d}w\right)\mathrm{d}s\\&+\left[\int_{y_0^+}^{y}\beta^u(s)\left(\int_{y_0^+}^{s}r^u(w)\mathrm{d}w\right)\mathrm{d}s\right]\frac{\partial\tilde{U}}{\partial t}.\end{aligned} \tag{A.1.58}$$

By using the method of integration by parts for the following integral while taking care near discontinuities at the interface, we find

$$\int_{y_0^+}^{y}\left(\int_{y_0^+}^{s}\beta^u(w)\mathrm{d}w\right)\mathrm{d}s=y\int_{y_0^+}^{y}\beta^u(s)\mathrm{d}s-\int_{y_0^+}^{y}s\beta^u(s)\mathrm{d}s. \tag{A.1.59}$$

This allows us to simplify (A.1.58) to

$$\begin{aligned}\tilde{\Gamma}_2^u(x,y,t)=\Bigg[&-\left(\langle\beta^u\rangle^{-1}y\int_{y_0^+}^{y}\beta^u(s)\mathrm{d}s-\frac{y^2}{2}\right)\frac{\partial^2\tilde{U}}{\partial x^2}\\&-\int_{y_0^+}^{y}\beta^u(s)\left(\int_{y_0^+}^{s}\beta^u(w)^{-1}F(\tilde{U},\tilde{V},w)\mathrm{d}w\right)\mathrm{d}s\\&+\left(\int_{y_0^+}^{y}\beta^u(s)\left(\int_{y_0^+}^{s}r^u(w)\mathrm{d}w\right)\mathrm{d}s\right)\frac{\partial\tilde{U}}{\partial t}\Bigg]\\&+\Bigg[\left(\langle\beta^u\rangle^{-1}y_0\int_{y_0^+}^{y}\beta^u(s)\mathrm{d}s\right)\frac{\partial^2\tilde{U}}{\partial x^2}\\&+a_2(x,t)\int_{y_0^+}^{y}\beta^u(s)\mathrm{d}s-(y-y_0)\frac{\partial b_1(x,t)}{\partial x}\Bigg]\end{aligned}$$

$$+\left[-(\frac{y_0^2}{2})\frac{\partial^2\tilde{U}}{\partial x^2}+\tilde{\Gamma}_2^u(x,y_0,t)\right]. \tag{A.1.60}$$

In the above equation, the three terms in the first square brackets are $O(y^2)$, the three terms in the next brackets are $O(y)$, and the two terms in the last square brackets are $O(y^0)$ as $y\to\infty$. In order for $\tilde{\Gamma}_2^u$ to remain bounded, it is necessary for the $O(y^2)$ terms to be balanced in this limit. Thus, we get

$$\left(\int_{y_0^+}^{y}\beta^u(s)\left(\int_{y_0^+}^{s}r^u(w)\mathrm{d}w\right)\mathrm{d}s\right)\frac{\partial\tilde{U}}{\partial t}=\left(\langle\beta^u\rangle^{-1}y\int_{y_0^+}^{y}\beta^u(s)\mathrm{d}s-\frac{y^2}{2}\right)\frac{\partial^2\tilde{U}}{\partial x^2}$$
$$+\int_{y_0^+}^{y}\beta^u(s)\left(\int_{y_0^+}^{s}\beta^u(w)^{-1}F(\tilde{U},\tilde{V},w)\mathrm{d}w\right)\mathrm{d}s. \tag{A.1.61}$$

Next, we begin to simplify equation (A.1.61). We assumed $l_1+l_2=1$. Then β^u and r^u are periodic with period 1:

$$\beta^u(y+1)=\beta^u(y)\quad\text{and}\quad r^u(y+1)=r^u(y). \tag{A.1.62}$$

For convenience, we set the lower limits of integration to $y_0^+=-\frac{1}{2}$. First, we start with the integral on the left-hand side of (A.1.61). So, we define $\eta^u(y)$ as follows

$$\eta^u(y)=\int_{y_0^+}^{y}r^u(w)\mathrm{d}w=\int_{-\frac{1}{2}}^{y}r^u(w)\mathrm{d}w. \tag{A.1.63}$$

Since we are interested in the limit as $y\to\infty$ in (A.1.61), we may assume that $y>0$ in the following calculations. In this case, $\eta^u(y)$ can be expressed as the sum

$$\eta^u(y)=\int_{\frac{1}{2}(2m-1)}^{y}r^u(w)\mathrm{d}w+\sum_{i=0}^{m-1}\int_{\frac{1}{2}(2i-1)}^{\frac{1}{2}(2i+1)}r^u(w)\mathrm{d}w, \tag{A.1.64}$$

where m is chosen so that

$$\frac{1}{2}(2m-1)\le y<\frac{1}{2}(2m+1). \tag{A.1.65}$$

Since r^u is periodic with period 1, each of the last m terms on the right-hand side of (A.1.64) are equal to $\int_{-\frac{1}{2}}^{\frac{1}{2}}r^u(w)\mathrm{d}w$. As a result, we obtain

$$\eta^u(y)=m\int_{-\frac{1}{2}}^{\frac{1}{2}}r^u(w)\mathrm{d}w+\int_{\frac{1}{2}(2m-1)}^{y}r^u(w)\mathrm{d}w. \tag{A.1.66}$$

Now, we express the integral in the left-hand side of (A.1.61) similar to above as follows

$$\int_{-\frac{1}{2}}^{y} \beta^u(s)\eta^u(s)\mathrm{d}s = \int_{\frac{1}{2}(2n-1)}^{y} \beta^u(s)\eta^u(s)\mathrm{d}s + \sum_{i=0}^{n-1} \int_{\frac{1}{2}(2i-1)}^{\frac{1}{2}(2i+1)} \beta^u(s)\eta^u(s)\mathrm{d}s, \quad \text{(A.1.67)}$$

where n is chosen so that

$$\frac{1}{2}(2n-1) \leq y < \frac{1}{2}(2n+1). \quad \text{(A.1.68)}$$

We will develop bounds for the last n terms on the right-hand side of (A.1.67). The limit of integration of these integrals restricts the relevant values of s, so that $\eta^u(s)$ needs only to be considered for $\frac{1}{2}(2i-1) \leq s < \frac{1}{2}(2i+1)$. Thus, according to (A.1.65) and (A.1.66), these integrals can be written as,

$$\begin{aligned}\int_{\frac{1}{2}(2i-1)}^{\frac{1}{2}(2i+1)} \beta^u(s)\eta^u(s)\mathrm{d}s = &\int_{\frac{1}{2}(2i-1)}^{\frac{1}{2}(2i+1)} \beta^u(s)\left(\int_{\frac{1}{2}(2i-1)}^{s} r^u(w)\mathrm{d}w\right)\mathrm{d}s \\ &+i\int_{\frac{1}{2}(2i-1)}^{\frac{1}{2}(2i+1)} \beta^u(s)\left(\int_{-\frac{1}{2}}^{\frac{1}{2}} r^u(w)\mathrm{d}w\right)\mathrm{d}s.\end{aligned} \quad \text{(A.1.69)}$$

Since $\beta^u(y)$ is periodic with period 1, we get $\int_{\frac{1}{2}(2i-1)}^{\frac{1}{2}(2i+1)} \beta^u(s)\mathrm{d}s = \int_{-\frac{1}{2}}^{\frac{1}{2}} \beta^u(s)\mathrm{d}s$. Thus we can rewrite (A.1.69) as

$$\begin{aligned}\int_{\frac{1}{2}(2i-1)}^{\frac{1}{2}(2i+1)} \beta^u(s)\eta^u(s)\mathrm{d}s = &\int_{\frac{1}{2}(2i-1)}^{\frac{1}{2}(2i+1)} \beta^u(s)\left(\int_{\frac{1}{2}(2i-1)}^{s} r^u(w)\mathrm{d}w\right)\mathrm{d}s \\ &+i\left(\int_{-\frac{1}{2}}^{\frac{1}{2}} r^u(s)\mathrm{d}s\right)\left(\int_{-\frac{1}{2}}^{\frac{1}{2}} \beta^u(s)\mathrm{d}s\right).\end{aligned} \quad \text{(A.1.70)}$$

Because r^u and β^u are positive, the double integral on the right-hand side of equation (A.1.70) also must be positive. Furthermore, $r^u(s)$ and $\beta^u(s)$ are piecewise constants, so, without loss of generality, we can assume

$$0 < \beta^u_m \leq \beta^u(s) \leq \beta^u_M < \infty \quad \text{(A.1.71)}$$

and

$$0 < r^u_m \leq r^u(s) \leq r^u_M < \infty, \quad \text{(A.1.72)}$$

where β^u_m and r^u_m are the minimum values and β^u_M and r^u_M are the maximum values, for all $s \in \mathbb{R}$. Consequently, based on these assumptions and also $\frac{1}{2}(2i-1) \leq s < \frac{1}{2}(2i+1)$, we obtain

$$0 < \int_{\frac{1}{2}(2i-1)}^{\frac{1}{2}(2i+1)} \beta^u(s)\left(\int_{\frac{1}{2}(2i-1)}^{s} r^u(w)\mathrm{d}w\right)\mathrm{d}s \leq r^u_M\beta^u_M. \quad \text{(A.1.73)}$$

Now we can find a bound for the first integral on the right-hand side of equation (A.1.70). Therefore, the second term in (A.1.67) is bounded as

$$\sum_{i=0}^{n-1} i\left(\int_{-\frac{1}{2}}^{\frac{1}{2}} r^u(s)\mathrm{d}s\right)\left(\int_{-\frac{1}{2}}^{\frac{1}{2}} \beta^u(s)\mathrm{d}s\right) \leq \sum_{i=0}^{n-1}\int_{\frac{1}{2}(2i-1)}^{\frac{1}{2}(2i+1)} \beta^u(s)\eta^u(s)\mathrm{d}s \\ \leq \sum_{i=0}^{n-1} i\left(\int_{-\frac{1}{2}}^{\frac{1}{2}} r^u(s)\mathrm{d}s\right)\left(\int_{-\frac{1}{2}}^{\frac{1}{2}} \beta^u(s)\mathrm{d}s\right) + n\beta_M^u r_M^u. \tag{A.1.74}$$

After simplification, the above inequality implies that

$$\left(\frac{n(n-1)}{2}\right)\left(\int_{-\frac{1}{2}}^{\frac{1}{2}} r^u(s)\mathrm{d}s\right)\left(\int_{-\frac{1}{2}}^{\frac{1}{2}} \beta^u(s)\mathrm{d}s\right) \leq \sum_{i=0}^{n-1}\int_{\frac{1}{2}(2i-1)}^{\frac{1}{2}(2i+1)} \beta^u(s)\eta^u(s)\mathrm{d}s \\ \leq \left(\frac{n(n-1)}{2}\right)\left(\int_{-\frac{1}{2}}^{\frac{1}{2}} r^u(s)\mathrm{d}s\right) \times \left(\int_{-\frac{1}{2}}^{\frac{1}{2}} \beta^u(s)\mathrm{d}s\right) + n\beta_M^u r_M^u. \tag{A.1.75}$$

Next, we develop bounds for the first term on the right-hand side of equation (A.1.67). But first we note that, since $\eta^u(s)$ is positive and we have $y \geq \frac{1}{2}(2n-1)$, we get

$$0 \leq \int_{\frac{1}{2}(2n-1)}^{y} \eta^u(s)\mathrm{d}s \leq \eta^u(y)\Big(y - \frac{1}{2}(2n-1)\Big). \tag{A.1.76}$$

On the other hand, inequality (A.1.68) also implies that

$$y - \frac{1}{2}(2n-1) \leq 1. \tag{A.1.77}$$

The two preceding inequalities, along with (A.1.71), give the following bound:

$$0 \leq \int_{\frac{1}{2}(2n-1)}^{y} \beta^u(s)\eta^u(s)\mathrm{d}s \leq \beta_M^u \eta^u(y). \tag{A.1.78}$$

By using inequalities (A.1.75) and (A.1.78) and equation (A.1.67), we find the following upper bound

$$\int_{-\frac{1}{2}}^{y} \beta^u(s)\eta^u(s)\mathrm{d}s \leq \left(\frac{n(n-1)}{2}\right)\left(\int_{-\frac{1}{2}}^{\frac{1}{2}} r^u(s)\mathrm{d}s\right)\left(\int_{-\frac{1}{2}}^{\frac{1}{2}} \beta^u(s)\mathrm{d}s\right) \\ +n\beta_M^u r_M^u + \beta_M^u \eta^u(y) \tag{A.1.79}$$

and the lower bound

$$\int_{-\frac{1}{2}}^{y} \beta^u(s)\eta^u(s)\mathrm{d}s \geq \left(\frac{n(n-1)}{2}\right)\left(\int_{-\frac{1}{2}}^{\frac{1}{2}} r^u(s)\mathrm{d}s\right)\left(\int_{-\frac{1}{2}}^{\frac{1}{2}} \beta^u(s)\mathrm{d}s\right). \tag{A.1.80}$$

Inequality (A.1.68) implies that

$$y - \frac{1}{2} < n \leq y + \frac{1}{2}, \tag{A.1.81}$$

which means that

$$n = y + \mathcal{O}(y^0) \tag{A.1.82}$$

and

$$\left(\frac{n(n-1)}{2}\right) = \frac{y^2}{2} + \mathcal{O}(y^1), \tag{A.1.83}$$

as $y \to \infty$. Furthermore, the last two terms on the right-hand side of the upper bound (A.1.79) satisfy

$$\beta_M^u r_m^u n = \mathcal{O}(y^1) \tag{A.1.84}$$

and

$$\beta_M^u \eta^u(y) = \mathcal{O}(y^1). \tag{A.1.85}$$

Finally, we arrive at the upper bound of (A.1.79)

$$\int_{-\frac{1}{2}}^{y} \beta^u(s)\eta^u(s)\mathrm{d}s \leq \left(\frac{y^2}{2} + \mathcal{O}(y^1)\right)\left(\int_{-\frac{1}{2}}^{\frac{1}{2}} r^u(s)\mathrm{d}s\right)\left(\int_{-\frac{1}{2}}^{\frac{1}{2}} \beta^u(s)\mathrm{d}s\right) + 2\mathcal{O}(y^1), \tag{A.1.86}$$

and the lower bound

$$\int_{-\frac{1}{2}}^{y} \beta^u(s)\eta^u(s)\mathrm{d}s \geq \left(\frac{y^2}{2} + \mathcal{O}(y^1)\right)\left(\int_{-\frac{1}{2}}^{\frac{1}{2}} r^u(s)\mathrm{d}s\right)\left(\int_{-\frac{1}{2}}^{\frac{1}{2}} \beta^u(s)\mathrm{d}s\right). \tag{A.1.87}$$

By dividing the both sides of above inequalities by y^2 and then evaluating the limits as $y \to \infty$, we get

$$\begin{aligned}\frac{1}{2}\left(\int_{-\frac{1}{2}}^{\frac{1}{2}} r^u(s)\mathrm{d}s\right)\left(\int_{-\frac{1}{2}}^{\frac{1}{2}} \beta^u(s)\mathrm{d}s\right) &\leq \lim_{y\to\infty} \frac{1}{y^2}\int_{-\frac{1}{2}}^{y} \beta^u(s)\eta^u(s)\mathrm{d}s \\ &\leq \frac{1}{2}\left(\int_{-\frac{1}{2}}^{\frac{1}{2}} r^u(s)\mathrm{d}s\right)\left(\int_{-\frac{1}{2}}^{\frac{1}{2}} \beta^u(s)\mathrm{d}s\right).\end{aligned} \tag{A.1.88}$$

Thus, by the Squeeze Theorem, the limit (A.1.88) is given by

$$\lim_{y\to\infty}\frac{1}{y^2}\int_{-\frac{1}{2}}^{y}\beta^u(s)\eta^u(s)\mathrm{d}s=\frac{1}{2}\left(\int_{-\frac{1}{2}}^{\frac{1}{2}}r^u(s)\mathrm{d}s\right)\left(\int_{-\frac{1}{2}}^{\frac{1}{2}}\beta^u(s)\mathrm{d}s\right). \tag{A.1.89}$$

Since we also have

$$\int_{-\frac{1}{2}}^{\frac{1}{2}}r^u(s)\mathrm{d}s=r_1^u l_1+r_2^u l_2=\langle r^u\rangle \tag{A.1.90}$$

and

$$\int_{-\frac{1}{2}}^{\frac{1}{2}}\beta^u(s)\mathrm{d}s=\beta_1^u l_1+\beta_2^u l_2=\langle\beta^u\rangle, \tag{A.1.91}$$

equation (A.1.89) is given by

$$\lim_{y\to\infty}\frac{1}{y^2}\int_{-\frac{1}{2}}^{y}\beta^u(s)\eta^u(s)\mathrm{d}s=\frac{1}{2}\langle r^u\rangle\langle\beta^u\rangle. \tag{A.1.92}$$

Then we want to calculate the second integral on the right-hand side of equation (A.1.61). Hence, we first assume that $(\beta^u)^{-1}$ and $F(\tilde{U},\tilde{V})$ are periodic with period 1, so

$$(\beta^u)^{-1}(y+1)=(\beta^u)^{-1}(y) \tag{A.1.93}$$

and

$$F(\tilde{U},\tilde{V},y+1)=F(\tilde{U},\tilde{V},y). \tag{A.1.94}$$

Then we define $\bar{\eta}^u(y)$ as follows

$$\bar{\eta}^u(y)=\int_{-\frac{1}{2}}^{y}(\beta^u)^{-1}(w)F(\tilde{U},\tilde{V},w)\mathrm{d}w. \tag{A.1.95}$$

We need to perform the same calculations as we did for the expression on the left-hand side of equation (A.1.61). By evaluating the limit as $y\to\infty$, we get

$$\lim_{y\to\infty}\frac{1}{y^2}\int_{-\frac{1}{2}}^{y}\beta^u(s)\bar{\eta}^u(s)\mathrm{d}s=\frac{1}{2}\left(\int_{-\frac{1}{2}}^{\frac{1}{2}}(\beta^u)^{-1}(s)F(\tilde{U},\tilde{V},s)\mathrm{d}s\right)\left(\int_{-\frac{1}{2}}^{\frac{1}{2}}\beta^u(s)\mathrm{d}s\right). \tag{A.1.96}$$

Since we have equation (A.1.24) so that $F_i(\tilde{U},\tilde{V})=\beta_i^u f_i(r_i^u\tilde{U},r_i^v\tilde{V})$, we can write the first integral of above equation on the right-hand side as follows

$$\int_{-\frac{1}{2}}^{\frac{1}{2}}(\beta^u)^{-1}(s)F(\tilde{U},\tilde{V},s)\mathrm{d}s=l_1f_1(r_1^u\tilde{U},r_1^v\tilde{V})+l_2f_2(r_2^u\tilde{U},r_2^v\tilde{V})=\langle f(r^u\tilde{U},r^v\tilde{V})\rangle. \tag{A.1.97}$$

Next, by using equations (A.1.91) and (A.1.97), equation (A.1.96) leads to

$$\lim_{y\to\infty}\frac{1}{y^2}\int_{-\frac{1}{2}}^{y}\beta^u(s)\bar{\eta}^u(s)\mathrm{d}s=\frac{1}{2}\langle f(r_1^u\tilde{U},r_2^v\tilde{V})\rangle\langle\beta^u\rangle, \tag{A.1.98}$$

which gives the limit of second term on the right-hand side of equation (A.1.61) as $y\to\infty$.

Finally, we need to evaluate the limit of the first term on the right-hand side of equation (A.1.61) as $y\to\infty$. In this case, we also set the lower limits of integration to $y_0=-\frac{1}{2}$. $\beta^u(s)$ can be expressed as the following sum

$$\int_{-\frac{1}{2}}^{y}\beta^u(s)\mathrm{d}s=\int_{\frac{1}{2}(2n-1)}^{y}\beta^u(s)\mathrm{d}s+\sum_{i=0}^{n-1}\int_{\frac{1}{2}(2i-1)}^{\frac{1}{2}(2i+1)}\beta^u(s)\mathrm{d}s, \tag{A.1.99}$$

where n is chosen so that

$$\frac{1}{2}(2n-1)\le y<\frac{1}{2}(2n+1). \tag{A.1.100}$$

We can find the bounds for the first term on the right-hand side of equation (A.1.99), with the same procedures that we have done before for inequalities (A.1.76) and (A.1.77) to get (A.1.78). We obtain

$$0\le\int_{\frac{1}{2}(2n-1)}^{y}\beta^u(s)\mathrm{d}s\le\beta_M^u(y-\frac{1}{2}(2n-1))\le\beta_M^u. \tag{A.1.101}$$

Then we want to find the bound for the second term on the right-side of equation (A.1.99). Again, since β^u is periodic with period 1, each of the last n are equal to $\int_{-\frac{1}{2}}^{\frac{1}{2}}\beta^u\mathrm{d}s$. Consequently,

$$\sum_{i=0}^{n-1}\int_{\frac{1}{2}(2i-1)}^{\frac{1}{2}(2i+1)}\beta^u(s)\mathrm{d}s=n\int_{-\frac{1}{2}}^{\frac{1}{2}}\beta^u(s)\mathrm{d}s. \tag{A.1.102}$$

By using inequalities (A.1.101) and (A.1.102) and equation (A.1.99), we arrive at the upper bound

$$\int_{-\frac{1}{2}}^{y}\beta^u(s)\mathrm{d}s\le\beta_M^u+n\int_{-\frac{1}{2}}^{\frac{1}{2}}\beta^u(s)\mathrm{d}s \tag{A.1.103}$$

and the lower bound

$$\int_{-\frac{1}{2}}^{y}\beta^u(s)\mathrm{d}s\ge n\int_{-\frac{1}{2}}^{\frac{1}{2}}\beta^u(s)\mathrm{d}s. \tag{A.1.104}$$

Inequality (A.1.100) implies that

$$y - \frac{1}{2} < n \leq y + \frac{1}{2}, \tag{A.1.105}$$

which results in

$$n = y + \mathcal{O}(y^0), \tag{A.1.106}$$

as $y \to \infty$. Consequently, the two terms on the right-hand side of the upper bound (A.1.103) satisfy

$$n \int_{-\frac{1}{2}}^{\frac{1}{2}} \beta^u(s)\mathrm{d}s \leq (y + \frac{1}{2}) \int_{-\frac{1}{2}}^{\frac{1}{2}} \beta^u(s)\mathrm{d}s = y \int_{-\frac{1}{2}}^{\frac{1}{2}} \beta^u(s)\mathrm{d}s + \mathcal{O}(y^0) \tag{A.1.107}$$

and

$$\beta_M^u = \mathcal{O}(y^0). \tag{A.1.108}$$

Furthermore, the lower bound in equation (A.1.104) satisfies

$$n \int_{-\frac{1}{2}}^{\frac{1}{2}} \beta^u(s)\mathrm{d}s \geq (y - \frac{1}{2}) \int_{-\frac{1}{2}}^{\frac{1}{2}} \beta^u(s)\mathrm{d}s = y \int_{-\frac{1}{2}}^{\frac{1}{2}} \beta^u(s)\mathrm{d}s + \mathcal{O}(y^0). \tag{A.1.109}$$

Finally, we arrive at the lower and upper bound (A.1.99)

$$y \int_{-\frac{1}{2}}^{\frac{1}{2}} \beta^u(s)\mathrm{d}s + \mathcal{O}(y^0) \leq \int_{-\frac{1}{2}}^{\frac{1}{2}} \beta^u(s)\mathrm{d}s \leq y \int_{-\frac{1}{2}}^{\frac{1}{2}} \beta^u(s)\mathrm{d}s + \mathcal{O}(y^0). \tag{A.1.110}$$

At this step, we want to evaluate the first term on the right-hand side of equation (A.1.61) as $y \to \infty$, so we can rewrite the above inequality as

$$\begin{aligned} \langle\beta^u\rangle^{-1} y^2 \int_{-\frac{1}{2}}^{\frac{1}{2}} \beta^u(s)\mathrm{d}s - \frac{y^2}{2} + \mathcal{O}(y^0) \leq \langle\beta^u\rangle^{-1} y \int_{-\frac{1}{2}}^{\frac{1}{2}} \beta^u(s)\mathrm{d}s - \frac{y^2}{2} \\ \leq \langle\beta^u\rangle^{-1} y^2 \int_{-\frac{1}{2}}^{\frac{1}{2}} \beta^u(s)\mathrm{d}s - \frac{y^2}{2} + \mathcal{O}(y^0). \end{aligned} \tag{A.1.111}$$

By dividing the both sides of the above inequality by y^2 and then evaluating the limit as $y \to \infty$, we find

$$\begin{aligned} \langle\beta^u\rangle^{-1} \int_{-\frac{1}{2}}^{\frac{1}{2}} \beta^u(s)\mathrm{d}s - \frac{1}{2} \leq \lim_{y\to\infty} \frac{1}{y^2} \left(\langle\beta^u\rangle^{-1} y \int_{-\frac{1}{2}}^{\frac{1}{2}} \beta^u(s)\mathrm{d}s - \frac{y^2}{2} \right) \\ \leq \langle\beta^u\rangle^{-1} \int_{-\frac{1}{2}}^{\frac{1}{2}} \beta^u(s)\mathrm{d}s - \frac{1}{2}. \end{aligned} \tag{A.1.112}$$

Next, by the Squeeze Theorem, the above limit is given by

$$\lim_{y\to\infty}\frac{1}{y^2}\left(\langle\beta^u\rangle^{-1}y\int_{-\frac{1}{2}}^{\frac{1}{2}}\beta^u(s)\mathrm{d}s-\frac{y^2}{2}\right)=\langle\beta^u\rangle^{-1}\int_{-\frac{1}{2}}^{\frac{1}{2}}\beta^u(s)\mathrm{d}s-\frac{1}{2}. \tag{A.1.113}$$

Since $\int_{-\frac{1}{2}}^{\frac{1}{2}}\beta^u(s)\mathrm{d}s=\langle\beta^u\rangle$, the above equation can be written as

$$\lim_{y\to\infty}\frac{1}{y^2}\left(\langle\beta^u\rangle^{-1}y\int_{-\frac{1}{2}}^{\frac{1}{2}}\beta^u(s)\mathrm{d}s-\frac{y^2}{2}\right)=\frac{1}{2}. \tag{A.1.114}$$

Now we have all the ingredients (A.1.92), (A.1.98) and (A.1.114) to evaluate equation (A.1.61) as $y\to\infty$. We divide both sides of equation (A.1.61) by y^2 and then evaluate the limit as $y\to\infty$. Thus, we get

$$\left(\frac{1}{2}\langle r^u\rangle\langle\beta^u\rangle\right)\frac{\partial\tilde{U}}{\partial t}=\frac{1}{2}\frac{\partial^2\tilde{U}}{\partial x^2}+\left(\frac{1}{2}\langle f(r^u\tilde{U},r^v\tilde{V})\rangle\langle\beta^u\rangle\right). \tag{A.1.115}$$

As a result, the homogenized model becomes

$$\frac{\partial\tilde{U}}{\partial t}=\hat{D}^u\frac{\partial^2\tilde{U}}{\partial x^2}+F(\tilde{U},\tilde{V}), \tag{A.1.116}$$

where

$$\hat{D}^u=\langle\beta^u\rangle^{-1}\langle r^u\rangle^{-1} \tag{A.1.117}$$

and

$$F(\tilde{U},\tilde{V})=\langle r^u\rangle^{-1}\langle f(r^u\tilde{U},r^v\tilde{V})\rangle. \tag{A.1.118}$$

Here $\langle r^u\rangle$ is the arithmetic average of the residence index as defined in (A.1.8) and $\langle f(r^u\tilde{U},r^v\tilde{V})\rangle$ is the arithmetic average of the reaction term, which is defined as

$$\langle f(r^u\tilde{U},r^v\tilde{V})\rangle=\frac{f_1(r_1^u\tilde{U},r_1^v\tilde{V})l_1+f_2(r_2^u\tilde{U},r_2^v\tilde{V})l_2}{l_1+l_2}. \tag{A.1.119}$$

Remark A.1.3. *Applying the same procedure to (A.1.19), we find the homogenized equation for v as well.*

We can rescale the dynamic level so that it approximates the average density over a period. We define

$$\Gamma^u(x,y,t)=u(x,y,t)\left(\frac{r^u(y)}{\langle r^u\rangle}\right)^{-1}=\langle r^u\rangle\tilde{\Gamma}^u(x,y,t) \tag{A.1.120}$$

to be the rescaled dynamic level for prey. Similarly, we can define the rescaled dynamical level for predator. The leading-order approximation to the rescaled dynamic level of prey is also independent of y

$$U(x,t) = \Gamma_0(x,y,t) = \langle r^u \rangle \tilde{\Gamma}_0^u(x,y,t) = \langle r^u \rangle \tilde{U}(x,t) \tag{A.1.121}$$

and satisfies the homogenized model (A.1.116) after a corresponding rescaling. The rescaled homogenized model for the prey is

$$\frac{\partial U}{\partial t} = \hat{D}^u \frac{\partial^2 U}{\partial x^2} + \hat{f}(U,V), \tag{A.1.122}$$

where the homogenized diffusion coefficient for prey, $\hat{D}^u$, given by equation (A.1.117), is unchanged, and the rescaled homogenized reaction term is given by

$$\hat{f}(U,V) = \langle f(\frac{r^u(y)}{\langle r^u \rangle} U, \frac{r^v(y)}{\langle r^v \rangle} V) \rangle. \tag{A.1.123}$$

A similar rescaling can be carried out for the predator equation.

As a summary, the homogenized model of predator–prey model (5.2.1) with interface conditions (5.2.2) in a heterogeneous landscape is given by

$$\begin{cases} \dfrac{\partial U(x,t)}{\partial t} = \hat{D}^u \dfrac{\partial^2 U(x,t)}{\partial x^2} + \hat{f}(U,V), \\ \dfrac{\partial V(x,t)}{\partial t} = \hat{D}^v \dfrac{\partial^2 V(x,t)}{\partial x^2} + \hat{g}(U,V), \end{cases} \tag{A.1.124}$$

where $x \in \mathbb{R}$. Here, $U(x,t)$ and $V(x,t)$ denote the population densities for prey and predator, respectively. In fact, they are originally the leading-order approximations to the dynamic levels for species u and v, scaled as (A.1.120), so that they reflect the average population densities.

Appendix B

Expression of the DDI conditions in terms of patch level quantities

We express the DDI conditions for the homogenized model in Chapter 5 in terms of the patchy growth functions, f_i and g_i, in order to evaluate them at the steady state in the patch-level model. It may sometimes be easier to evaluate the DDI conditions on the patchy level rather than on the homogenized level.

We derive these conditions on the patch-level by applying the chain rule for each of the following partial derivatives to obtain

$$\begin{aligned}\frac{\partial f_i}{\partial U}\left(\frac{r_i^u U}{\langle r^u\rangle}, \frac{r_i^v V}{\langle r^v\rangle}\right)\Big|_{(U^*,V^*)} &= \left(\frac{\partial f_i}{\partial u_i}\frac{\partial u_i}{\partial U}\right)(u_i, v_i)\big|_{(U^*\frac{r_i^u}{\langle r^u\rangle}, V^*\frac{r_i^v}{\langle r^v\rangle})} \\ &= \left(\frac{\partial f_i}{\partial u_i}\left(\frac{r_i^u}{\langle r^u\rangle}\right)\right)(u_i, v_i)\big|_{(U^*\frac{r_i^u}{\langle r^u\rangle}, V^*\frac{r_i^v}{\langle r^v\rangle})}\end{aligned} \tag{B.0.1}$$

and

$$\begin{aligned}\frac{\partial f_i}{\partial V}\left(\frac{r_i^u U}{\langle r^u\rangle}, \frac{r_i^v V}{\langle r^v\rangle}\right)\Big|_{(U^*,V^*)} &= \left(\frac{\partial f_i}{\partial v_i}\frac{\partial v_i}{\partial V}\right)(u_i, v_i)\big|_{(U^*\frac{r_i^u}{\langle r^u\rangle}, V^*\frac{r_i^v}{\langle r^v\rangle})} \\ &= \left(\frac{\partial f_i}{\partial v_i}\left(\frac{r_i^v}{\langle r^v\rangle}\right)\right)(u_i, v_i)\big|_{(U^*\frac{r_i^u}{\langle r^u\rangle}, V^*\frac{r_i^v}{\langle r^v\rangle})}.\end{aligned} \tag{B.0.2}$$

We have similar expressions for partial derivatives of function g_i.

As a result, conditions DDI 1–DDI 4 in terms of f_i and g_i are given by

$$1.\ l_1\left[\frac{r_1^u}{\langle r^u\rangle}\frac{\partial f_1}{\partial u_1} + \frac{r_1^v}{\langle r^v\rangle}\frac{\partial g_1}{\partial v_1}\right] + l_2\left[\frac{r_2^u}{\langle r^u\rangle}\frac{\partial f_2}{\partial u_2} + \frac{r_2^v}{\langle r^v\rangle}\frac{\partial g_2}{\partial v_2}\right] < 0, \tag{B.0.3}$$

$$2.\ \frac{l_1}{l_2}(r_1^u r_1^v)\left[\frac{\partial f_1}{\partial u_1}\frac{\partial g_1}{\partial v_1}-\frac{\partial g_1}{\partial u_1}\frac{\partial f_1}{\partial v_1}\right]+(r_1^u r_2^v)\left[\frac{\partial f_1}{\partial u_1}\frac{\partial g_2}{\partial v_2}-\frac{\partial g_1}{\partial u_1}\frac{\partial f_2}{\partial v_2}\right]$$
$$+(r_2^u r_1^v)\left[\frac{\partial f_2}{\partial u_2}\frac{\partial g_1}{\partial v_1}-\frac{\partial f_1}{\partial v_1}\frac{\partial g_2}{\partial u_2}\right]+\frac{l_2}{l_1}(r_2^u r_2^v)\left[\frac{\partial f_2}{\partial u_2}\frac{\partial g_2}{\partial v_2}-\frac{\partial f_2}{\partial v_2}\frac{\partial g_2}{\partial u_2}\right]>0, \tag{B.0.4}$$

$$3.\ l_1\left[\frac{r_1^u}{\langle\beta^v\rangle}\frac{\partial f_1}{\partial u_1}+\frac{r_1^v}{\langle\beta^u\rangle}\frac{\partial g_1}{\partial v_1}\right]+l_2\left[\frac{r_2^u}{\langle\beta^v\rangle}\frac{\partial f_2}{\partial u_2}+\frac{r_2^v}{\langle\beta^u\rangle}\frac{\partial g_2}{\partial v_2}\right]>0, \tag{B.0.5}$$

$$4.\ \left(l_1\left[\frac{r_1^u}{\langle\beta^v\rangle}\frac{\partial f_1}{\partial u_1}+\frac{r_1^v}{\langle\beta^u\rangle}\frac{\partial g_1}{\partial v_1}\right]+l_2\left[\frac{r_2^u}{\langle\beta^v\rangle}\frac{\partial f_2}{\partial u_2}+\frac{r_2^v}{\langle\beta^u\rangle}\frac{\partial g_2}{\partial v_2}\right]\right)^2$$
$$-4l_1l_2\langle\beta^u\rangle^{-1}\langle\beta^v\rangle^{-1}\left(\frac{l_1}{l_2}(r_1^u r_1^v)\left[\frac{\partial f_1}{\partial u_1}\frac{\partial g_1}{\partial v_1}-\frac{\partial g_1}{\partial u_1}\frac{\partial f_1}{\partial v_1}\right]\right.$$
$$+(r_1^u r_2^v)\left[\frac{\partial f_1}{\partial u_1}\frac{\partial g_2}{\partial v_2}-\frac{\partial g_1}{\partial u_1}\frac{\partial f_2}{\partial v_2}\right]+(r_2^u r_1^v)\left[\frac{\partial f_2}{\partial u_2}\frac{\partial g_1}{\partial v_1}-\frac{\partial f_1}{\partial v_1}\frac{\partial g_2}{\partial u_2}\right]$$
$$\left.+\frac{l_2}{l_1}(r_2^u r_2^v)\left[\frac{\partial f_2}{\partial u_2}\frac{\partial g_2}{\partial v_2}-\frac{\partial f_2}{\partial v_2}\frac{\partial g_2}{\partial u_2}\right]\right)>0, \tag{B.0.6}$$

where all these expressions are evaluated at the steady state $(U^*\frac{r_i^u}{\langle r^u\rangle}, V^*\frac{r_i^v}{\langle r^v\rangle})$. Expressions of $\langle\beta^u\rangle^{-1}$ and $\langle r^u\rangle^{-1}$ were derived in Appendix A.

Bibliography

[1] D. Alonson, F. Bartumeus, and J. Catalan. Mutual interference between predators can give rise to Turing spatial patterns. *The Ecological Society of America*, 83(1):28–34, 2002.

[2] Y. Alqawasmeh and F. Lutscher. Movement behaviour of fish, harvesting-induced habitat degradation and the optimal size of marine reserves. *Journal of Theoretical Ecology*, 12:453–466, 2019.

[3] Y. Alqawasmeh and F. Lutscher. Persistence and spread of stage-structured populations in heterogeneous landscapes. *Journal of Mathematical Biology*, 78(5):1485–1527, 2019.

[4] D. A. Andow, P. Kareiva, S. A. Levin, and A. Okubo. Spread of invading organisms. *Journal of Landscape Ecology*, 4(2/3):177–188, 1990.

[5] R. Arditi and L. R. Ginzburg. Coupling in predator-prey dynamics: ratio dependence. *Journal of Theoretical Biology*, 139:311–326, 1989.

[6] R. Arditi, C. Lobry, and T. Sari. Is dispersal always beneficial to carrying capacity? New insights from the multi-patch logistic equation. *Theoretical Population Biology*, 106:45–59, 2015.

[7] R. Arditi, C. Lobry, and T. Sari. Asymmetric dispersal in the multi-patch logistic equation. *Theoretical Population Biology*, 120:11–15, 2018.

[8] J. R. Beddington. Mutual interference between parasites or predators and its effect on searching efficiency. *Journal of Animal Ecology*, 44:331–340, 1975.

[9] C. M. Bender and S. A. Orszag. *Advanced mathematical methods for scientists and engineers*. Springer, New York, 1999.

[10] D. L. Benson, P. K. Maini, and J. A. Sherratt. Analysis of pattern formation in reaction-diffusion models with spatially inhomogeneous coefficients. *Mathematical and Computer Modelling*, 17(2):29–34, 1993.

[11] D. L. Benson, P. K. Maini, and J. A. Sherratt. Diffusion driven instability in an inhomogeneous domain. *Bulletin of Mathematical Biology*, 55(2):365–384, 1993.

[12] H. Brezis. *Functional analysis, Sobolev spaces and partial differential equations*. Springer, New York, 2010.

[13] R. S. Cantrell and C. Cosner. *Spatial Ecology via Reaction-Diffusion Equations*. Wiley, 2003.

[14] C. Cobbold and F. Lutscher. Mean occupancy time: linking mechanistic movement models, population dynamics and landscape ecology to population persistence. *Mathematical Biology*, 68:549–579, 2014.

[15] C. A. Cobbold, F. Lutscher, and J. A. Sherratt. Diffusion-driven instabilities and emerging spatial patterns in patchy landscapes. *Ecological Complexity*, 24:69–81, 2015.

[16] C. Cosner. Existence of global solutions to a model of a myelinate nerve axon. *SIAM Journal on Applied Mathematics*, 18(3):703–710, 1987.

[17] F. Courchamp, L. Berec, and J. Gascoinge. *Allee effects*. Oxford University Press, 2008.

[18] E. E. Crone, L. M. Brown, J. A. Hodgson, F. Lutscher, and C. B. Schultz. Faster movement in nonhabitat matrix promotes range shifts in heterogeneous landscapes. *Ecology*, 100(7):e02701, 2019.

[19] G. C. Cruywagen, P. Kareiva, M. A. Lewis, and J. D. Murray. Competition in a spatially heterogeneous environment: Modelling the risk of spread of a genetically engineered population. *Theoretical Population Biology*, 49(1):1–38, 1996.

[20] D. DeAngelis, W-M. Ni, and B. Zhang. Dispersal and spatial heterogeneity: single species. *Journal of Mathematical Biology*, 72(1):239–254, 2016.

[21] D. DeAngelis, W-M. Ni, and B. Zhang. Effect of diffusion on total biomass in heterogeneous continuous and discrete-patch systems. *Theoretical Ecology*, 9(4):443–453, 2016.

[22] L. C. Evans. *Partial differential equations*. American Mathematical Society, 2010.

[23] S. Fasani and S. Rinaldi. Factors promoting or inhibiting Turing instability in spatially extended prey-predator systems. *Ecological Modelling*, 222:3449–3452, 2011.

[24] R. Fisher. The advance of advantageous genes. *Annals of Eugenics*, 7:355–369, 1937.

[25] H. I. Freedman. *Deterministic mathematical models in population ecology*. Marcel Dekker, New York, 1980.

[26] H. I. Freedman, J. B. Shukla, and Y. Takeuchi. Population diffusion in a two patch environment. *Mathematical Biosciences*, 95(1):111–123, 1989.

[27] H. I. Freedman and P. Waltman. Mathematical models of population interactions with dispersal. I: stability of two habitats with and without a predator. *SIAM Journal on Applied Mathematics*, 32(3):631–648, 1977.

[28] A. Friedman. *Partial differential equations*. New York: Holt, Rinehart and Winston, 1969.

[29] M. J. Garlick, J. A. Powel, M. B. Hooten, and L. R. MacFarlane. Homogenization of large-scale movement models in ecology. *Bulletin of Mathematical Biology*, 73:2088–2108, 2011.

[30] M. J. Garlick, J. A. Powell, M. B. Hooten, and L. R. MacFarlane. Homogenization, sex, and differential motility predict spread of chronic wasting disease in mule deer in southern Utah. *Journal of Mathematical Biology*, 69(2):369–399, 2014.

[31] A. Gierer and H. Meinhardt. A theory of biological pattern formation. *Kybernetik*, 12:30–39, 1972.

[32] Q. Guo, X. He, and W-M. Ni. On the effects of carrying capacity and intrinsic growth rate on single and multiple species in spatially heterogeneous environments. *Journal of Mathematical Biology*, 81:403–433, 2020.

[33] C. S. Holling. The components of predation as revealed by a study of small-mammal predation of the European pine sawfly. *The Canadian Entomologist*, 91:293–320, 1959.

[34] C. S. Holling. Some characteristics of simple types of predation and parasitism. *The Canadian Entomologist*, 91:385–398, 1959.

[35] T. Kato. *Perturbation theory for linear operators*. Springer-Verlag, Berlin, 1966.

[36] L. E. Keshet. *Mathematical models in biology*. SIAM: Society for Industrial and Applied Mathematics, Philadelphia, 2005.

[37] M. Kot. *Elements of Mathematical Ecology*. Cambridge University Press, 2001.

[38] J. Langebrake, L. Riotte-Lambert, C. W. Osenberg, and P. De Leenheer. Differential movement and movement bias models for marine protected areas. *Journal of Mathematical Biology*, 64:667–696, 2012.

[39] S. Levin and L. Segel. Hypothesis for origin of planktonic patchiness. *Nature*, 259:659, 1976.

[40] M. A. Lewis, S. V. Petrovskii, and J. R. Potts. *The mathematics behind biological invasions*. Springer, New York, 2016.

[41] Y. Lou. On the effect of migration and spatial heterogeneity on single and multiple species. *Journal of Differential Equations*, 223(2):400–426, 2006.

[42] Y. Lou and G. Sell. *Dynamics of evolutionary equations*. Springer, New York, 2002.

[43] F. Lutscher, M. A. Lewis, and E. McCauley. The effects of heterogeneity on population persistence and invasion in rivers. *Bulletin of Mathematical Biology*, 68(8):2129–2160, 2006.

[44] F. Lutscher and J. Musgrave. Behavioral responses to resource heterogeneity can accelerate biological invasions. *Ecology*, 98(5):1229–1238, 2017.

[45] G. Maciel, C. Cosner, R. S. Cantrell, and F. Lutscher. Evolutionary stable movement strategies in reaction-diffusion models with edge behavior. *Journal of Mathematical Biology*, 80(1-2):61–92, 2020.

[46] G. A. Maciel and F. Lutscher. How individual movement response to habitat edge affects population persistence and spatial spread. *The American Naturalist*, 182(1):42–52, 2013.

[47] G. A. Maciel and F. Lutscher. Allee effects and population spread in patchy landscapes. *Journal of Biological Dynamics*, 9(1):109–123, 2015.

[48] R. M. May. *Stability and complexity in model ecosystems*. Princeton University Press, 1974.

[49] B. Mukhopadhyay and R. Bhattacharyya. Modeling the role of diffusion coefficients on Turing instability in a reaction-diffusion predator-prey system. *Bulletin of Mathematical Biology*, 68:293–313, 2006.

[50] J. D. Murray. *Mathematical Biology II: Spatial models and biomedical applications*. Springer, New York, 2001.

[51] N. Nagel and K-J. Engel. *One operator semigroups for linear evolution equations*. Springer, 2000.

[52] A. Novruzi. *An introduction to partial differential equations*. Lecture notes, University of Ottawa.

[53] A. Okubo and S. A. Levin. *Diffusion and ecological problems: modern perspectives*. Springer, New York, 2001.

[54] H. G. Othmer. A continuum model of coupled cells. *Journal of Mathematical Biology*, 17(3):351–369, 1983.

[55] O. Ovaskainen and S. Cornell. Biased movement at a boundary and conditional occupancy times for diffusion processes. *Journal of Applied Probability*, 40(3):557–580, 2003.

[56] S. W. Pacala and J. Roughgarden. Spatial heterogeneity and interspecific competition. *Theoretical Population Biology*, 21:92–113, 1982.

[57] K. Page, P. K. Maini, and N. A. M. Monk. Pattern formation in spatially heterogeneous Turing reaction-diffusion models. *Physica D*, 181:80–101, 2003.

[58] K. Page, P. K. Maini, and N. A. M. Monk. Complex pattern formation in reaction-diffusion systems with spatially varying patterns. *Physica D*, 202:95–115, 2005.

[59] L. Perko. *Differential equations and dynamical systems*. Springer, New York, 2001.

[60] R. Precup. *Methods in non-linear integral equations*. Springer, Netherlands, 2002.

[61] M. Renardy and R. Rogers. *An introduction to partial differential equations. Texts in Applied Mathematics 13*. Springer-Verlag, Berlin/New York, 1993.

[62] M. Rosenzweig and R. MacArthur. Graphic representation and stability conditions of predator-prey interaction. *The American Naturalist*, 97(895):209–223, 1963.

[63] L. Segel and J. Jackson. Dissipative structure: an explanation and an ecological example. *Journal of Theoretical Biology*, 37:545–559, 1972.

[64] E. Sheffer, J. Von Hardenberg, H. Yizhaq, M. Shachak, and E. Meron. Emerged or imposed: a theory on the role of physical templates and self-organisation for vegetation patchiness. *Ecology Letters*, 16:127–139, 2013.

[65] N. Shigesada, K. Kawasaki, and E. Teramoto. Traveling periodic waves in heterogeneous environments. *Theoretical Population Biology*, 30:143–160, 1986.

[66] J. G. Skellam. Random dispersal in theoretical populations. *Biometrika*, 38:196–218, 1951.

[67] J. C. Strikwerda. *Finite difference schemes and partial differential equations*. SIAM: Society for Industrial and Applied Mathematics, Philadelphia, 2004.

[68] P. Turchin. *Quantitative analysis of movement: measuring and modeling population redistribution of plants and animals*. Sinauer Associates, Sunderland, 1998.

[69] P. Turchin. *Complex population dynamics*. Princeton University Press, 2001.

[70] A. Turing. The chemical basis of morphogenesis. *Philosophical Transactions of the Royal Society B*, 237:37–72, 1952.

[71] V. Voltera. Variations and fluctuations of the number of individuals in animal species living together. *Journal du Conseil permanent international pour l'Exploration de la Mer*, 3:3–51, 1926.

[72] W. Wang, L. Zhang, Y. Xue, and Z. Jin. Spatiotemporal pattern formation of Beddington–Deangelis-type predator-prey model. 2008.

[73] B. Yurk. Homogenization of a directed dispersal model for animal movement in a heterogeneous environment. *Bulletin of Mathematical Biology*, 87(10):2034–2056, 2016.

[74] B. Yurk and C. Cobbold. Homogenization techniques for population dynamics in strongly heterogeneous landscapes. *Journal of Biological Dynamics*, 12(1):171–193, 2018.

[75] B. Yurk, F. Lutscher, and C. Cobbold. Prey refuge homogenization. *Submitted to Methods in Ecology and Evolution*.

[76] N. Zaker, L. Ketchemen, and F. Lutscher. The effect of movement behavior on population density in patchy landscapes. *Bulletin of Mathematical Biology*, 82(1):1, 2019.

[77] B. Zhang, A. Kula, K. Mack, L. Zhai, A. Ryce, W-M. Ni, D. DeAngelis, and J. D. Van Dyken. Carrying capacity in a heterogeneous environment with habitat connectivity. *Ecology letters*, 20(9):1118–1128, 2017.

[78] B. Zhang, X. Liu, D. L. DeAngelis, W-M. Ni, and G. Geoff Wang. Effects of dispersal on total biomass in a patchy, heterogeneous system: Analysis and experiment. *Mathematical Biosciences*, 264:54–62, 2015.